STRUCTURAL DAMAGE IDENTIFICATION USING VIBRATION-BASED MODEL UPDATING

by

Shuxuan Li

B.Sc.E. (Civil Engineering), University of New Brunswick, 2016

A Thesis Submitted in Partial Fulfillment
of the Requirements for the Degree of

Master of Science in Engineering

in the Graduate Academic Unit of Civil Engineering

Supervisor: Kaveh Arjomandi, PhD, PEng., Department of Civil Engineering

Examining Board: Peter Bischoff, PhD, P.Eng., Department of Civil Engineering, Chair
Won Taek Oh, PhD, P.Eng., Department of Civil Engineering
Mohsen Mohammadi, PhD, Department of Mechanical Engineering

This thesis is accepted by the Dean of Graduate Studies

THE UNIVERSITY OF NEW BRUNSWICK

October, 2018

©Shuxuan Li, 2019

ABSTRACT

In this thesis, topics relevant to structural damage identification using vibration-based model updating are discussed. First, a seven-story scale building model is designed and constructed following the similitude law. Then the finite element models of the scale building are developed using SAP2000 and ABAQUS with appropriate modelling assumptions. Different vibration tests are conducted on the physical model, and the dynamic characteristics of the scale building are successfully extracted using the operational modal analysis (OMA). It is shown that the results of OMA are highly dependent on the sensor configuration, excitation type, block size, and model order. Lastly, identification of four damage scenarios of the scale building are investigated by assessing the change in modal frequencies. Major structural damage causing a significant effect on the modal frequencies is successfully identified using the model updating technique.

ACKNOWLEDGEMENT

I would like to thank the following people:

- My supervisor Dr. Kaveh Arjomandi for his guidance, encouragement and continuously inspiring me throughout my degree.
- The administrative staff (Joyce Moore, MaryBeth Nicholson, Angela Stewart and Alisha Hanselpacker) and laboratory technicians (Andrew Sutherland, Min-Seop Song, and Chris Forbes) at the Civil Engineering Department for their assistance and patience during my time at UNB.
- My parents, Bomin Li and Jinghua Chen for their continuous support and encouragement.
- My colleagues Ethan MacLeod and Wanrong Zhu for their accompanying, assistance and continuous encouragement.
- And my fur child Loki for always making me smile and accompanied when I needed the most.

Table of Contents

ABSTRACT ii

ACKNOWLEDGEMENT iii

Table of Contents iv

List of Tables vii

List of Figures ix

List of Symbols xii

1 Introduction 1

1.1 Overview 1
1.2 Thesis Structure 3
1.3 Contribution of the Candidate 3

2 Development of Small-Scale Building Model 4

2.1 Introduction 4
2.2 Physical Modeling Theory 9
2.2.1 Classification of Models 9
2.2.2 Buckingham's Pi Theorem 10
2.2.3 Similitude Law 11
2.3 Case-study Building 12
2.3.1 Scale Factor 14
2.3.2 Section Summary 15
2.3.3 Construction Details 20
2.4 Summary 30

3 Finite Element Model of the Scale Building 31

3.1 Introduction 31
3.2 Modelling Assumptions 32
3.2.1 Material 33
3.2.2 Member Cross-section 34
3.2.3 Boundary Condition 34
3.2.4 Assembling of Elements 35
3.3 Mesh and Element Convergence studies 35
3.3.1 SAP2000 38

3.3.2 ABAQUS 40
3.3.3 FEMtools 44
3.4 Modeling of Columns and Connection End-Plates 45
3.5 Modelling of Brace Members 47
3.6 Finite Element Analysis Result 51
3.7 Conclusion 54
4 Operational Modal Analysis of the Scale Building 55
4.1 Introduction 55
4.2 Technical Background 58
4.2.1 Time Domain PolyReference (TDPR) 58
4.2.2 Frequency Domain Decomposition (FDD) 62
4.3 Vibration Tests 64
4.3.1 Sensor Configuration 67
4.3.2 Input Excitation and Monitoring Time 69
4.4 Operational Model Analysis 72
4.4.1 Modal Parameter Extractor 72
4.4.2 Correlation Analysis 75
4.4.3 Parametric Study Summary 76
4.5 Validation of FEMs and OMA Results 81
4.5.1 Validation of Finite Element Models 81
4.5.2 OMA Results of Moment and Braced Frame 83
4.6 Discussion 88
4.7 Conclusions 89
5 Vibration-Based Damage Detection Using Model Updating 90
5.1 Introduction 90
5.2 Model updating 94
5.2.1 Technical background 94
5.2.2 Damage Detection using Model Updating 97
5.3 Experimental Studies on Undamaged Models 99
5.3.1 Moment Frame 99
5.3.2 Braced Frame 105
5.4 Experimental Studies on Damaged Models 112
5.4.1 Damage Condition 112
5.4.2 Baseline FEM 114

5.4.3 Moment Frame 114
5.4.4 Braced Frame 116
5.5 Conclusion 122
6 General Conclusions and Recommendations 123
6.1 General Conclusions 123
6.2 Recommendations 125
7 References 126
Appendix A: FEMtools Command Script for OMA 133
Curriculum Vitae

List of Tables

Table 2.1: Summary of previous studies 8
Table 2.2: Summary of scale factors 14
Table 2.3: Summary of the prototype and scale model sections 19
Table 3.1: Summary of material properties 34
Table 3.2: Summary of member cross-section. All dimension in mm. 34
Table 3.3: Summary of finite elements 37
Table 3.4: Number of elements and nodes for each seed size for the moment frame 40
Table 3.5: Number of elements and nodes for each seed size for the braced frame 44
Table 3.6: Conversion scheme between ABAQUS and FEMtools element type 44
Table 3.7: Frequencies and mode shapes for the moment frame 52
Table 3.8: Frequencies and mode shapes for the braced frame 53
Table 4.1: Monitoring time for type 1 excitation tests 71
Table 4.2: Summary of test parameters 72
Table 4.3: Extracted and paired modes from vibration tests 81
Table 4.4: Validation of the moment frame finite element model 82
Table 4.5: Validation of the braced frame finite element model 82
Table 4.6: OMA results of moment frame 84
Table 4.7: OMA results of brace frame 86
Table 5.1: Parameter limits of undamaged MF 99
Table 5.2: Summary of Response Combination (RC) of undamaged MF 100
Table 5.3: Mode shape pairs of MF before updating 100
Table 5.4: Results of model updating of MF using different response combination 101
Table 5.5: Summary of response combinations for the undamaged BF 106
Table 5.6: Parameter limits of undamaged BF 106
Table 5.7: Mode shape pairs of BF before updating 106
Table 5.8: Results of model updating of BF using different response combination 107

Table 5.9: Comparison of OMA results of undamaged and damaged MF 115
Table 5.10: Parameter limits for MF..... 115
Table 5.11: Comparison of OMA results of undamaged and damaged BF 117
Table 5.12: Selected response for model updating to detect the damage of the BF 117
Table 5.13: Parameter limits for BF damage detection..... 117

List of Figures

Figure 2.1: 1:40 Suspension Bridge, Tongji University, China [5] 5

Figure 2.2: 1:3 Reinforced Concrete Frame, IZIIS Laboratory, Macedonia [6]..... 6

Figure 2.3: 1:4 AAC Building, Bovec, Slovenia [7]..... 7

Figure 2.4: 1:110 Lions Gate, Ottawa, Canada [4] 8

Figure 2.5: Case study building a) Full scale b) Small Scale. All dimensions are in mm. 13

Figure 2.6: a) Moment-resisting frame with brace members b) Moment-resisting frame c) Braced frame d) Displacement of frame shown in Figure 2.6.a e) Displacement of frame shown in Figure 2.6.b f) Displacement of frame shown in Figure 2.6.c..... 17

Figure 2.7: 1/12 scale model a). Plan view b) Elevation view at A and C c) Elevation view at 1and 3 d) Elevation view at B and 2. All dimension are in mm. 20

Figure 2.8: Foundation skid connected to the strong floor a) Foundation skid at elevation -2 5/16'' b) Anchor bolt connected to the strong floor c) Elevation view of the connection. All units are in inches (1 inch = 25.4 mm)..... 22

Figure 2.9: Foundation skid at elevation 0.0..... 23

Figure 2.10: Foundation skid elevation. All unites are in inches (1 inch = 25.4 mm).... 23

Figure 2.11: Dimensions of the shaft mounts a) 3-D b) Elevation c) Cross section [15] All unites are in inches (1 inch = 25.4 mm)..... 24

Figure 2.12: Dimensions of the steel shafts a) 3D b) Cross section [15] All unites are in inches (1 inch = 25.4 mm) 25

Figure 2.13: Dimensions of the ball bearing a) 3-D view b) Plan c) Cross section d) Elevation [15] All unites are in inches (1 inch = 25.4 mm)..... 26

Figure 2.14: Moment frame end-plate connection detail a) Elevation b) Plan All unites are in inches (1 inch = 25.4 mm) 27

Figure 2.15: Braced frame end-plate connection detail a) Elevation b) Plan All unites are in inches (1 inch = 25.4 mm) 27

Figure 2.16: Construction of the building foundation a) Skid assembly b) Arrangement of the shaft mount supports 28

Figure 2.17: Assembly of columns and end plates 28

Figure 2.18: Detail of diagonal braces a) Tie down ring b) Turn buckles c) Ring-end plate connection d) Brace assembly..... 29

Figure 2.19: Moment frame building 30
Figure 2.20: Braced frame building 30
Figure 3.1: Braced frame FE models a) SAP2000 b) ABAQUS 33
Figure 3.2: Boundary condition a) SAP2000 b) ABAQUS 35
Figure 3.3: Common three-dimensional elements 36
Figure 3.4: Mesh convergence result for the moment frame using SAP2000 38
Figure 3.5: Mesh convergence result for the braced frame using SAP2000 39
Figure 3.6: Mesh convergence study results for the moment frame using ABAQUS 41
Figure 3.7: Processing time for the moment frame FE model 42
Figure 3.8: First six frequencies result for the braced frame versus seed size using C3D20R 43
Figure 3.9: Small gap between floor plate and column end-plate connection 45
Figure 3.10: Idealization of the column end-plate a) No end-plate b) Fully bonded end-plate 46
Figure 3.11: Free body diagram a) Column without end-plate b) Column with end-plate 47
Figure 3.12: Brace connection 48
Figure 3.13: Equivalent brace member stiffness using a system springs in series 48
Figure 3.14: Cantilever beam assumption 49
Figure 3.15: Location of brace connection in ABAQUS model 51
Figure 4.1: Procedure of applying PR method 58
Figure 4.2: Procedure of applying FDD method 62
Figure 4.3: a) Tri-axial wireless accelerometer b) Wireless router 65
Figure 4.4: Rubber hammer on the scale 66
Figure 4.5: Mounted sensors 66
Figure 4.6: Monitoring station 67
Figure 4.7: Sensor setup 1 a) Plan view b) Elevation view 68
Figure 4.8: Sensor setup 2: a) Plan view b) Elevation 69

Figure 4.9: Excitation configurations a) Type 1 b) Type 2 c) Type 3 d) Type 4 70
Figure 4.10: Flowchart for finding the optimum block size and model order values 74
Figure 4.11: Model order parametric study for test 2 76
Figure 4.12: Parametric study of block size for test 2 77
Figure 4.13: Parametric study of model order for test 5 78
Figure 4.14: Parametric study of block size for test 5 78
Figure 4.15: MAC matrix plots a) Test 1 b) Test 2 c) Test 3 d) Test 4 e) Test 5 f) Test 6 81
Figure 5.1: Procedure of damage detection using model updating 98
Figure 5.2: Changes in Young's modulus using 1st response combination [%] 102
Figure 5.3: Changes in Young's modulus using 2nd response combination [%] 103
Figure 5.4: Changes in Young's modulus using 3rd response combination [%] 104
Figure 5.5: Changes in Young's modulus using 4th response combination [%] 105
Figure 5.6: Changes in Young's modulus using 1st response combination [%] 108
Figure 5.7: Changes in Young's modulus using 2nd response combination [%] 109
Figure 5.8: Changes in Young's modulus using 3rd response combination [%] 110
Figure 5.9: Changes in Young's modulus using 4th response combination [%] 111
Figure 5.10: Damage conditions a) MF b) BF case 1 c) BF case 2 d) BF case 3 113
Figure 5.11: Parameter change in Young's modulus for damage detection of MF 116
Figure 5.12: Parameter change in Young's modulus for damage detection of BF case 1 119
Figure 5.13: Parameter change in Young's modulus for damage detection of BF case 2 120
Figure 5.14: Parameter change in Young's modulus for damage detection of BF case 3 121

List of Symbols

S_L	Dimension scale factor
S_V	Velocity scale factor
S_A	Area scale factor
S_I	Moment of inertia scale factor
S_E	Modulus of elasticity scale factor
L_{model}	Dimension of scale model
$L_{Prototype}$	Dimension of prototype model
V_{model}	Velocity of scale model
$V_{prototype}$	Velocity of prototype model
f_{model}	Force of scale model
$f_{prototype}$	Force of prototype model
I	Moment of inertia
TYP	Typical
K	Stiffness
Δ	Deflection
$R(\tau)$	Correlation function
E	Expected value
$y(n)$	System response
$x(n)$	System input

$\boldsymbol{\varphi_d}$	Discrete eigenvector
$\boldsymbol{\mu}$	Discrete time pole
$\boldsymbol{\lambda_n}$	Pole
$\boldsymbol{\omega_n}$	Undamped natural frequency [Hz]
$\boldsymbol{\omega_d}$	Damped natural frequency [Hz]
$\mathbf{G_y(f)}$	Power spectra density matrix
$\boldsymbol{g_n^2(f)}$	Diagonal elements of the power spectra density matrix
$\mathbf{f_s}$	Sampling frequency
$\mathbf{T_{req}}$	Required time
$\boldsymbol{\zeta}$	Damping ratio
$\boldsymbol{\psi}$	Mode shape vector
$\mathbf{R}$	Response
$\mathbf{S}$	Sensitivity matrix
$\mathbf{P}$	Parameter
$\mathbf{G}$	Gain matrix
$\boldsymbol{C_R}$	Weighting coefficients of response
$\boldsymbol{C_p}$	Weighting coefficients of parameter

1 Introduction

1.1 Overview

Structural condition assessment is an important step in maintenance and operation of civil infrastructures. Structural damage can be caused by various sources such as ageing, material deterioration and natural disaster. Visual inspection is the most common method to assess structural damage. However, with increasing complexity of civil structures, visual inspection can be very expensive and time-consuming. Also, the damage that results in the structural changes may not be visible. Therefore, visual inspection methods are often inadequate for detecting such damage. To complement visual inspection, non-destructive testing methods such as acoustic, ultrasonic, magnetic field, radiography and thermal field methods were developed in the late 1980s [1]. However, successful application of these methods requires prior knowledge of damage location, and in most cases, the damage location needs to be accessible for inspection, which makes these methods inadequate for comprehensive damage identification of civil infrastructure.

Vibration-based damage detection methods have been introduced to the civil engineering community for more accurate and efficient damage identification. These methods incorporate Operation Modal Analysis (OMA) and model updating technique. The current structural dynamic characteristics such as natural frequency, mode shape, and damping ratio can be extracted from the vibration test using OMA [2]. Model updating uses the physical model response for calibrating the finite element model [3], which means if a physical model is altered through experiencing damage, it would be identified in the updating process.

OMA and finite element model updating began to draw attention in the civil engineering community in the early 1990s. These methods have been well established in the academic field, and there has been a growing interest in the practical engineering field in recent years. To successfully identify the structural damage, it involves the development of an accurate FE model and the selection of efficient responses for the model updating procedure. However, little literature is available for investigating the efficiency and practical limitations of applications of vibration-based damage identification using model updating.

In this thesis, four topics are addressed to investigate the efficiency and practical limitation of vibration-based damage identification using model updating:

a) A physical model of a seven-story scale building is designed and constructed (Chapter 2). The proper condition of similarity between prototype and scale model is established using similitude law, and necessary modifications are made.
b) Different FE models of the scale building are developed using SAP2000 and ABAQUS in Chapter 3. Mesh and element convergence studies are conducted for developing the accurate FE models.
c) The effects of vibration test parameters on OMA results are investigated in Chapter 4. To maximize the number of valuable extracted mode shapes from OMA, a procedure of parametric study for finding the optimal parameters is developed.
d) Different levels of structural damage can result in different change in structural dynamic characteristics. Using the OMA results from Chapter 4, model updating was used to identify different damage scenarios in Chapter 5.

The relevant FEMtools command script for Chapter 4 and Chapter 5 can be found in Appendix A.

1.2 Thesis Structure

This thesis has been prepared following the traditional thesis format; four main sections are included as Chapter 2, 3, 4 and 5. Introductory and concluding chapters are also included.

Chapter 2 presents the development of the scale building model. This chapter provides details of the design and construction process.

Chapter 3 presents the development of the finite element models. The mesh and element convergence studies are conducted and the modelling assumptions are discussed.

Chapter 4 presents the results of OMA from different vibration test setups.

A practical application of vibration-based damage identification using model updating on the scale building is presented in Chapter 5. Different damage scenarios are investigated.

1.3 Contribution of the Candidate

Dr. Kaveh Arjomandi proposed investigation of the efficiency and practical limitation of structural damage identification using model updating and provided valuable guidance and mentorship throughout the duration of this work. The candidate designed and implemented the experimental and analysis procedures under the supervision of Dr Arjomandi. Based on the proposed idea, the candidate developed the analytical model, conducted the parametric studies, analysed the data, and prepared this thesis.

2 Development of Small-Scale Building Model

2.1 Introduction

Numerical models are the most common tools for engineers in simulating the behaviour of structures. In the development of numerical models, several assumptions must be made which can cause discrepancies between the actual structural behaviour and the response estimated by the numerical models. Hence, numerical models are often calibrated against the test results from actual structures. However, civil engineers often work with large structures which makes performing full-scale tests of actual structures challenging. Hence, it is common to use scale models for better understanding of the actual behaviour of large structure as well as verification of numerical models.

Physical scale models also known as structural models have played a significant role in the advancement of structural engineering. It is helpful to develop a reduced scale model (small-scale model) when it is difficult to perform a test on a prototype structure, as well as when calculations and computer simulation are not completely reliable [4]. Small-scale modelling has been applied to different types of structures in the past. An example is using scale models to evaluate the structural response to seismic load. For example, a scale model of a 2940 meter long two-span suspension bridge with a scale factor of 1:40 was constructed at Tongji University, China [5]. This model was used to investigate the seismic performance of the bridge (Figure 2.1). In this case study, additional masses were used to create realistic dead loads and internal forces. Also, the seismic responses of the suspension bridge using eight different seismic structural systems (different damping ratio) were compared.



Figure 2.1: 1:40 Suspension Bridge, Tongji University, China [5]

A study for simulating the behaviour of a reinforced concrete structure that collapsed during the Izmit earthquake was conducted on a 1:3 scale model (Figure 2.2) using the scale model that was built in IZIIS Laboratory, Skopje, Macedonia [6]. Two different retrofitting techniques were compared for improving the seismic response of the typical structural system. The experiments discovered that the structural behaviour under seismic excitation can be improved significantly by using carbon fibre reinforced polymer strips to strengthen the infill wall.



Figure 2.2: 1:3 Reinforced Concrete Frame, IZIIS Laboratory, Macedonia [6]

A 1:4 scale autoclaved aerated concrete (AAC) confined masonry building model was constructed in Bovec, Slovenia [7]. The purpose of this study was to investigate the response of AAC confined masonry buildings to seismic ground motion. In this study, the important role of vertical tie columns for AAC masonry was discovered and the test result concluded the structural behaviour factor from Eurocode 8 for confined masonry buildings is adequate for AAC masonry buildings.



Figure 2.3: 1:4 AAC Building, Bovec, Slovenia [7]

The 1:110 scale full aeroelastic model and 1:24 scale sectional models of the Lion's Gate Bridge were constructed at the National Research Council of Canada in Ottawa [4]. A modification for using sidewalks to extend the three-lane roadway was proposed. The model was used to determine the aerodynamic characteristic of the present bridge and the bridge with the proposed change. The full aeroelastic model was tested using a 9x9m wind tunnel to simulate turbulent flow and smooth flow. The results showed the behaviour of two models are in good agreement in smooth flow. Excellent correlation was found between experimental and analytical results for the mode shapes.

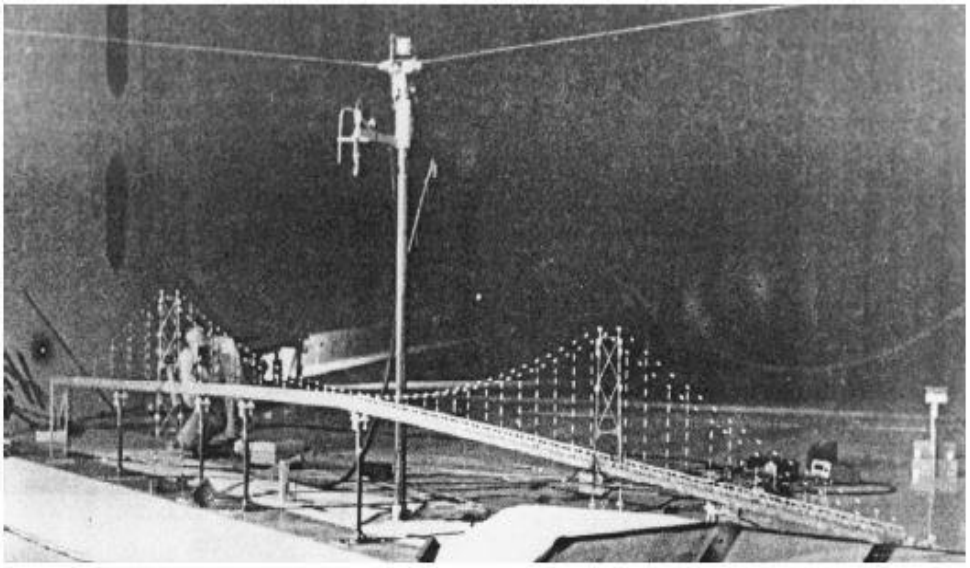


Figure 2.4: 1:110 Lions Gate, Ottawa, Canada [4]

Table 2.1 summarizes some previous experimental scale model studies, including, scale factors, structure types and materials that were used.

Table 2.1: Summary of previous studies

Structure	Scale Factor	Model material	Type of Studies
Suspension bridge [5]	1:40	Microconcrete pylon, steel box deck	Seismic response
Reinforce concrete building [6]	1:3	Reinforced concrete	Seismic response
AAC masonry building [7]	1:4	AAC masonry	Seismic response
Cable-stayed bridge [8]	1:33.3	Steel and aluminum sheet	Aerodynamic response
Masonry shear wall [9]	1:3	Masonry	Shear and flexural strength
Earthquake-resistant building [10]	1:5	Reinforced microconcrete	Seismic response
Long curved bridge [11]	1:30	Reinforced microconcrete	Seismic response
Twin suspension bridge [12]	1:211	Aluminum, piano wire	Aerodynamic response

In this chapter, the procedure that was used in designing and constructing a seven-story aluminum small-scale building model is presented. The physical modelling theories that were used for designing the scale model, including the model's classification, Buckingham's Pi theorem and similitude law are also briefly explained.

2.2 Physical Modeling Theory

2.2.1 Classification of Models

Physical models fall into different categories, each type able to simulate a specific response, capacity, and dynamic properties. Hence, it is important to define the purpose of the model and expected outcomes. Structural models can be classified into direct and indirect models [13]:

- Indirect Model: The model does not resemble the prototype directly; the main purpose of this model is to obtain the influence diagrams for reactions. In this model, the applied load does not correspond to the load on the prototype. This is known as a special form of the elastic model. Due to the efficiency of modern computers, this model is not popular nowadays.
- Direct Model: The geometric form of this model resembles the prototype and the applied loads correspond to the loads on the prototype. An elastic model can also be a direct model.

Structural models can also be categorized into the following four classes:

- Elastic Model: The geometric form of this type of model resembles the prototype directly, and is made of homogeneous, elastic materials that do not need to

replicate the material properties of the prototype. This model is not capable of predicting any inelastic behaviour such as post cracking and post yield behaviour; only elastic behaviour can be captured using this model. The common material used for elastic models are plastic and wood.

- Strength Model: This model is also a direct model that not only is geometrically similar to the prototype but also uses similar materials as the prototype. This type of model is expected to predict the strength of the prototype. It is commonly made for concrete, steel and timber structures.
- Wind Effects Model: This model can be categorized in two classifications: Rigid model, which is made for measuring the wind pressures on the structure; and Aeroelastic model, which is made for measuring the dynamic interaction of the structure with the wind.
- Dynamic Model: These models are made for vibration and dynamic loading studies, such as earthquake effects and aeroelastic effects as well as impact effects.

Physical models can also be classified according to their use as, an instructional, research, and design model. Instructional models are simple models that are often made for demonstration; Research models are made for structure theories study; and design models are similar to the other two types of models. However, the accuracy of these models is based on the requirements.

2.2.2 Buckingham's Pi Theorem

Buckingham's Pi theorem is an important theory of dimensional analysis; it states that a set of dimensionless pi groups can be determined from any dimensionally homogeneous equation of physical quantities. Generally, the procedure for forming the pi groups

depends on personal preference and experience. The following procedure is a general guideline for the formation of pi terms [4]:

a) To determine all n variables involved such as stress, density, modulus of elasticity, etc.
b) To determine the fundamental measures (r) for expressing each variable of the problem that are dimensionally independent such as force, length and time.
c) To isolate the parameters of interest into one Pi group, $\boldsymbol{\pi}_i = n - r$, and group them in order to have dimensionless terms.

In order to achieve similarity, the dimensionless Pi terms of the model must be set to be equal to the corresponding prototype pi term.

2.2.3 Similitude Law

Similitude law is essential to establish the proper condition of similarity between the prototype and scale model. The three main categories of similarity conditions are as follows [4]:

d) Geometric similarity: The prototype and scale model have the same ratio of the corresponding dimensions. This means the scale model is geometrically similar to the prototype. The following equation shows the geometric relationship between scale model and prototype which is the dimension scale factor S_L:

$$\frac{L_{Prototype}}{L_{model}} = S_L \tag{2.1}$$

e) Kinematic similarity: It represents the similarity of motion between the model and prototype. The following equation shows the kinematic relationship between scale model and prototype which is the scale factor of velocity S_V:

$$\frac{V_{prototype}}{V_{model}} = S_V \tag{2.2}$$

f) Dynamic similarity: The magnitudes of forces of a dynamically similar system have the same ratio at correspondingly similar points in the prototype and model. In order to achieve dynamic similarity, geometric and kinematic similarity are required. The following equation shows the dynamic similarity relationship between the scale model and prototype which is the force ratio S_f:

$$\frac{f_{prototype}}{f_{model}} = S_f \tag{2.3}$$

2.3 Case-study Building

A preliminary design of a full-scale seven-story building was conducted following the requirements of the 2010 National Building Code of Canada [14]. The full-scale building was designed as a residential steel structure in Fredericton, New Brunswick, Canada. Fredericton wind and seismic design loads, and the related load combinations were considered. The prototype building height is 26.6 m with an individual story height of 3.8 m. The plan area of the building is considered to be 7.6 m by 7.6 m. The building's height and foot print were chosen to create a relatively slender structure that is dynamically sensitive. Figure 2.5.a shows the full-scale building dimensions.

The footprint of the small-scale model was selected according to the available area in the Civil Engineering high-bay structural laboratory at the University of New Brunswick. The available area resulted in a geometry scale S_L of 12. T6061 aluminum was used to build the scale model. The model has a plan area 0.63 m x 0.63 m and 2.2 m high (Figure 2.5.b).

The small-scale building is designed to be adjustable as a braced or moment resisting frame. The building was constructed on a custom-build shake table which can be excited manually or by using an actuator.

The small-scale model was designed as an elastic model, however adequate adjustments were made in the member sections according to the section availability.

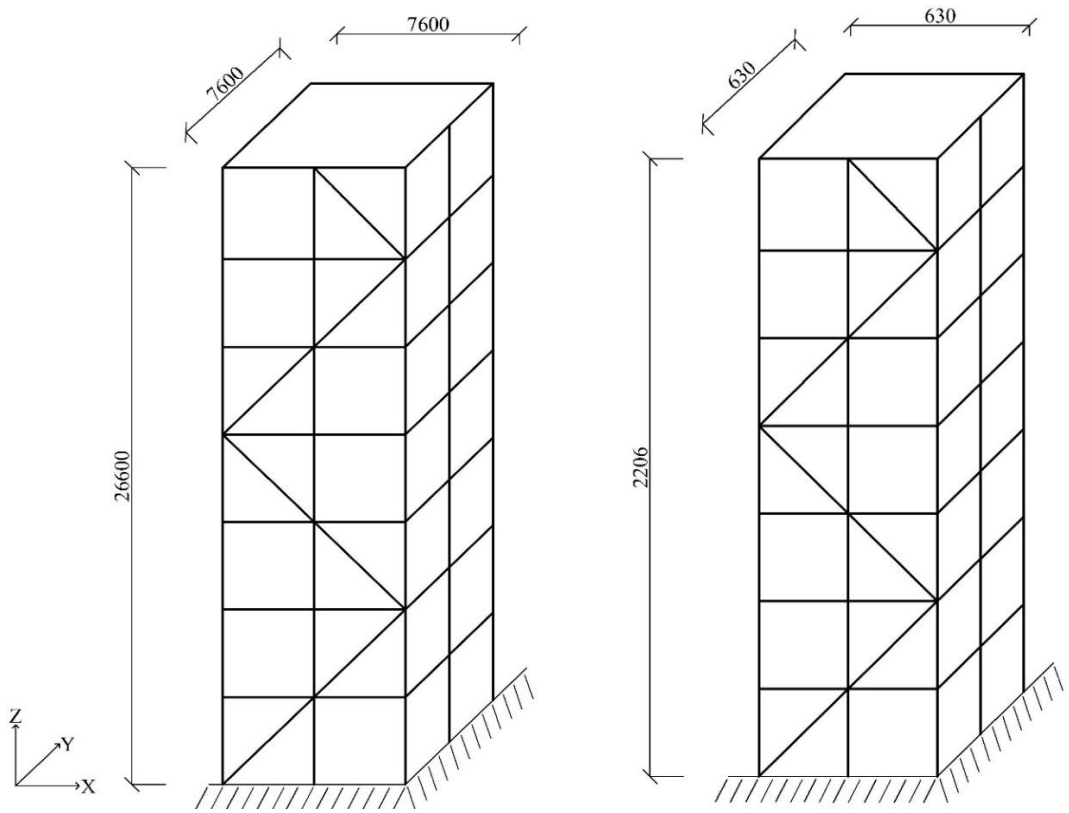


Figure 2.5: Case study building a) Full scale b) Small Scale. All dimensions are in mm.

2.3.1 Scale Factor

Scale factors are applied to prototype models to fulfill the geometric and kinematic similitude requirements [4]. The dimension scale factor S_L can be determined using Equation (2.1). Using the linear dimension scale factor, the area scale and moment of inertia scale factors can be calculated from [4]:

$$S_A = S_L^2 \tag{2.4}$$

$$S_I = S_L^4 \tag{2.5}$$

As the material of the prototype structure (steel) is different from the scale model (T6061 Aluminum), a scale factor for the modulus of elasticity is considered as:

$$S_E = \frac{E_P}{E_M} \tag{2.6}$$

where, E_P is the modulus of elasticity of the prototype, E_M is the modulus of elasticity of the model.

Table 2.2 provides a summary of the scale model scale factors

Table 2.2: Summary of scale factors

Linear Dimension [S_L]	Area [S_A]	Moment of Inertia [S_I]	Modulus of Elasticity [S_E]
12	144	20736	2.86

2.3.2 Section Summary

The Cross-section area and moment of inertia about the strong axis of the prototype member were used for the design of scale model beam and column sections. To consider the flexural rigidity of the flexural members, first, the moment of inertia of the prototype member was converted from steel to an equivalent moment of inertia of aluminum by using the following equation:

$$E_S I_S = E_A I_A \tag{2.7}$$

where, E is the Young's modulus and I is the moment of inertia. To calculate the moment of inertia for the scale model, the following equation can be formed:

$$I_M = \frac{E_S}{E_A}\frac{I_S}{S_I} = S_E \frac{I_S}{S_I} \tag{2.8}$$

where, I_M is the moment inertia of the model and I_S is the moment inertia of the prototype.

The area scale factor (S_A) was used to calculate the brace section sizes.

Due to availability and constructability of the sections, columns were designed as square sections that were calculated using the following equation:

$$a = \sqrt[4]{12 I_M} \tag{2.9}$$

This assumption introduces an error in the simulation between the scale model and the prototype. However, this error is acceptable for the purpose of this study as it is aiming at investigating damage detection methods and not simulating the exact behaviour of the prototype structure.

Table 2.3 provides the summary of the prototype and small-scale model structural members. Table 2.3 includes sections calculated as per theory of similitude law. However, due to the constructability and availability of the material, adjustments were made to the model. Also, the density and weight similarity were not considered for designing the scale model building. This is considering that the model will be used for conducting vibration tests to validate the numerical models and to assess the efficiency of model updating methods for damage detection application. To simplify the construction process, a square plate was used for each story instead of using interior, and exterior beam members and horizontal brace members. Also, an adjustment was made on the column section based on material availability.

A turnbuckle mechanism is used as the brace members. The braced frame (BF) structure (Figure 2.6.a) for this research is created by attaching braces to the moment-resisting frame (Figure 2.6.b) where the connections are moment-resisting connection. The general braced frame where all the connections are pinned (Figure 2.6.c). To compare the stiffness difference, the sections of the full-scale building were used to model each frame in SAP2000, an assumption of 15 kN point load was assigned at left top corner. The displacement results are shown in Figure 2.6. d to Figure 2.6. f.

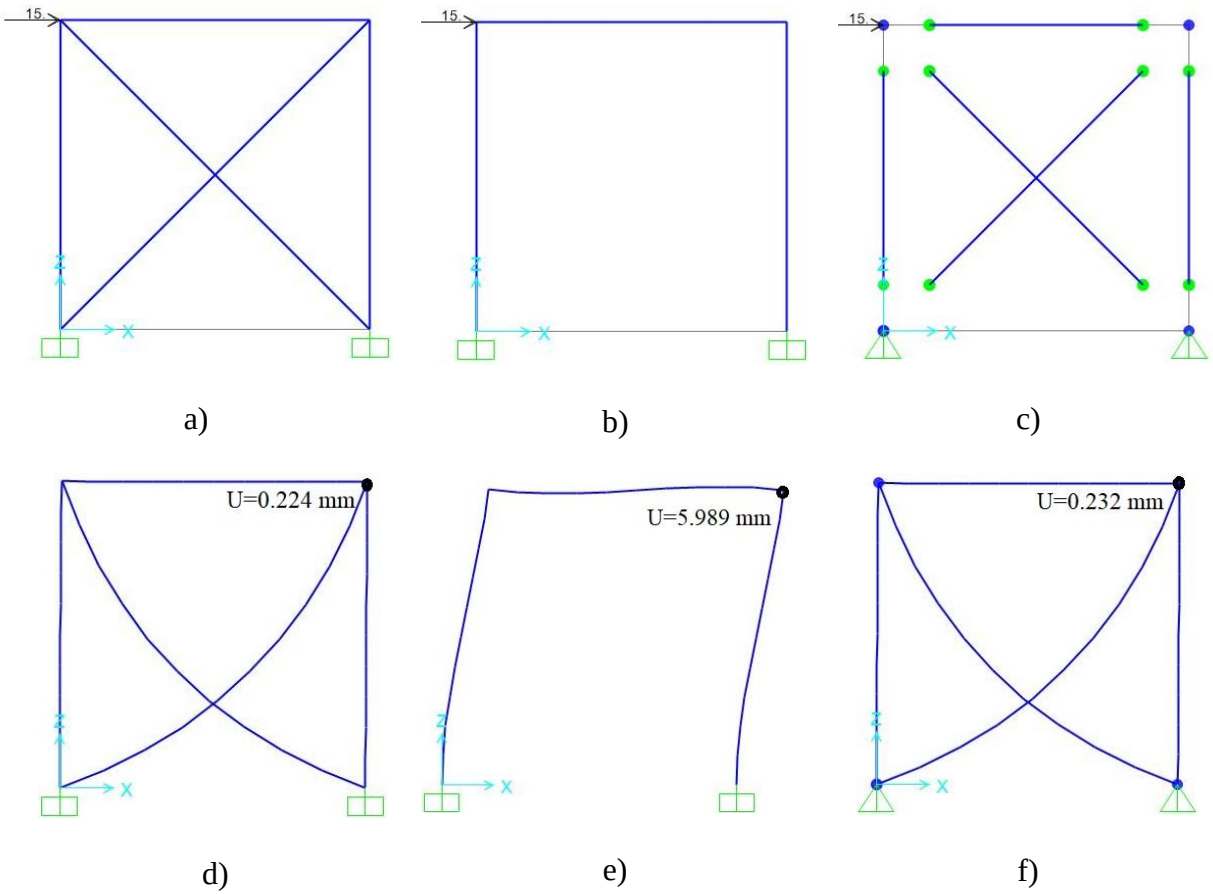


Figure 2.6: a) Moment-resisting frame with brace members b) Moment-resisting frame c) Braced frame d) Displacement of frame shown in Figure 2.6.a e) Displacement of frame shown in Figure 2.6.b f) Displacement of frame shown in Figure 2.6.c

The stiffness of frame shown in Figure 2.6. a to Figure 2.6. c where calculated to be 66.96 kN/mm, 2.50 kN/mm, and 64.60 kN/mm respectively, using:

$$K = \frac{F}{\Delta} \tag{2.10}$$

where, F is force, Δ is the displacement.

The stiffness contribution ratio of moment-resisting frame (SCRMF) system shown in Figure 2.6.a was calculated to be 4%, using:

$$SCRMF = \frac{K_1 - K_3}{K_1} * 100\% \quad (2.11)$$

where, K_1 is the stiffness of frame shown in Figure 2.6.a, K_3 is the stiffness of frame shown in Figure 2.6.c

The stiffness contribution ratio of braced mechanism (SCRBF) shown in Figure 2.6.a was calculated to be 96%, using:

$$SCRBF = \frac{K_1 - K_2}{K_1} * 100\% \quad (2.12)$$

where, K_2 is the stiffness of frame shown in Figure2.6.b.

The contribution of the moment-resisting system is significantly smaller than the contribution of the braced mechanism. Therefore, the stiffness of the moment-resisting frame with brace members is considered approximately the same as the braced frame with pin connections.

Table 2.3: Summary of the prototype and scale model sections

Structural Member	Prototype	Small Scale (As calculated) [mm]	Small Scale (As built) [mm]	Small Scale (As built) [inch]
Column		Solid square, Aluminum		
Story 1-3	W250x167	27x27	31.75x31.75	1.25
Story 4-7	W200x100	21x21	19.05x19.05	0.75
Interior Beam		Solid square, Aluminum	Plate (Approximation), Aluminum	
Story 1-4	HS254x254x13	21x21	630x630x6.35	30x30x0.25
Story 5-7	HSS228.6x228.6x15.9	20x20	630x630x6.35	30x30x0.25
Exterior Beam Moment Frame		Solid square, Aluminum	Plate (Approximation), Aluminum	
Story 1-4	HSS254x203.2x12.7	20x20	630x630x6.35	30x30x0.25
Story 5-7	HS203x152x6.4	14x14	630x630x6.35	30x30x0.25
Exterior Beam Braced Frame		Solid square, Aluminum	Plate (Approximation), Aluminum	
Story 1-4	HSS177.8x177.8x7.9	14x14	630x630x6.35	30x30x0.25
Story 5-7	HS178x178x6.4	14x14	630x630x6.35	30x30x0.25
Vertical Brace		Solid square, Aluminum	Round, Steel	
Story 1-7	HSS152.4x127x6.4	4.5x4.5	Turn Buckle	Turn Buckle
Horizontal Brace		Solid square, Aluminum		
Story 1-7	HSS127x127x4.8	3.8x3.8	N/A	N/A

2.3.3 Construction Details

The scale model dimensions are shown in Figure. 2.7.

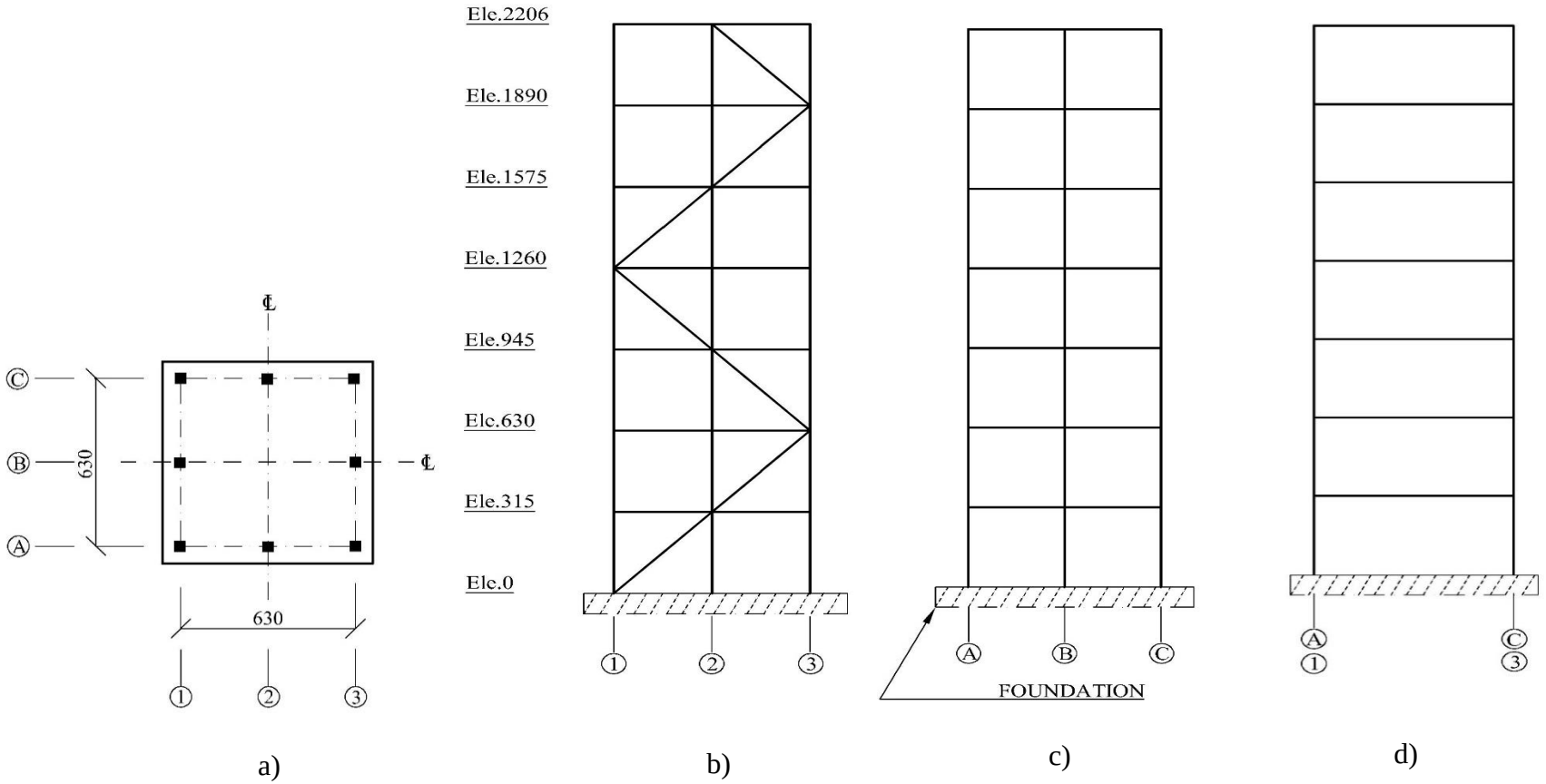
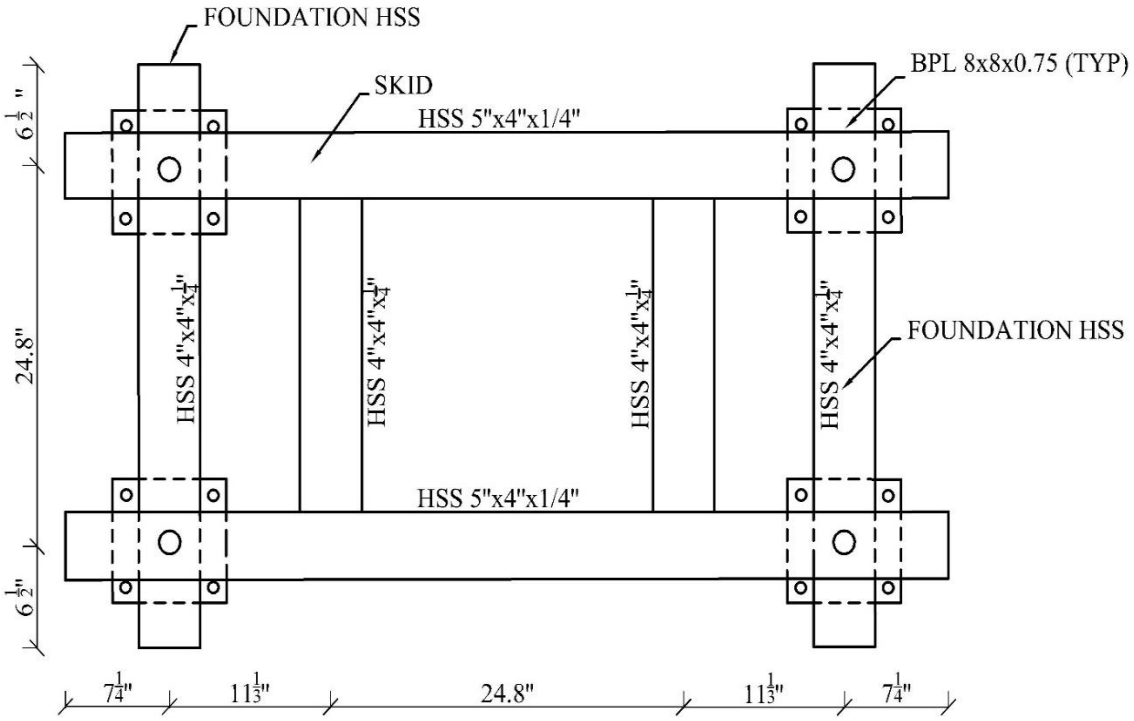
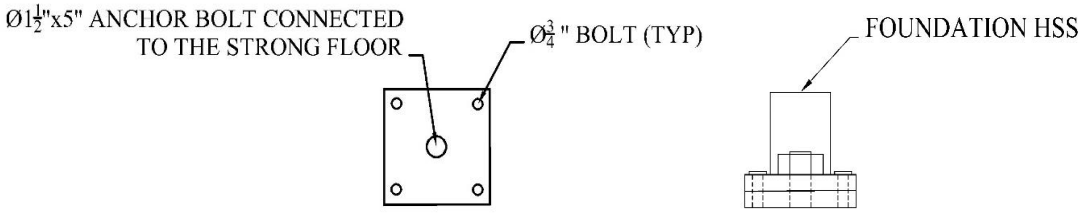


Figure 2.7: 1/12 scale model a). Plan view b) Elevation view at A and C c) Elevation view at 1and 3 d) Elevation view at B and 2. All dimension are in mm.

The foundation skid was designed to fit the layout of the structural lab strong floor anchor bolts pattern. Eight 0.75'' thick steel plates were designed to support the shake table linear motion shafts. These plates are attached to an HSS skid connected to the strong floor using anchor bolts (Figure 2.8). The steel plates are mounted to the top of the skid using eight steel plates at the bottom and four 3/8''x8'' threaded rods per plate (Figure 2.9). The shaft mounts shown in (Figure 2.11) are connected to the foundation plate, using the Rockwell c60 hardness steel shafts (shown in Figure 2.12) are installed on the mount, and the shaker system is completed with ball bearings that are shown in Figure 2.13. Ball bearings are connected to a floor plate that provides stability and uniform sliding feature. As per manufacture specs, ball bearings have 470lbs load capacity per bearing.



a)



b) c)

Figure 2.8: Foundation skid connected to the strong floor a) Foundation skid at elevation $-2\frac{5}{16}$'' b) Anchor bolt connected to the strong floor c) Elevation view of the connection. All units are in inches (1 inch = 25.4 mm).

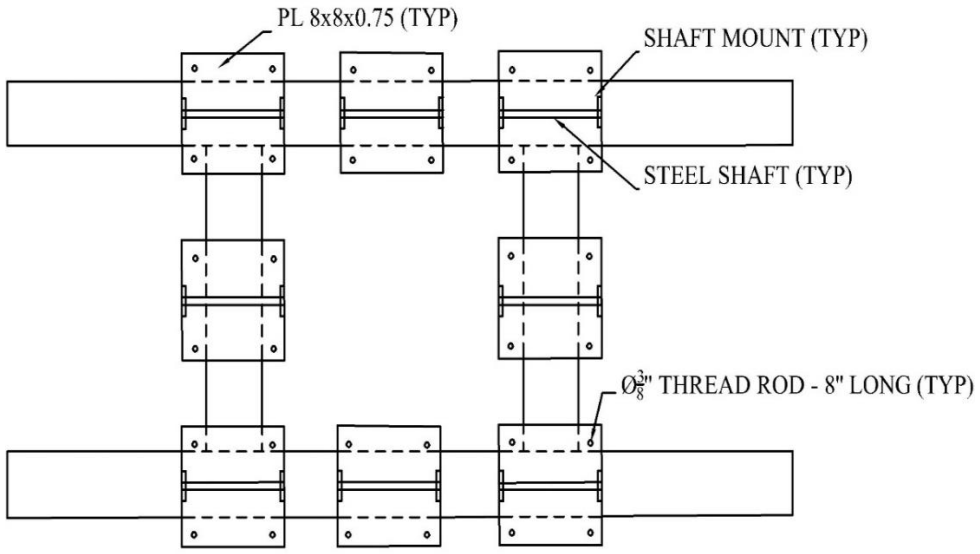


Figure 2.9: Foundation skid at elevation 0.0

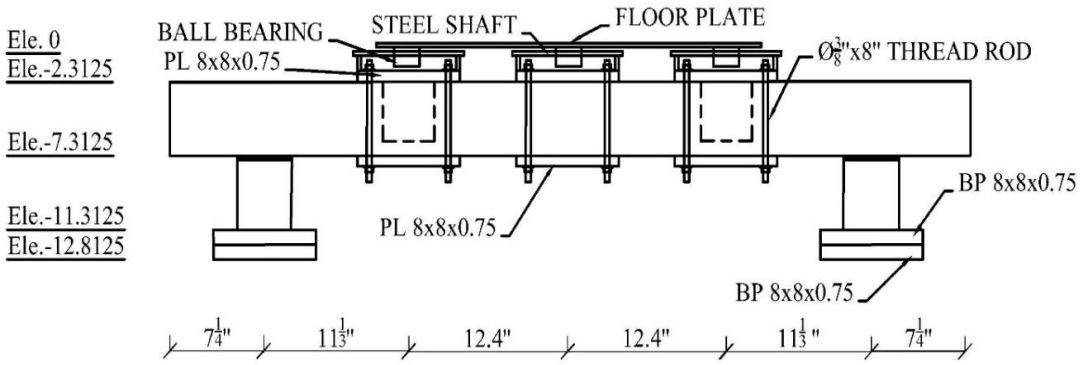
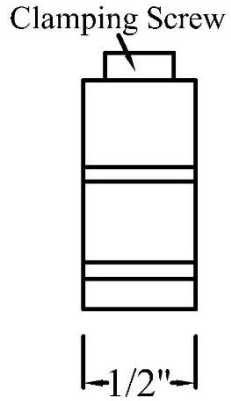


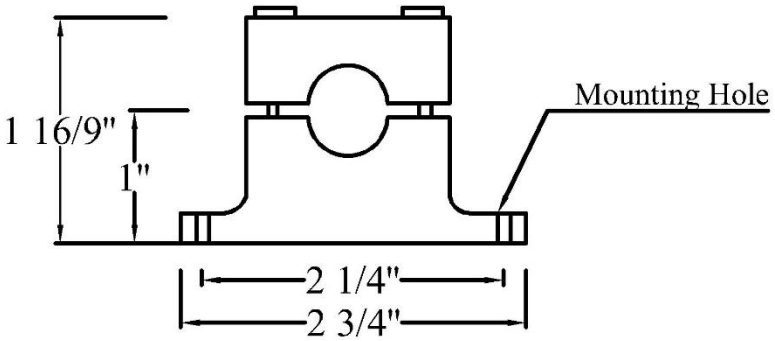
Figure 2.10: Foundation skid elevation. All unites are in inches (1 inch = 25.4 mm).



a)



b)



c)

Figure 2.11: Dimensions of the shaft mounts a) 3-D b) Elevation c) Cross section [15]
All unites are in inches (1 inch = 25.4 mm)



a) b)

Figure 2.12: Dimensions of the steel shafts a) 3D b) Cross section [15] All unites are in inches (1 inch = 25.4 mm)

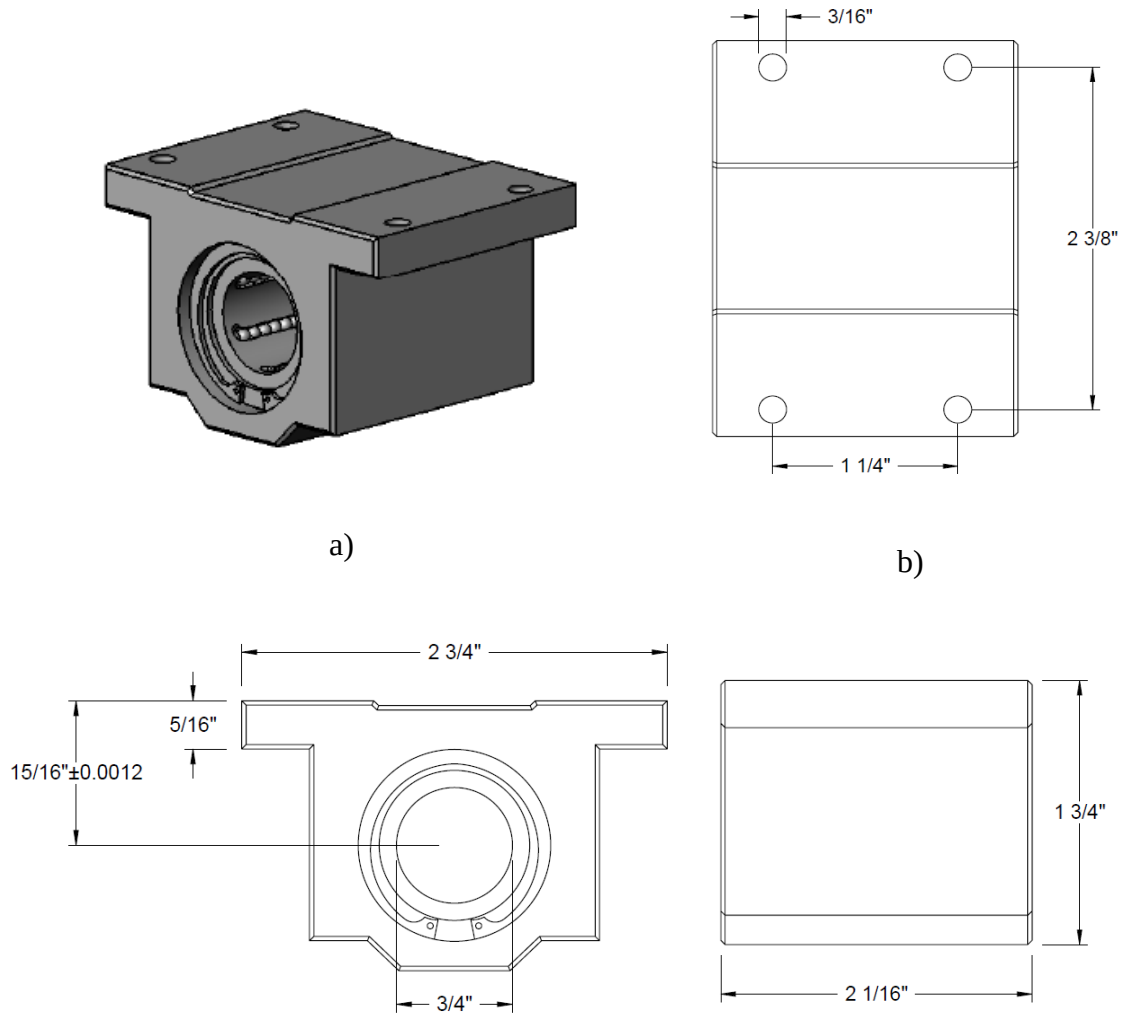
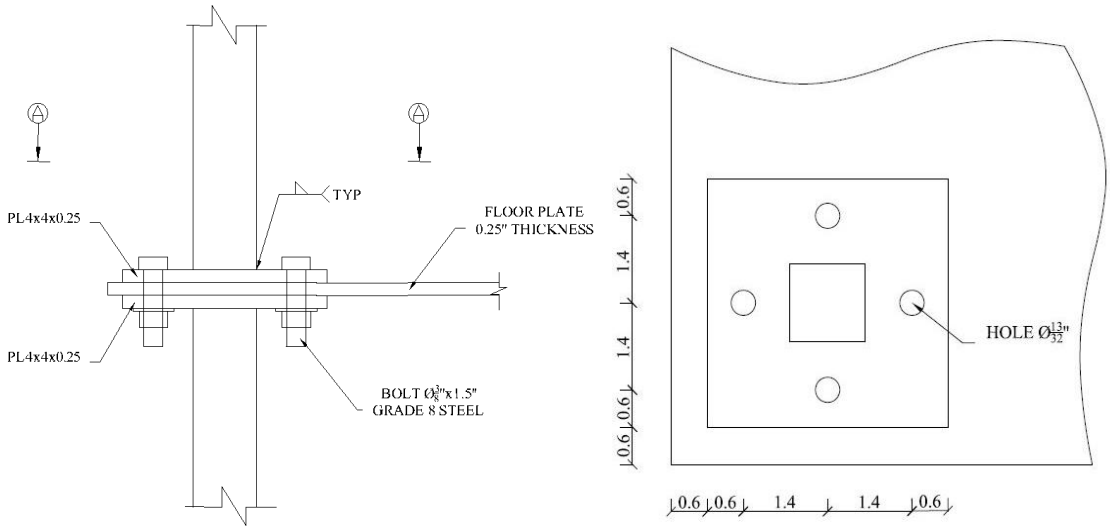


Figure 2.13: Dimensions of the ball bearing a) 3-D view b) Plan c) Cross section d) Elevation [15] All unites are in inches (1 inch = 25.4 mm)

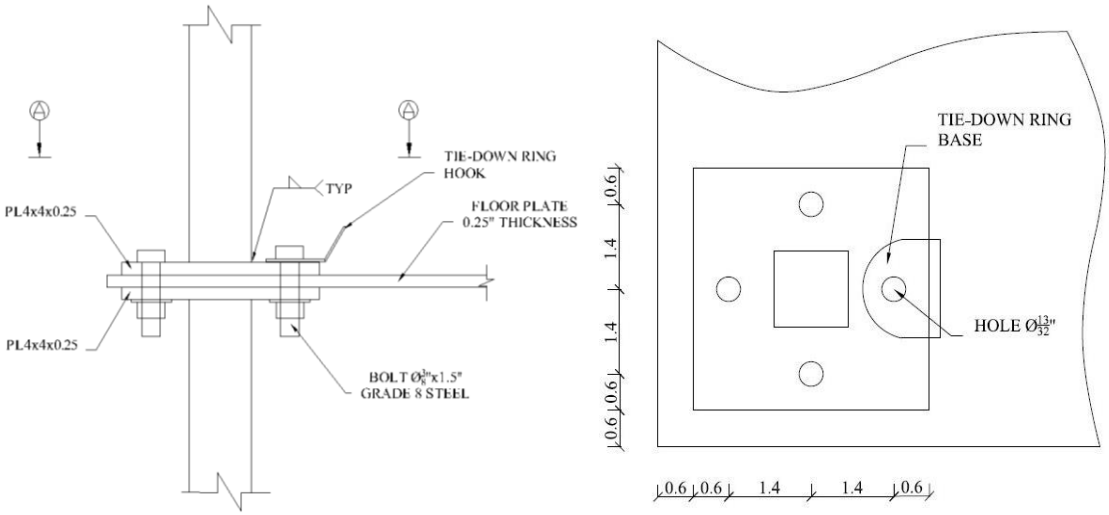
A 4’’x4’’ square aluminum plate was welded to the column ends, four 3/8’’ bolts were used to connect the columns end plates to the floor plates. Figure 2.14 shows the detail of column connections for moment frames.



a) b)

Figure 2.14: Moment frame end-plate connection detail a) Elevation b) Plan All unites are in inches (1 inch = 25.4 mm)

Figure 2.15 shows the tie down ring that used to contact a turn buckle braced system.



a) b)

Figure 2.15: Braced frame end-plate connection detail a) Elevation b) Plan All unites are in inches (1 inch = 25.4 mm)

Figure 2.16-2.20 show the as-built details of the scale model foundation.



a) b)

Figure 2.16: Construction of the building foundation a) Skid assembly b) Arrangement of the shaft mount supports



Figure 2.17: Assembly of columns and end plates



a) b)



c) d)

Figure 2.18: Detail of diagonal braces a) Tie down ring b) Turn buckles c) Ring-end plate connection d) Brace assembly



Figure 2.19: Moment frame building



Figure 2.20: Braced frame building

2.4 Summary

A seven-story aluminum scale model was designed and constructed on a custom-built shake table. The procedure of designing a small-scale model following the similitude law is presented. Necessary modifications were made to the member sections to account for constructability and availability of sections. This chapter also presents the construction details of the scale model.

3 Finite Element Model of the Scale Building

3.1 Introduction

Understanding the structural behaviour is a crucial step in the engineering design process. Engineers often use finite element numerical models for structural design and analysis. The Finite Element (FE) procedure simplifies the structure by transforming a complex structural system into an equivalent system of small elements. In the mathematical perspective, the equivalent of large systems with a large number of elements yield a large number of algebraic equations [16]. Solving such a large amount of equations used to be challenging, however, advancements in computing technologies have made the analysis of large complex FE models feasible.

Numerous commercial finite element analysis software are available. Some of the most common ones for structural engineers are SAP2000 [17], ETABS [18], MIDAS [19], ANSYS [20], and ABAQUS [21]. The fundamental algorithms used in these software are very similar. However, the built-in interface, specific analysis types and design package makes each more suitable for a specialty field. In this thesis, SAP2000 and ABAQUS were used for the development of finite element models.

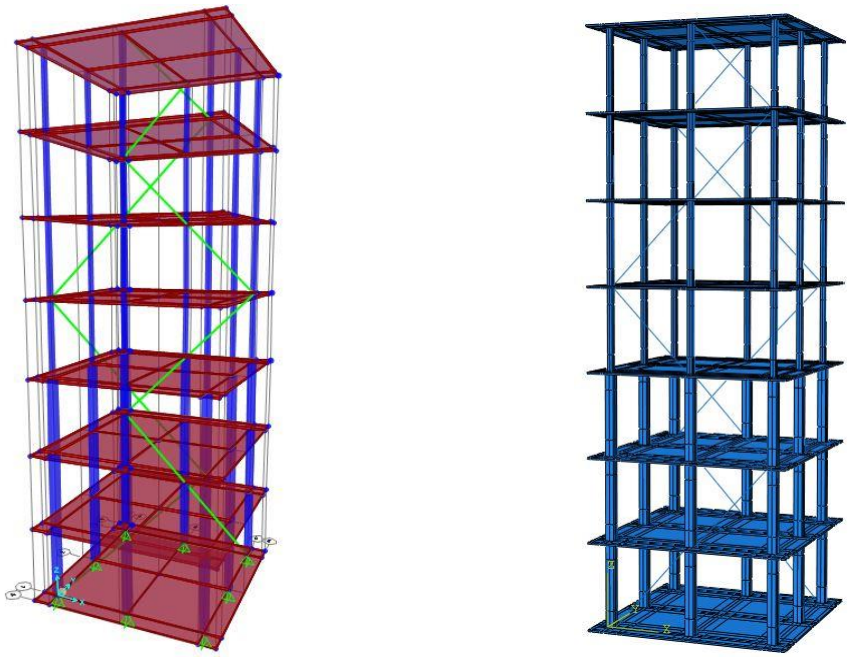
SAP2000 is one of the most common analysis and design software in structural engineering. It has integrated design codes that are necessary for practicing engineers. Furthermore, it allows for generating complex models and advanced analytical techniques applicable to a wide range of structures [17]. On the other hand, the finite element software package ABAQUS is one of the most powerful finite element analysis software packages that are available commercially. It benefits from various types of elements and

is capable of solving linear and nonlinear, coupled physics, structural acoustics, and thermal-electrical problems. ABAQUS supports complex materials modelling, contact behaviour, fracture, and failure conditions [21].

In this chapter, the finite element models of the scale model are developed using SAP2000 and ABAQUS. Details of the modeling procedure, mesh and element convergence studies are discussed in detail. FEMtools [22] is the software that is used to perform operational model analysis in the next chapter. Therefore, in order to create a compatible finite element model that is supported by FEMtools, certain adjustments are also made in the SAP2000 and ABAQUS models.

3.2 Modelling Assumptions

Figure 3.1 illustrates the FE models of the braced structure using SAP2000 and ABAQUS. Certain modelling assumptions must be made to create a finite element model of the small-scale building model that was introduced in the previous chapter. In this section, the assumptions regarding material, section members, boundary conditions, connections, and brace members are discussed in detail.



a) b)

Figure 3.1: Braced frame FE models a) SAP2000 b) ABAQUS

3.2.1 Material

The columns and floor plates of the small-scale model were made of T6061 Aluminum and the braces are made of steel. The modulus of elasticity of T6061 Aluminum is the same under tension and compression within the elastic range [23]. For this research the impact that is applied on the scale building would not lead to the inelastic stage, therefore, a constant value for the modulus of elasticity of aluminum is used in the finite element models. Table 3.1 summarizes the Modulus of elasticity, mass density and Poisson ratio that were used in FE models.

Table 3.1: Summary of material properties

	Modulus of Elasticity [kN/mm^2]	Weight Density [kN/mm^3]	Poisson's Ratio
Aluminum	70	2.70E-08	0.35
Steel Brace	200	8.03E-08	0.30

3.2.2 Member Cross-section

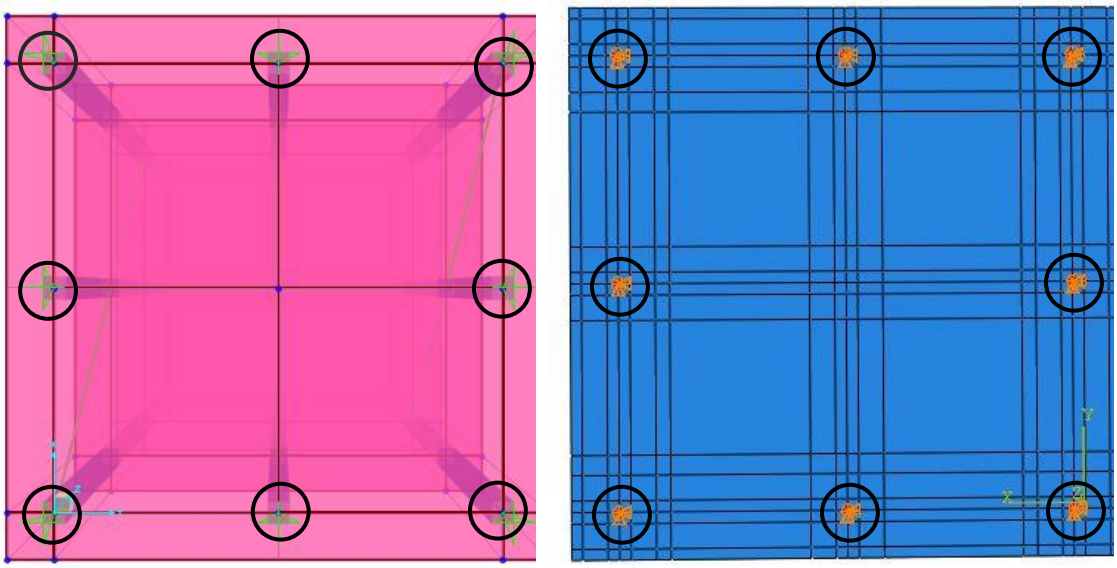
The dimensions of the member cross-sections are shown in Table 3.2.

Table 3.2: Summary of member cross-section. All dimension in mm.

	b	h	t	D
Storey 1-3 Column [mm]	31.75	31.75	N/A	N/A
Storey 4-7 Column [mm]	19.05	19.05	N/A	N/A
Floor Plate [mm]	762	762	6.35	N/A
Column End-Plate [mm]	101.6	101.6	6.35	N/A
Brace Diameter [mm]	N/A	N/A	N/A	4.8

3.2.3 Boundary Condition

The physical model was built on a shaker table. In this model, the supports are located at the column locations. In the finite element models, joint restraints were used to assign pin support conditions to the bottom of the first-floor plate. Pin supports restrain the translational movements and allow for rotational movements. Figure 3.2 shows the location of supports in SAP2000 and ABAQUS models.



a) b)

Figure 3.2: Boundary condition a) SAP2000 b) ABAQUS

3.2.4 Assembling of Elements

SAP2000 was created as a single model. Since the column connection plates were not modelled in SAP2000, to keep the overall height the same as the physical model, the additional height of 12.7 mm is added to the column grid lines for each story. The individual instance that defined in the previous section were used for assembling the ABAQUS model. As mentioned before the numerical model needs to be compatible with FEMtools. ABAQUS models with multiple instances are not supported by FEMtools [24]. Therefore, after assembling the model, all the instances were selected and then merged as one part. Fastener and welding details were neglected in both models.

3.3 Mesh and Element Convergence studies

Element type is an important factor for creating an accurate finite element model. In SAP2000, the floor plates were modelled using the shell elements, and linear beam

elements were used to model columns. ABAQUS provides a wide range of elements which includes standard elements, and explicit elements. In this project, columns, column connection plates, floor plates and braces are modelled using the 3D stress and truss element. In order to develop an adequate finite element model, a mesh and element convergence study was carried out in this section.

Figure 3.3 shows the examples of two common types of three-dimensional elements.

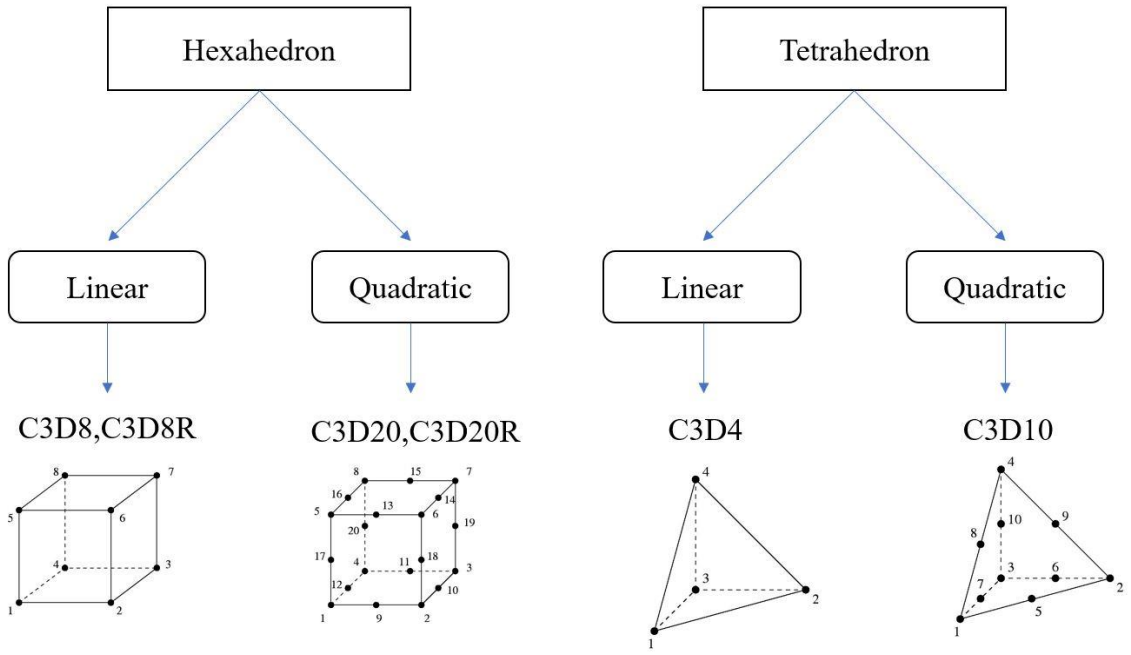


Figure 3.3: Common three-dimensional elements

In most situations, hexahedron elements are more accurate. Different types of elements also result in different processing time. The difference can be tremendous since the element with more nodes and higher element orders will form more algebraic equations. The accuracy of the numerical model also depends on the number of elements in the mesh. Often using more elements means a finer mesh and more accuracy. However, models having more elements take a longer time to process. In order to create the most efficient

numerical model, mesh and element convergence studies are essential [25]. These ensure the finite element analysis results are not affected by changing the mesh size. In this project, mesh convergence studies are performed to ensure the change in the calculated natural frequencies between two mesh refinements is less than five percent.

Table 3.3 summarizes the information about the finite elements that were used in SAP2000 and ABAQUS for this study. As can be seen, the C3D20R element is expected to provide the most accurate result, while the other elements are either too stiff or overall performance is not as good as C3D20R. Then comparing the ABAQUS model to the SAP2000 model using the 2D element, the frequency results of ABAQUS models are expected to be higher than SAP2000.

Table 3.3: Summary of finite elements

	Element Type	Dimensional	Element order	Advantage and limitation
SAP2000	shell	2D	linear	less process time reasonable for static analysis of panel member can't analyze the problem involving Z-direction
ABAQUS	C3D4	3D	linear	relatively stiff for structural calculation
	C3D8	3D	linear	relatively stiff for structural calculation
	C3D20	3D	quadratic	good for linear elastic analysis stiff in bending
	C3D20R	3D	quadratic	perform well for plastic behaviour perform well in bending

For this study, beam and truss members are used for modelling FE models, and the purpose of FEA for this study is to obtain the modal parameters.

3.3.1 SAP2000

The floor shell element mesh size was the studied mesh parameter in SAP2000. Using the area automatic mesh, a maximum mesh size of 120 mm was used for the first trial; the mesh size was decreased for other trials. A minimum seed size of 10 mm was considered. Figure 3.4 and Figure 3.5 show the mesh convergence result of the first three frequencies for the moment frame and braced frame respectively.

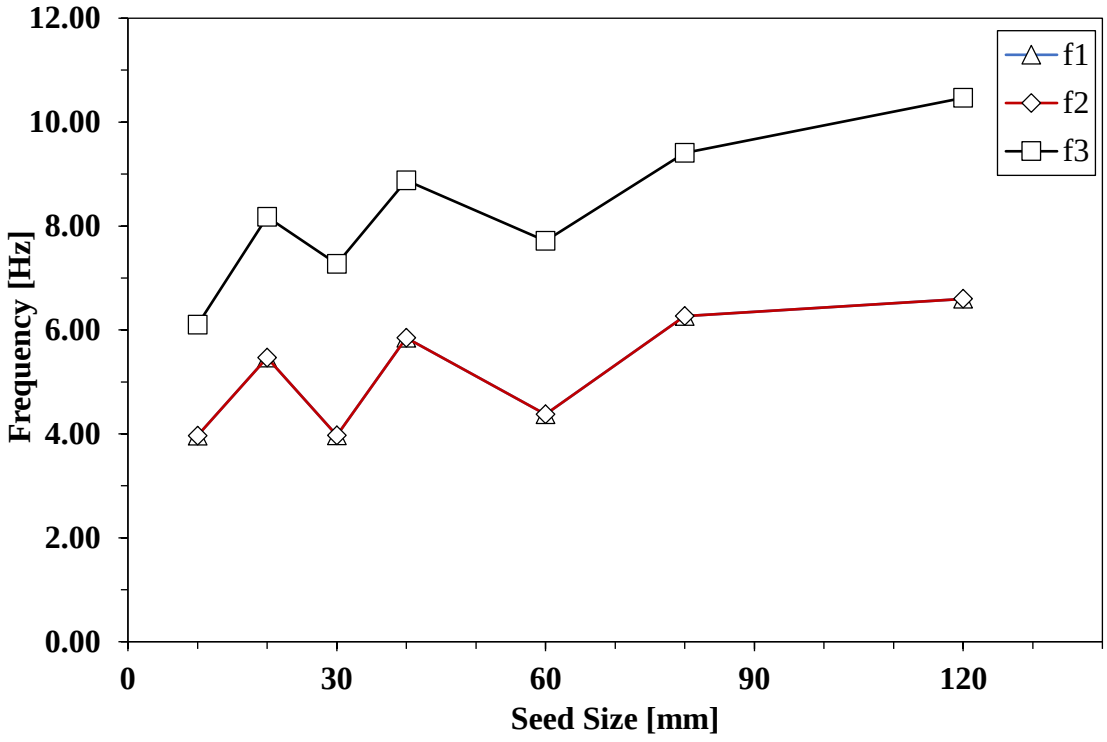


Figure 3.4: Mesh convergence result for the moment frame using SAP2000

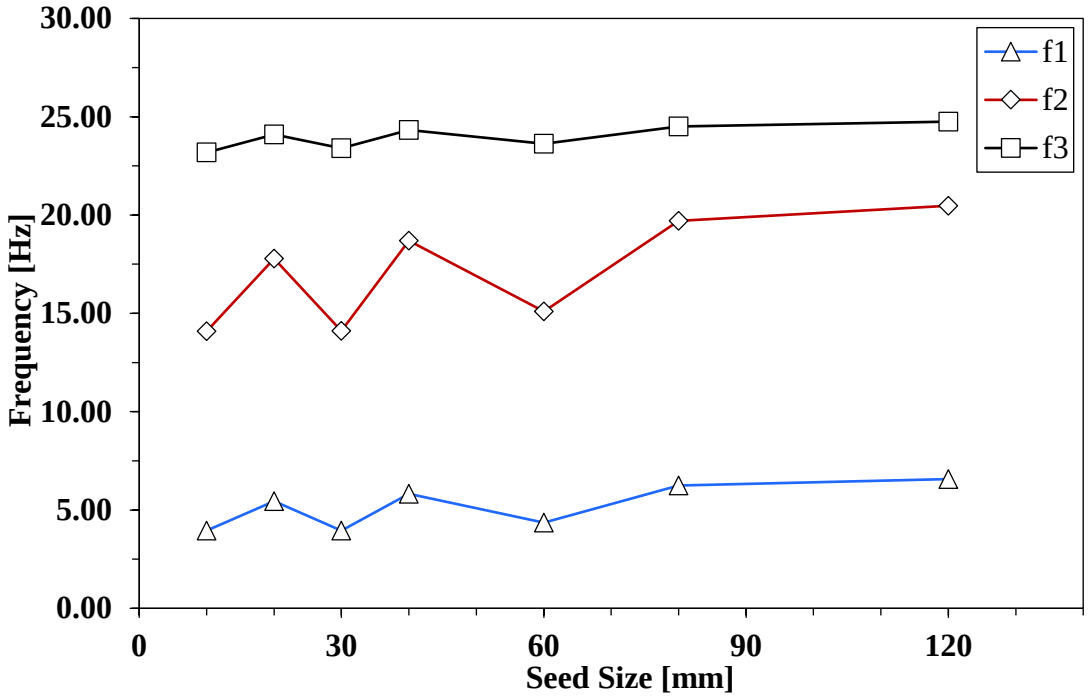


Figure 3.5: Mesh convergence result for the braced frame using SAP2000

From Figure 3.4 and Figure 3.5, the result from SAP2000 appears to be a nonmonotonic convergence which is not a preferred convergence type when dealing with numerical models.

3.3.2 ABAQUS

In this study, mesh convergence studies were performed on four ABAQUS 3D stress elements: C3D20, C3D20R, C3D8 and C3D4. A seed size range of 200 mm to 20 mm is studied. Table 3.4 shows the number of nodes associated with each seed size. Figure 3.6 shows the change in the first three frequencies against the seed size. In models using C3D8, C3D4, and C3D20, the frequency estimates monotonically decrease as the seed size decreases. The frequency estimates of C3D20R was not affected by changing the mesh size since a seed size of 200 mm, and the calculated natural frequencies between two refinements is smaller than five percent which means C3D20R converged at a seed size of 200 mm.

Table 3.4: Number of elements and nodes for each seed size for the moment frame

Seed Size [mm]	C3D20R/C3D20		C3D8/C3D4	
	Elements	Nodes	Elements	Nodes
200	7024	43024	7024	12032
160	7536	46144	7536	12920
145	7536	46144	7536	12920
120	8240	51232	8240	14392
100	8752	54352	8752	15280
70	10032	63008	10032	17768
50	11888	75232	11888	21272
20	28832	184304	28832	52240

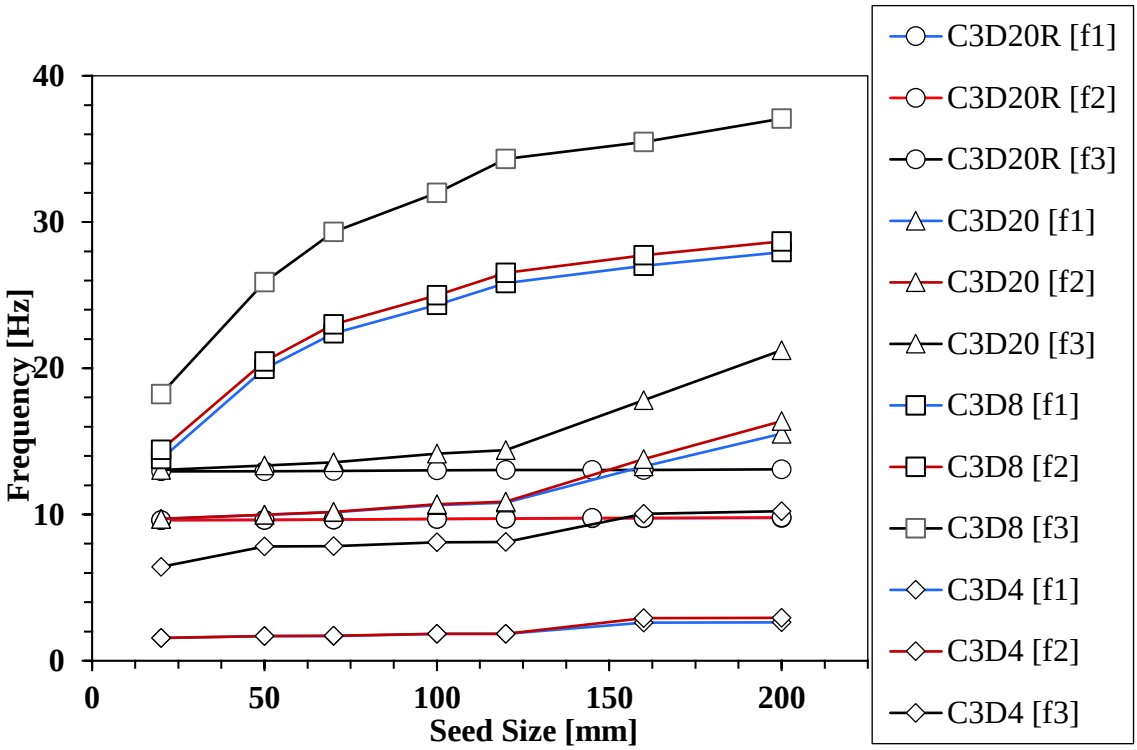


Figure 3.6: Mesh convergence study results for the moment frame using ABAQUS

The processing time depends on the seed size; a smaller seed size means a larger number of nodes which takes a longer processing time. As seen in Table 3.4, C3D4 and C3D8 have less number of nodes compared to C3D20 and C3D20R. Figure 3.7 shows the models made with C3D4 and C3D8 were taking less time to process the analysis. C3D20 was the slowest element to process. C3D20R was slightly faster than C3D20. At a seed size of 50 mm, the processing time of all the elements increased exponentially. In this project, a computer with 2.5GHz CORE i7 processor and 12GB RAM was used for the analysis.

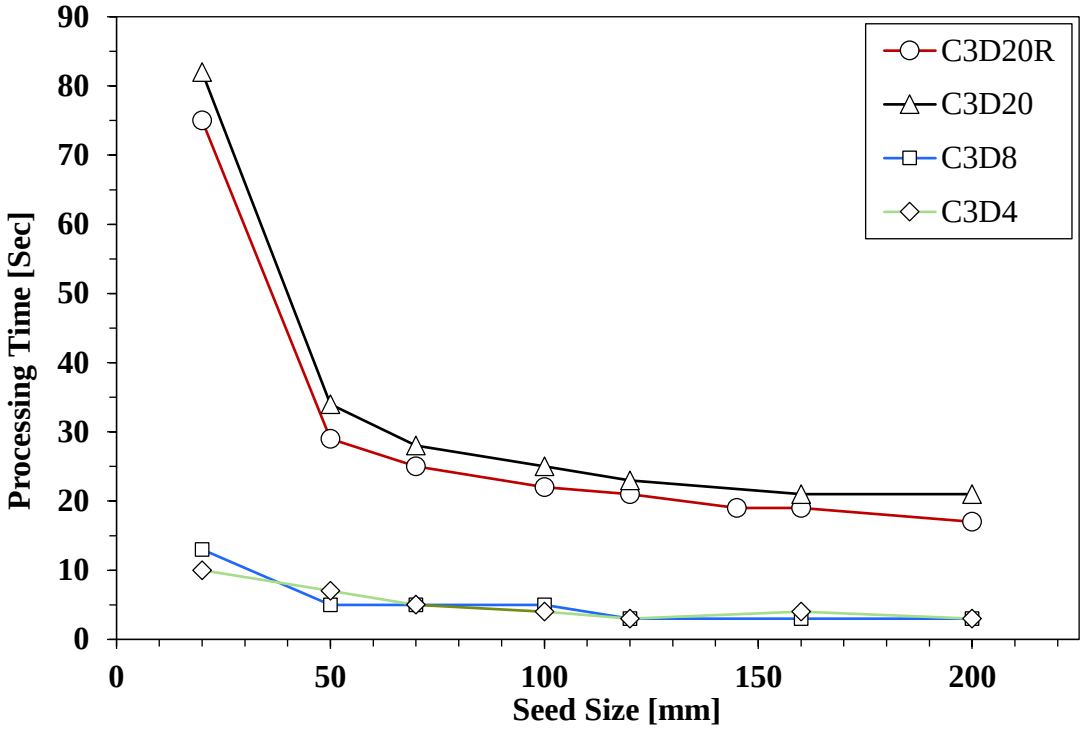


Figure 3.7: Processing time for the moment frame FE model

In the convergence result figure (Figure 3.6), C3D20R was determined as the element of choice for this model. However, as mentioned before, FEMtools supports a maximum of 50000 nodes. Considering this limitation, the seed size of 145 mm was chosen for the moment frame modelling.

The C3D20R was then used for modelling the braced frame. The brace members are modelled using the T3D2 truss element. The convergence study results for the braced frame model are shown in Figure 3.8. Similar to the result from the moment frame study, the result of braced frame starts to converge at seed size 200 mm. As can be observed in Table 3.5, adding the truss element results in the braced frame model having more number of nodes than the moment frame. In order to stay within the FEMtools node limitation, a 200 mm seed size was chosen for modelling the braced frame.

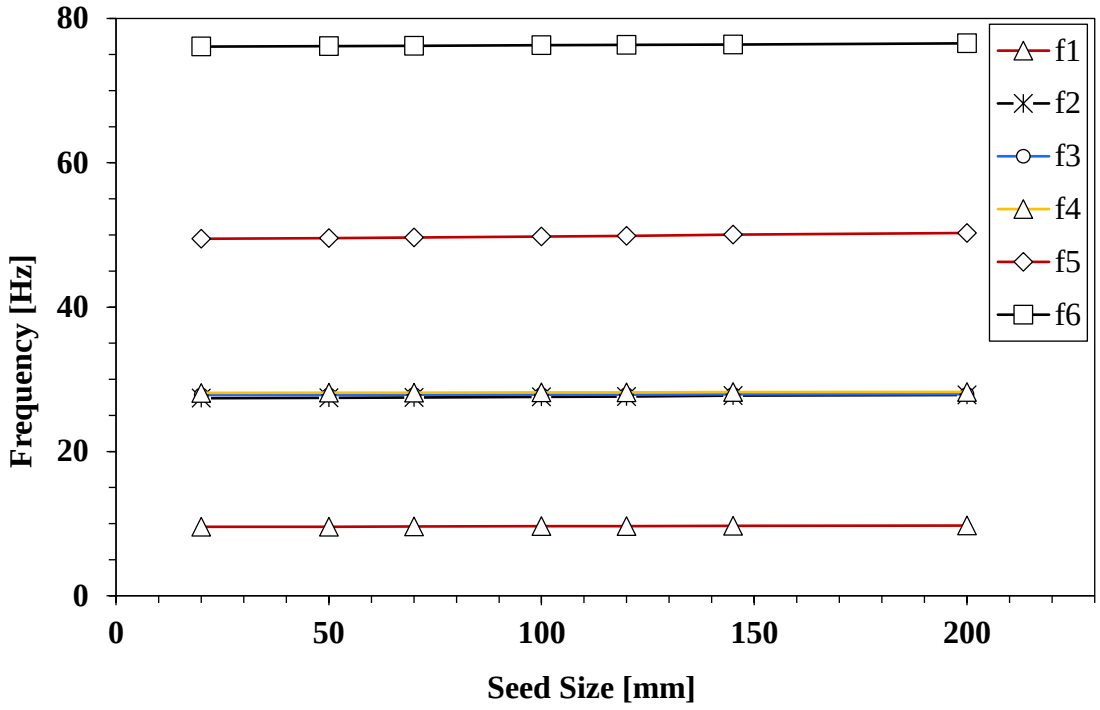


Figure 3.8: First six frequencies result for the braced frame versus seed size using C3D20R

Table 3.5: Number of elements and nodes for each seed size for the braced frame

Seed size [mm]	Number of nodes	Number of elements
200	47058	7722
145	50178	8234
120	51232	8970
100	58610	9482
70	67490	10794
50	79938	12682
20	152076	23478

3.3.3 FEMtools

The finite element model developed using ABAQUS can be imported into FEMtools, as long as the FEMtools requirements are fulfilled. However, not all ABAQUS element types are supported by FEMtools. Table 3.6 summarizes the conversion between ABAQUS and FEMtools element type. Only the elements that were used for the mesh and element convergence study are presented in this table.

Table 3.6: Conversion scheme between ABAQUS and FEMtools element type

ABAQUS element type	FEMtools element type	Element type
C3D4	TETR4	3D stress tetra linear
C3D8	HEXA8	3D stress hex linear
C3D20	HEX20	3D stress hex quadratic
C3D20R	HEX20	3D stress hex quadratic
T3D2	Line 2	Truss

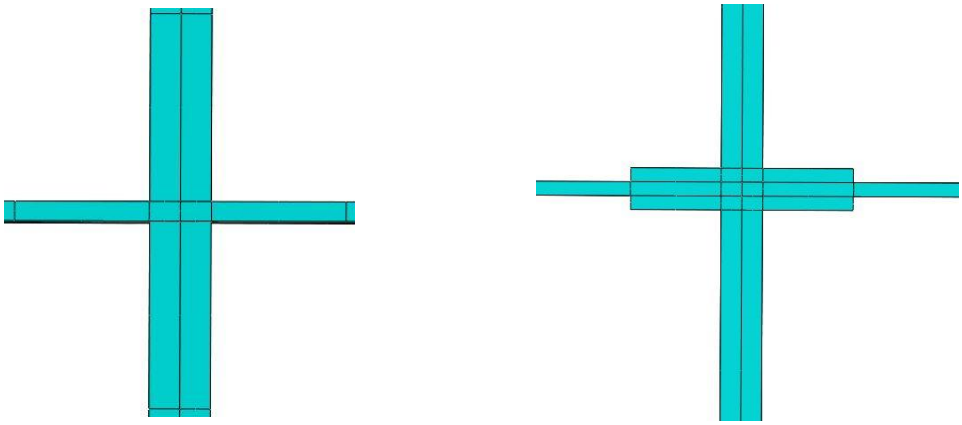
3.4 Modeling of Columns and Connection End-Plates

In this section, the idealization of the column-floor plate connections is investigated. The real condition of end-plate connections present that some of the end-plates are not in full contact with the floor plate (Figure 3.9).



Figure 3.9: Small gap between floor plate and column end-plate connection

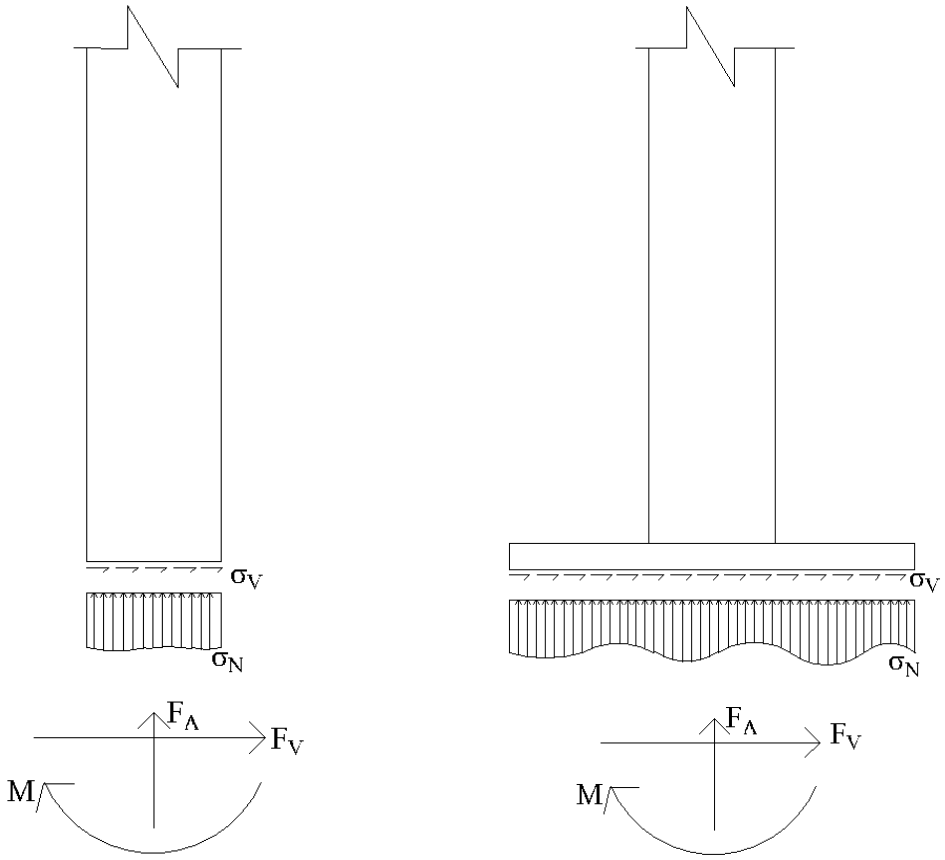
Two extreme conditions were considered as shown in Figure 3.10. This figure shows a connection where the column is directly connected to the floor plate without an end-plate. In the second model a fully bonded end-plate is used to connect the column to the floor plate.



a) b)

Figure 3.10: Idealization of the column end-plate a) No end-plate b) Fully bonded end-plate

Figure 3.11.a shows the free body diagram (FBD) of the column without end-plate, and Figure 3.11.b shows the FBD of the column with end-plate. As shown, the moment connection type is not changed by removing the end plate. However, the fully bonded end-plate condition creates much higher stiffness at the connection.



a) b)

Figure 3.11: Free body diagram a) Column without end-plate b) Column with end-plate

The effect of end-plate models on the realistic simulation of the structural behaviour is presented in the next chapter where the FE results are compared with the physical model test results.

3.5 Modelling of Brace Members

As seen in Figure 3.12, the tie-down ring is connected to the end-plate using a relatively flexible plate. Therefore, assuming braces as solid continuous members connecting the two columns ends is not accurate.



Figure 3.12: Brace connection

This condition is modelled by considering an equivalent stiffness for the braces. The brace members are considered as a series spring system as shown in Figure 3.13.

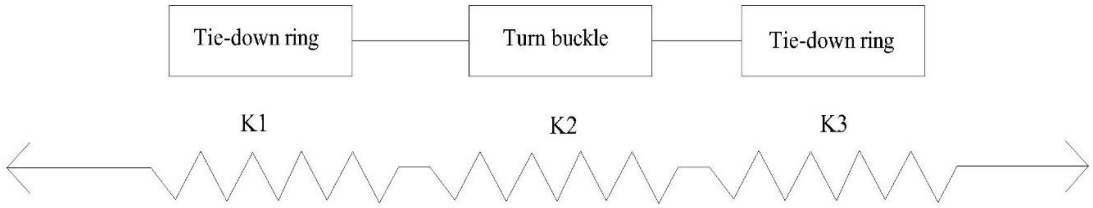


Figure 3.13: Equivalent brace member stiffness using a system springs in series

Equation (3.1) is the expression of K_{total} for a series spring system.

$$\frac{1}{K_{total}} = \frac{1}{K_1} + \frac{1}{K_2} + \frac{1}{K_3} \tag{3.1}$$

Where, K_1 and K_3 are the stiffness of the tie down ring connection plates, and K_2 is the stiffness of the turn buckle. Considering K_1 and K_3 are equal, Equation (3.1) can be rewritten as:

$$K_{total} = \frac{K_1}{2 + \frac{K_1}{K_2}} \tag{3.2}$$

For this bracing system, K_2 represents the stiffness of the turn buckle which has much higher stiffness than the tie down ring plate (K_1). Therefore, $\frac{K_1}{K_2} \approx 0$ and Equation (3.2) can be written as following:

$$K_{total} = \frac{K_1}{2} \tag{3.3}$$

The tie down ring connection was then assumed as a cantilever beam, shown as in Figure 3.14

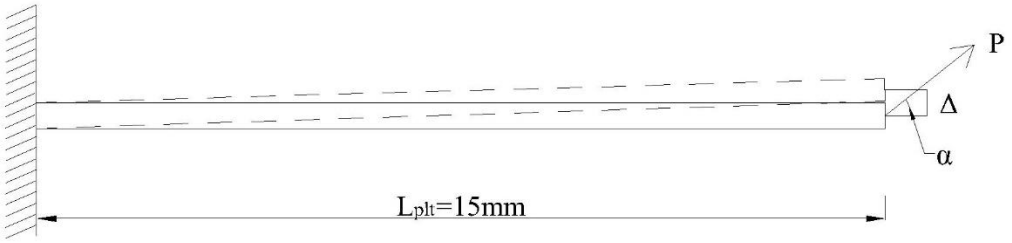


Figure 3.14: Cantilever beam assumption

Equation (3.4) is the expression of deflection at the beam tip. Substituting Equation (3.4) into Equation (3.5) results in Equation (3.6) for calculating the stiffness of the brace system.

$$\Delta = \frac{FL^3}{3EI} \tag{3.4}$$

$$K_1 = \frac{F}{\Delta \sin(\alpha)} \tag{3.5}$$

$$K_{total} = \frac{3EI}{2\sin(\alpha)L^3} \tag{3.6}$$

In the previous section, the brace member in the ABAQUS model was assumed as a rigid member of which the stiffness shall be calculated using Equation (3.7):

$$K = \frac{AE}{L} \tag{3.7}$$

In this scale model, the cross-section area (A) of the brace member was calculated to be 31.7 mm^2, the length of brace member of 390 mm was used in Equation (3.7). The moment of inertia (I) of the tie down ring plate was calculated to be 11.5 mm^4. Then using Equation (3.6), the stiffness of the tie down ring connection system is calculated to be 8% of Equation (3.7). An alternative model with reduced Young's modulus of the brace material was modelled. The eccentricity of brace connection is modelled in ABAQUS model as shown in Figure 3.15. The summarized results of FEA can be found in the following section.

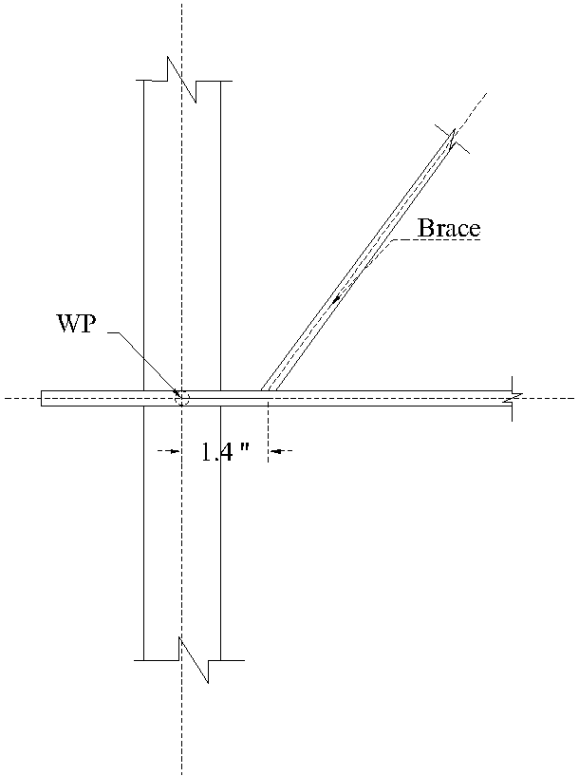
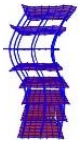
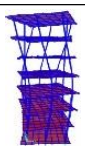
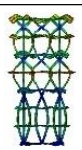


Figure 3.15: Location of brace connection in ABAQUS model

3.6 Finite Element Analysis Result

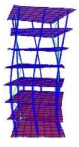
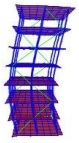
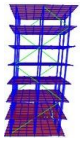
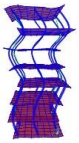
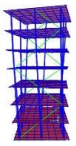
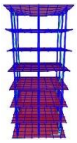
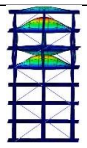
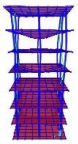
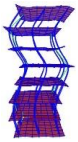
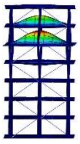
Table 3.7 and 3.8 summarized the first twelve modal vibration frequencies and mode shapes calculated using the ABAQUS and SAP2000 models for the moment and braced frames.

Table 3.7: Frequencies and mode shapes for the moment frame

Mode	ABAQUS with End-Plates [Hz]	ABAQUS without End-Plates [Hz]	SAP2000 [Hz]	Mode	ABAQUS with End-Plates [Hz]	ABAQUS without End-Plates [Hz]	SAP2000 [Hz]
1 First Y direction	 9.44	 7.06	 6.60	7 Third Y direction	 48.81	 42.61	 41.43
2 First X direction	 9.47	 7.06	 6.60	8 Third X direction	 48.89	 42.61	 41.43
3 First torsional	 12.54	 10.8	 10.47	9 Third torsional	 59.25	 54.49	 53.15
4 Second Y direction	 27.06	 21.28	 20.54	10 Fourth Y direction	 75.88	 70.80	 68.00
5 Second X direction	 27.12	 21.28	 20.54	11 Fourth X direction	 75.97	 70.80	 68.00
6 Second torsional	 34.04	 29.17	 28.61	12 Fourth torsional	 91.50	 89.58	 85.40

For the MF, the sequence of the mode shapes for all three models are matching. However, the ABAQUS model with end plates creates much higher frequencies than the other two models. These models will be validated against experimental results in the next chapters.

Table 3.8: Frequencies and mode shapes for the braced frame

Mode	ABAQUS [Hz]	ABAQUS modified brace stiffness [Hz]	SAP2000 [Hz]	Mode	ABAQUS [Hz]	ABAQUS modified brace stiffness [Hz]	SAP2000 [Hz]
1 First Y direction	 7.01	 7.01	 6.57	7 Second torsional/ Third Y direction	 85.21	 42.31	 69.54
2 Second Y /First X direction	 21.13	 12.43	 20.46	8 Second X/ Third X direction	 86.74	 63.93	 70.35
3 First X direction/ First torsional	 30.91	 14.82	 25.49	9 Fifth Y/ Fourth Y direction	 102.11	 70.27	 97.40
4 First torsional/ Second Y direction	 31.21	 21.13	 25.84	10 First vertical/ Third torsional	 104.83	 71.23	 102.78
5 Thrid Y/ Second X direction	 42.31	 35.86	 41.26	11 Second vertical/ Forth X direction	 111.44	 95.04	 108.18
6 Fourth Y direction/ Second torsional	 70.26	 40.03	 67.71	12 Third vertical/ Fifth Y direction	 113.86	 102.11	 109.94

For the BF, the mode shapes of the ABAQUS model using unmodified brace stiffness and SAP2000 model are matching. However, comparing these models to the ABAQUS model using a reduced Young's modulus, the models with rigid brace members have much higher frequencies. Also, the sequence of mode shapes for the reduced brace stiffness

model does not match with the other two models. These models will be validated against experimental results in the next chapters.

3.7 Conclusion

The finite element model of the moment and braced frame structures were developed using SAP2000 and ABAQUS. The details of the FE models were presented. Mesh and element convergence studies were carried out to develop the most efficient and adequate finite element model. The convergence results of the ABAQUS FE model appeared to be better than SAP2000. Therefore, the ABAQUS model using C3D20R will be used for the studies that presented in the next chapters. The effect of column end plates and brace stiffness were investigated; adequate assumptions were made to create alternative models that will be validated against the experimental results.

4 Operational Modal Analysis of the Scale Building

4.1 Introduction

Modal analysis is used for extracting the modal parameters of a structural system. Classical modal analysis uses frequency response functions which can be obtained from measuring the relationship between input excitations and responses. However, it is challenging and expensive to create large enough excitation forces for civil structures that would require very large actuators or impact forces. Instead, it is common to use the ambient operational conditions as a source of input excitation. As the input in such cases is unknown, operational modal analysis (OMA) which is an output only approach is used for extracting the modal parameters.

OMA has drawn great attention in the civil engineering community since the late 20th century. In 2003, Ventura summarized the advantages of OMA such as its simplified testing and analysis procedure [26]. OMA has been applied to structures such as footbridges [27-28], football stadiums [29], tall buildings [30], pedestrian walkways [31], historic masonry structures [32–34], cable-stayed bridges [35], steel truss cantilever bridges [36], and arch bridges [37]. In the last decade, more applications of OMA have been explored, and it has become an indispensable tool for model updating, damage detection, and structural health monitoring.

One of the earliest case studies of using OMA for model updating was applied on a fifteen-story reinforced concrete building in Vancouver, BC, Canada in 2005. The study demonstrated that OMA techniques can be effectively used with model updating

technique to improve the accuracy of FE models [30]. OMA has been also used for damage detection purposes. One of the popular applications is to aid with making decisions regarding rehabilitation and preservation of heritage structures [38].

The identification methods using OMA can be categorized into two main classes which are time domain and frequency domain identifications. In the late 1970's, Ibrahim Time Domain (ITD) method that is one of the first techniques for the identification of output only systems was developed [39]. Shortly after the ITD, the polyreference method (PR) that is based on the modal decomposition of impulse response functions was proposed by Vold [40]. The Stochastic Subspace Identification (SSI) method which uses semi-infinite block Hankel matrices to identify the stochastic state space models from given output data was proposed by Overschee and Moor in 1993 [41].

As for the frequency domain identification, the earliest technique is the Peak Peaking (PP) method which is known as the Basic Frequency Domain (BFD) method [42]. It obtains the modal frequencies directly from the peaks of the Power Spectral Density (PSD) plot [43]. As an enhanced version of the BFD, the Frequency Domain Decomposition (FDD) method was proposed in 2000 [44]. The FDD method computes the singular value decomposition of the PSD matrix which enables it to overcome the difficulty of identifying closely spaced modes. The Least-Squares Complex Frequency-domain (LSCF) estimation was introduced in 1998 [45]. Shortly after LSCF, a Poly-reference of the Least-Squares Complex Frequency domain (p-LSCF) estimator (also known as Polymax method) was proposed in 2003 [46]. The original LSCF and p-LSCF methods were developed for experimental modal analysis, and they are based on the modal

decomposition of the frequency response function matrix. In 2005, the polymax method that is based on the modal decomposition of PSD was adopted [47].

Among the above-mentioned methods, two of the most popular methods are SSI and Polymax. They have been adopted by commercial software such as ARTeMIS [48], and FEMtools [22]. The SSI method was used to estimate the modal parameters of the Ironworkers Memorial Second Narrows Bridge, Vancouver, Canada. In this project, OMA was used to perform model updating in order to create an accurate finite element model of the structure. Then the updated FE model was used for fatigue and damage studies as part of the real-time seismic and health monitoring system [36]. One of the earliest applications of the Polymax method was to analyze the ambient vibration data obtained from the roof of a football stadium (Bradford and Bingley Stadium, Bradford city, UK). Both Polymax and SSI methods were applied, and the results were compared. It was found that the two methods gave approximately the same modal parameter estimates. However, Polymax has the advantage that it yields clear stabilization diagrams, and it is easier to automate [29].

In this chapter, a brief technical background of two OMA methods: Time Domain PolyReference (TDPR) and FDD are presented. The process of conducting different vibration tests on the scale building for finding the most adequate test setup is presented. The importance of finding the optimal parameters to perform the modal analysis was presented through a series of parametric studies. The correlation analysis is performed for pairing the OMA results and the FEM results. Finally, the paired mode shapes for the moment and braced frames are presented.

4.2 Technical Background

4.2.1 Time Domain PolyReference (TDPR)

The TDPR method is one of the methods of OMA in the time domain. It is an autoregressive (AR) based model identification approach [40]. The following flowchart (Figure 4.1) describes the procedure for applying the PR method.

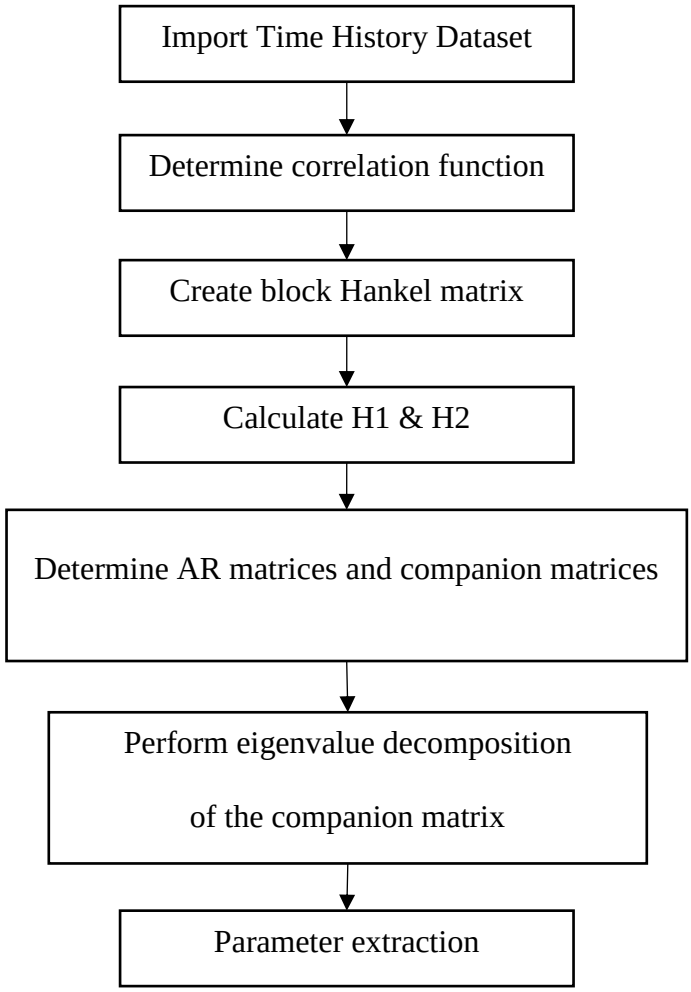


Figure 4.1: Procedure of applying PR method

In the following section the theoretical background for the TDPR is briefly presented. The first step after obtaining the data set is to calculate the correlation function (CF) using the definition of the CF:

$$R(\tau) = E[y(t)y^T(t+\tau)] \tag{4.1}$$

The autoregression moving average (ARMA) model of a dynamic system can be expressed as:

$$y(n) = \sum_{k=1}^{N} a_k y(n-k) + \sum_{k=0}^{M} b_k x(n-k) \tag{4.2}$$

Or

$$y(n) - A_1 y(n-1) - \cdots - A_{na} y(n-N) = B_0 x(n) + \cdots + B_M x(n-M) \tag{4.3}$$

Where, *y(n)* is the system response, *x(n*) is the system input, the coefficients a_k are the autoregressive (AR) part of the model, and the coefficients b_k are the moving average (MA) part of the model. The AR part represents the physical properties of the system, and the MA part represents the external forces acting on the system. The free response properties of the system can be obtained by setting the LHS of Equation (4.3) to zero:

$$y(n) - A_1 y(n-1) - \cdots - A_{na} y(n-N) = 0 \tag{4.4}$$

In order to use the TDPR method, AR matrices in the free decay (Equation (4.4)) must be obtained. To estimate the AR matrices, using the calculated CF matrix at a corresponding time step, a block Hankel matrix where each row begins one-time step behind the previous should be formed as:

$$H_1 = \begin{bmatrix} y(1) & y(2) & \cdots & y(np-na) \\ y(2) & y(3) & \ddots & y\big(np-(na-1)\big) \\ \vdots & & \cdots & \vdots \\ y(na) & y(na+1) & & y(np-1) \end{bmatrix} \quad (4.5\text{ a})$$

And a second block Hankel matrix should be formed as:

$$H_2 = [y(na+1)\ \ y(na+2)\ \ \ldots\ y(np)] \quad (4.5\text{ b})$$

where, *np* is the number of samples, na is the number of AR coefficients.

Using the two Hankel matrices, Equation (4.4) can be formulated as:

$$AH_1 = H_2 \quad (4.6)$$

Where, *A* is the matrix containing the AR matrices arranged with decreasing index na, na-1, …, 1, and it can be solved with the least squares approach, an estimate $\widehat{A}$ for A can be obtained as:

$$\hat{A} = [A_{na}, A_{na-1}, \ldots A_1] \quad (4.7)$$

Then the estimated matrix $\widehat{A}$ can be used to form the companion matrix A_C for discrete time as:

$$A_C = \begin{bmatrix} 0 & I & 0 & 0 \\ \vdots & 0 & \ddots & \vdots \\ 0 & \vdots & \ddots & I \\ A_{na} & A_{na-1} & \ldots & A_1 \end{bmatrix} \quad (4.8)$$

Using the concept of state vector and the companion matrix for discrete time, the following equation can be formed:

$$A_c\, U_d(n) = U_d(n+1) \tag{4.9}$$

Where, U_d is the discrete state vector, and can be expressed as:

$$U_d(n) = \varphi_d \mu^n \tag{4.10}$$

$$\mu = e^{\lambda_n \Delta t} \tag{4.11}$$

Where, φ_d is the discrete eigenvector, μ is the discrete time pole, λ_n is the pole, Δt is the discrete time increment. Using Equation (4.10), Equation (4.11) can be formed as an eigenvalue problem and written as:

$$A_C \varphi_d = \mu \varphi_d \tag{4.12}$$

Where, φ_d is the discrete mode shape, μ is the discrete time pole, and these are the eigenvector and eigenvalue to the companion matrix A_C. Therefore, once the companion matrix A_C (Equation (4.8)) is formed, the mode shapes and discrete time poles can be obtained by performing the eigenvalue decomposition of the companion matrix A_C. Then the natural frequency and damping ratio can be extracted from the pole:

$$\lambda_n = \zeta \omega_n \pm i \omega_d \tag{4.13}$$

Where, ζ is the damping ratio of mode n, ω_n is the undamped natural frequency, and ω_d is the damped natural frequency.

The TDPR method is one of the earliest developed modal analysis techniques. Since its introduction, several other techniques have been proposed based on the PR method concept. Nowadays, the original TDPR method is less popular in practice, since its computations become too demanding for large dimension structures [43].

4.2.2 Frequency Domain Decomposition (FDD)

The FDD method is based on a singular value decomposition of the spectral density matrix and is one of the most popular and basic methods in the frequency domain. The procedure for applying the FDD method is shown in Figure 4.2.

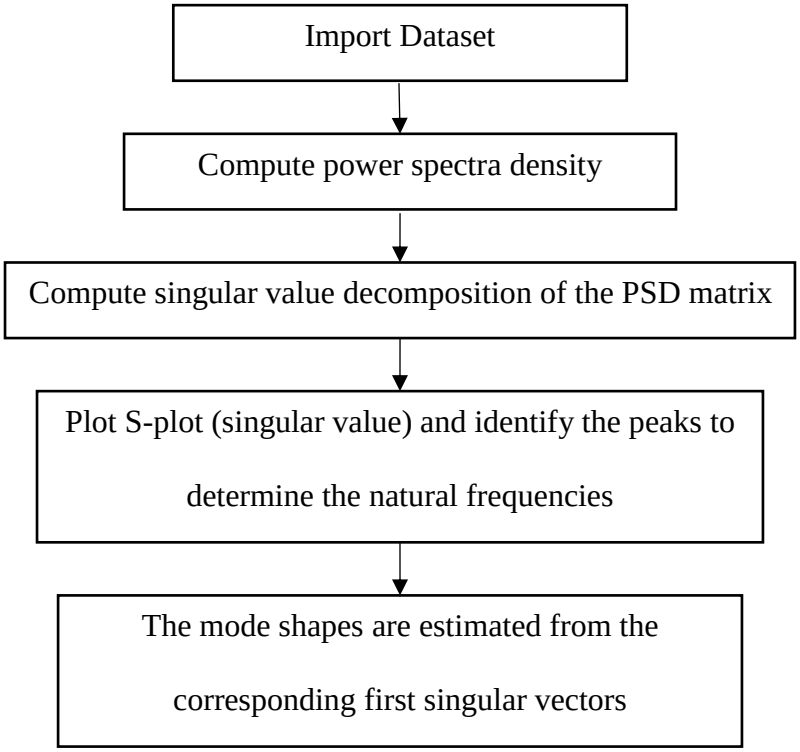


Figure 4.2: Procedure of applying FDD method

The theoretical background of FDD should begin with expressing the structural response using normal modes and modal coordinates:

$$y(t) = a_1 q_1(t) + a_2 q_2(t) + \cdots = Aq(t) \tag{4.14}$$

where, *y(t)* is the time history data, *A* is the mode shape matrix a= [a_1, a_2…] and $q(t)$ is the column vector of modal coordinates $q^T(t) = \{q_1(t), q_2(t), \ldots\}$

Using the concept of correlation function that is shown in Equation (4.1) and Equation (4.14), the following equation can be developed:

$$R(\tau) = E[y(t)y^T(t+\tau)] = AE[q(t)q^T(t+\tau)]A^T = AR_q(\tau)A^T \qquad (4.15)$$

Where, $R_q(\tau)$ is the correlation function matrix of modal coordinates. Taking the Fourier transform of Equation (4.15), the corresponding PSD matrix can be obtained:

$$G_y(f) = AG_q(f)A^T \qquad (4.16)$$

Where, G_y is the PSD matrix. If the input is a white noise, this means the off-diagonal elements in $G_q(f)$ are zero, and the matrix must be positive valued and diagonal. Also, because the PSD matrix is complex and the mode shapes might be complex, the Hermitian transpose should be used, and Equation (4.16) can be formed as:

$$G_y(f) = Ag_n^2(f)A^H \qquad (4.17)$$

Where, $g_n^2(f)$ are the diagonal elements of the PSD matrix of the modal coordinates ($G_q(f)$).

Then taking the singular value decomposition of the PSD matrix:

$$G_y(f) = USV^H \qquad (4.18)$$

The diagonal matrix *S* contains the singular values on the diagonal entries and U contains the singular vectors which are the mode shapes. The singular values are plotted against frequency, and the natural frequencies are estimated as the location of a peak in the first singular value. Then the corresponding mode shape can be found in the first column of the U matrix.

The main advantages of the FDD method compared to the PR method are FDD requires less calculation and it overcomes the difficulty of extracting the closely spaced modes. However, FDD is considered as a biased technique, because the method assumes all the inputs are white noise which is not always the case in practical applications.

In this study, the commercial software FEMtools is used to perform OMA. The software uses one of the most popular techniques which is the poly-reference of the least-squares complex frequency domain (p-LSCF) [49].

4.3 Vibration Tests

Vibration tests were performed on the scale building, for this study the building foundation was locked with clamps during the vibration tests. The monitored vibration response was recorded using tri-axial wireless LORD MicroStrain G-Link LXRS accelerometers (Figure 4.3 a). OMA was performed on the recorded time history data in order to obtain the structural dynamic characteristics, such as natural frequency, mode shapes, and damping ratio. Due to the large number of sensors required for monitoring the structure and the wireless communication bandwidth limits of the wireless router (Figure 4.3 b), the data logging configuration was used instead of the real-time streaming feature of the accelerometers. Based on the preliminary finite element analysis, the highest natural frequency of the first twenty modes of the moment and the braced frame is 120 HZ. Therefore, the sampling frequency was chosen according to the Nyquist's theorem [50]:

$$f_{max} = f_{Nyquist} = \frac{f_s}{2} \tag{4.19}$$

where, f_{max} is the maximum frequency, $f_{Nyquist}$ is the Nyquist frequency, and f_s is the sampling frequency. The sampling frequency of 256 Hz was used to capture all the desired modes. Accelerations in the global X and Y directions were recorded.



a) b)

Figure 4.3: a) Tri-axial wireless accelerometer b) Wireless router

A rubber hammer (shown in Figure 4.4) that weights 732 gram was used for creating impacts on the structure.



Figure 4.4: Rubber hammer on the scale

Strong double-sided tapes were used to mount the sensors on the floor plates. The test setup can be seen in Figure 4.5 to 4.6



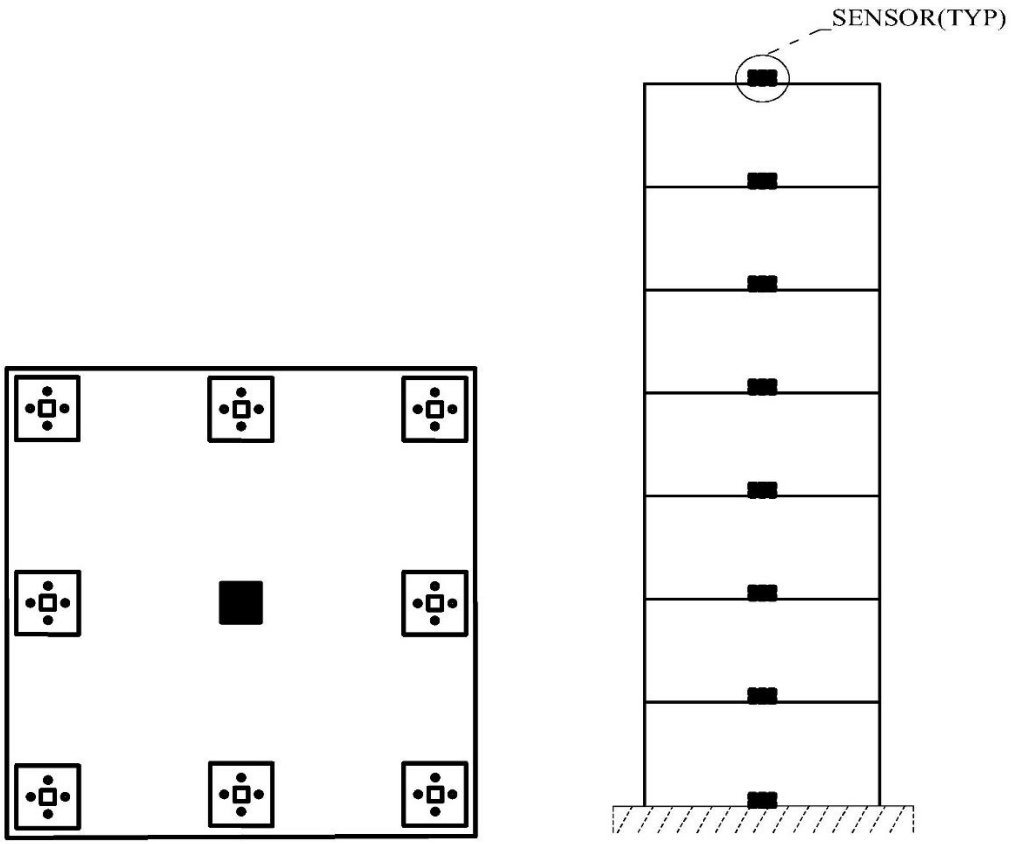
Figure 4.5: Mounted sensors



Figure 4.6: Monitoring station

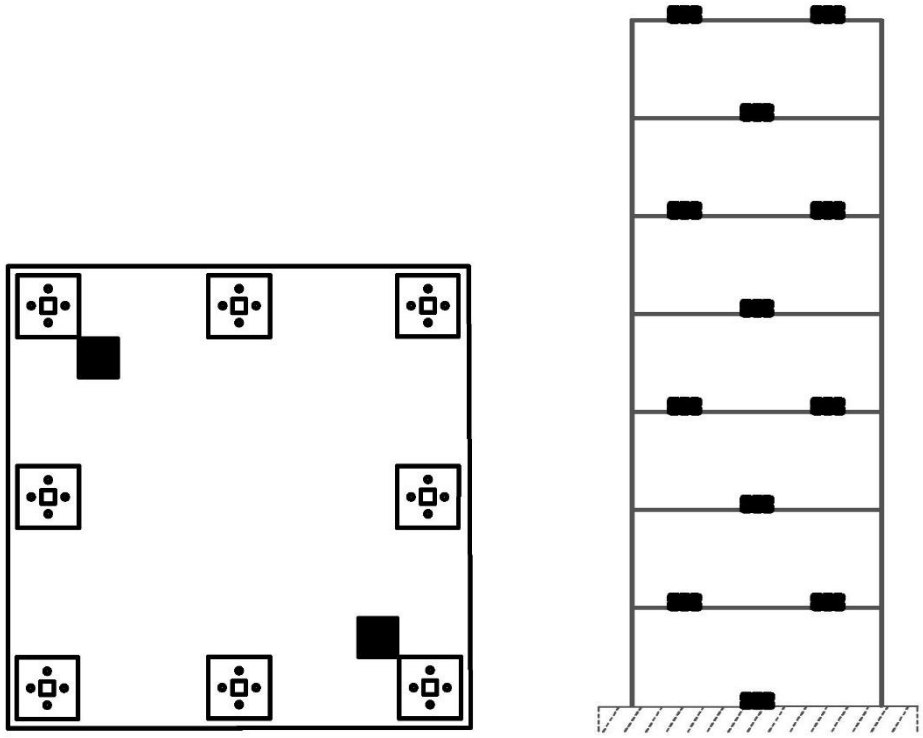
4.3.1 Sensor Configuration

Two sensor configurations were used. In setup 1 (shown in Figure 4.7) a single sensor was placed at the center of each floor plate. In this configuration, a total of eight sensors was used. In configuration setup 2 an alternating dual diagonal and single sensors combination was used. In this setup, twelve sensors were placed on the model as shown in Figure 4.8



a) b)

Figure 4.7: Sensor setup 1 a) Plan view b) Elevation view



a) b)

Figure 4.8: Sensor setup 2: a) Plan view b) Elevation

4.3.2 Input Excitation and Monitoring Time

Three types of input excitations were considered in this study. The first type of excitation was created by striking the two points (shown in Figure 4.9.a) along the edge of the floor plate, switching directions every 5 seconds. The second type of excitation was created by a single impulse impact (shown in Figure 4.9 b). The third and fourth types of excitations were created using two impulse impacts at different directions simultaneously (shown in Figure 4.9 c & d). The summary of input excitations, including the stories where the impacts were applied is shown in Table 4.2.

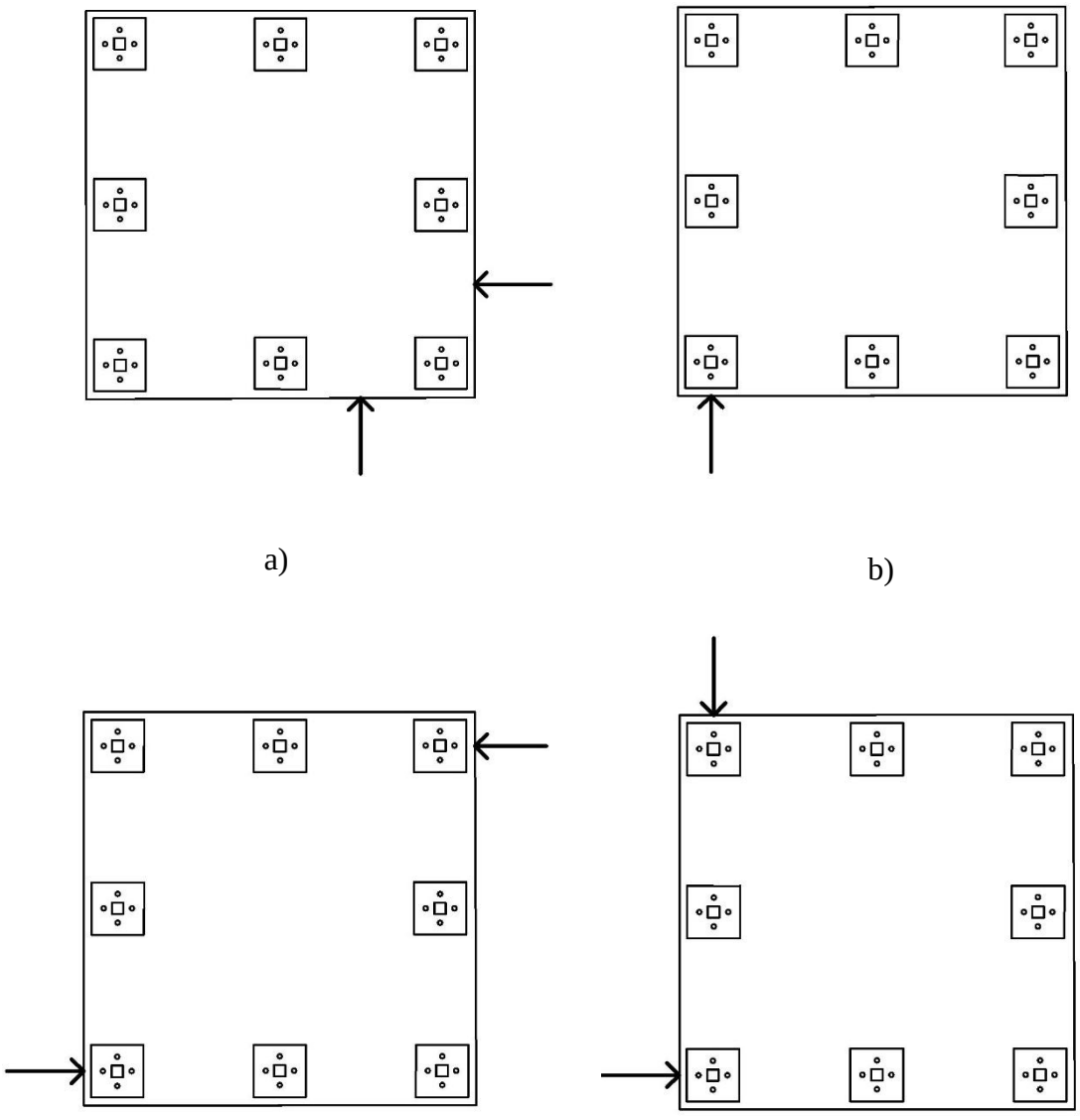


Figure 4.9: Excitation configurations a) Type 1 b) Type 2 c) Type 3 d) Type 4

The required monitoring time for the continuous excitation tests was calculated using Equation (4.20) [51], and Equation (4.21) [2]:

$$T_{req} = \frac{200}{\zeta f_n} \tag{4.20}$$

$$T_{req} = \frac{10}{\zeta f_{min}} \tag{4.21}$$

where, ζ is the damping ratio and f_n is the natural frequency of nth mode. f_{min} is the lowest frequency of interest.

In these equations, the minimum frequency of 7 Hz obtained from preliminary FE models was used. Table 4.1 summarizes the required monitoring time using two assumed values of damping ratio.

Table 4.1: Monitoring time for type 1 excitation tests

	Monitoring time [sec]	
Damping ratio	Equation 4.14	Equation 4.15
2%	1430	70
5%	570	30

In this case study, due to the limited internal memory of the accelerometers, the longest monitoring time of 1430 seconds was not possible. Thus a monitoring time of 600 seconds was used with the continuous excitation tests. 15 seconds was used for the impulse excitation tests.

Six vibration tests using different sensor configurations, input excitations, and monitoring times were initially conducted on the moment frame to discover the best setup. The details of these tests are summarized in Table 4.2. The results of different test setups are discussed in Section 4.4.3.

Table 4.2: Summary of test parameters

Test	1	2	3	4	5	6
Sensor configuration	Setup 1	Setup 2	Setup 2	Setup 2	Setup 2	Setup 2
Excitation type	Type 1 at 2nd floor	Type 1 at 2nd floor	Type 2 at 2nd floor	Type 2 at 7th floor	Type 3 at 8th floor	Type 4 at 8th floor
Monitoring time [sec]	600	600	15	15	15	15

4.4 Operational Model Analysis

The mean of the vibration time history data was removed for all tests, and for test 3 to 6 (impulse excitation tests), only the free vibration data was used in the operational modal analysis. The command script that generates the structure's mesh frame was written to replicate the sensor configuration as the trace line in FEMtools.

First, FEMtools was used to estimate cross-power spectra; then the modal parameters were extracted using its Model Parameter Extractor (MPE) module and the estimated cross-power spectra. The correlation analysis was then applied to compare the numerical and experimental mode shapes and to obtain the mode shape pairs.

4.4.1 Modal Parameter Extractor

The block size and model order are the two critical parameters which are required to be defined by the user in order to extract the desired modal parameters. The correlation function must be calculated before the cross-power spectra can be estimated. FEMtools

uses Equation (4.22) to calculate the correlation function. As can be seen in this equation, the block size is the time lag that divides the time series into a number of segments. The correlation function is computed for the individual segments and averaged.

$$R_{xy}(k) = \frac{1}{N-k} \sum_{i=0}^{N-k-1} x(i+k)y(i) \tag{4.22}$$

Where, x and y are the discrete time signal, k is the time lag, and N is the number of samples in the time series.

A small block size gives better noise reduction, and the result will be more stable. However, it may increase the damping. A large block size can reduce the impact on damping, but it will lead to a noisier spectra [52]. Therefore, choosing an optimal block size depends on the specific problem.

The model order is the number of the modes that are assumed to be present in the selected frequency range (for this study the frequency range was 0 to 120Hz). A small model order can fail to extract all modes of interest while a large model order will result in extracting noise modes. Thus, it is important to find the optimal values for model order and block size which optimize the extraction of the largest number of valuable modes. This was accomplished through a series of parametric studies following the procedure presented as a flowchart in Figure 4.10. Two criteria were considered for finding the optimal parameters in this study. The first one is the number of extracted mode shapes, as more extracted mode shapes could provide more information about the structural system. However, these extracted mode shapes are not necessarily valuable and may not be meaningful and pairable with numerical results. Therefore, a second criterion of the

number of paired mode shapes between the OMA and FE models was also considered. A summary of the parametric study results is presented in the Section 4.4.3.

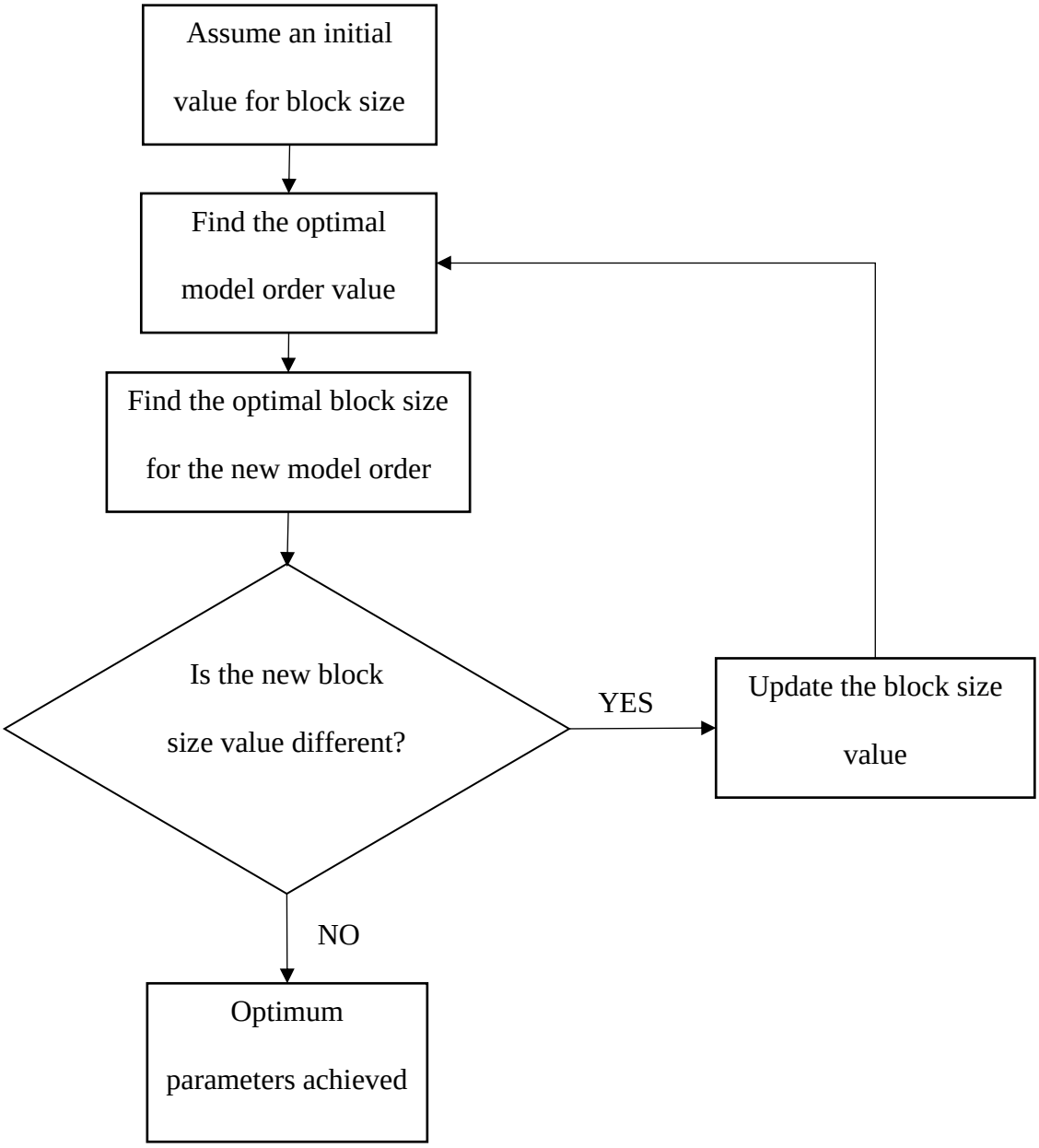


Figure 4.10: Flowchart for finding the optimum block size and model order values

4.4.2 Correlation Analysis

Correlation analysis is used to compare the numerical results with the experimental results, as well as to find the mode shape pairs. Modal Assurance Criterion (MAC) is the parameter that indicates the correlation between two mode shapes; MAC values are between zero and unity, a closer MAC value to unity means a better correlation between the two mode shapes. For this study, MAC values represent the correlation between mode shapes that are calculated from the numerical FEA and experimental OMA results. Equation (4.23) was used to calculate the MAC values.

$$MAC_{(\psi_a,\psi_e)} = \frac{|(\{\psi_a\}^t\{\psi_e\})|^2}{(\{\psi_a\}^t\{\psi_a\})(\{\psi_e\}^t\{\psi_e\})} \tag{4.23}$$

where, ψ_a is the mode shape vector from FEA, and ψ_e is the mode shape vector from OMA.

FEMtools correlation analysis was used to calculate the MAC value between all the possible combinations of numerical and experimental modes. For this study, the ABAQUS model was imported to FEMtools, and using the external solver feature in FEMtools, ABAQUS solver was selected to perform the modal analysis. The first 20 modes shapes of the FE model were selected. A minimum MAC value of 40% and maximum frequency difference of 50% were set to find the mode shape pairs. Based on the preliminary results of OMA, the moment frame model without end-plates was used for the correlation analysis. The results of this study can be found in Section 4.5.2.

4.4.3 Parametric Study Summary

It was assumed that one set of optimal block size and model order can be used for the tests that have the same signal length. Thus, two parametric studies were performed. The first parametric study (following the flowchart in Figure 4.10) was performed on test 2 (600 seconds monitor duration test). Initially, the block size was set as 15360 which represents a one-minute time lag at a sampling frequency of 256 Hz. The effects of changing the model order on the number of extracted mode shapes and paired mode shapes are plotted in Figure 4.11. As seen in this figure, the higher model order values resulted in extracting more mode shapes, but the number of paired mode shape converged to a value of 15 at model order 100. This was chosen as the optimal model order.

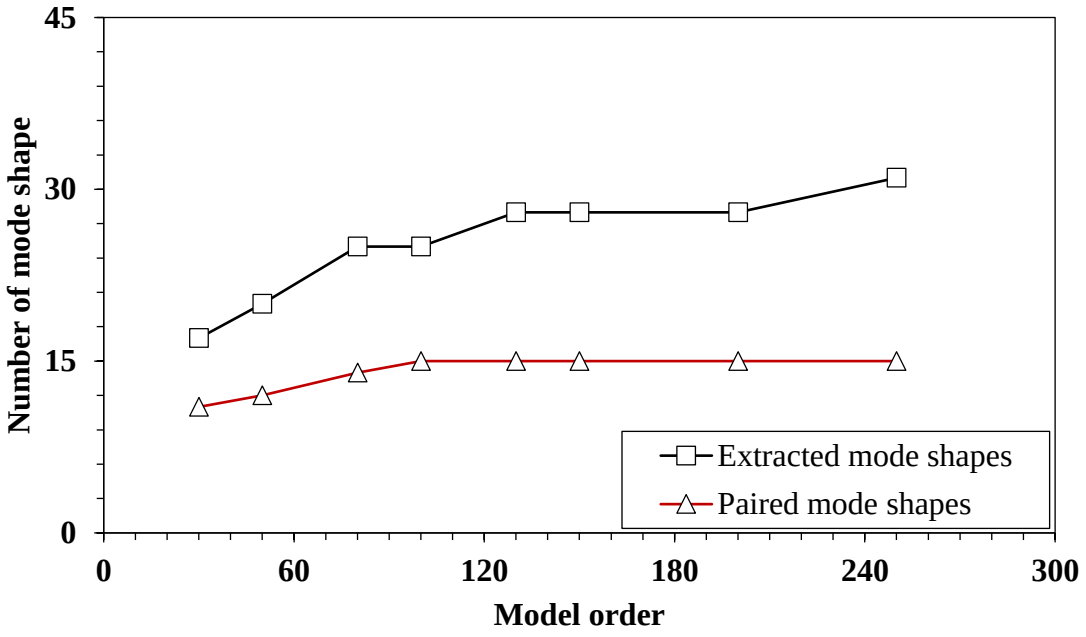


Figure 4.11: Model order parametric study for test 2

The model order of 100 was then used to find the optimal block size. The effect of changing the block size on the number of extracted mode shapes and paired mode shapes

are plotted in Figure 4.12. As shown in this figure, the number of extracted mode shapes increases as the block size decreases. However, the number of paired mode shapes converged at the block size of 15360. This block size value also results in the optimal model order of 100. Thus, the optimal block size of 15360 and optimal model order of 100 for 600 seconds monitor duration tests were selected.

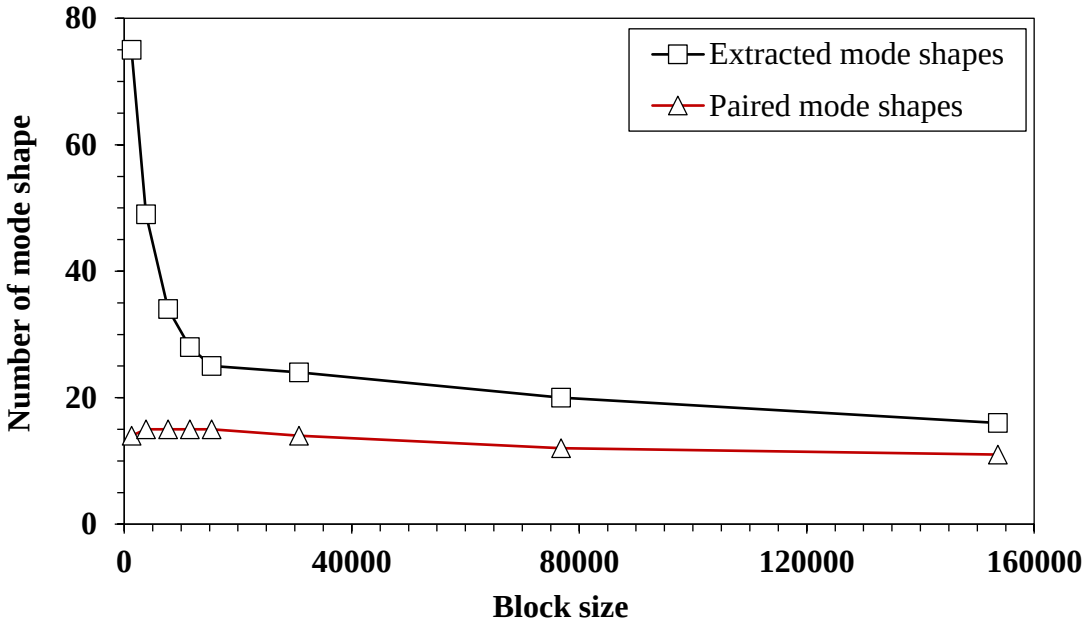


Figure 4.12: Parametric study of block size for test 2

The same parametric studies were performed for test 5 (15 seconds impulse test). The initial block size was chosen to be 768 which is a 3 seconds time lag at a sampling rate of 256 Hz. The block size of 768 and model order of 200 were determined to be the optimum parameters for the impulse tests (Figure 4.13).

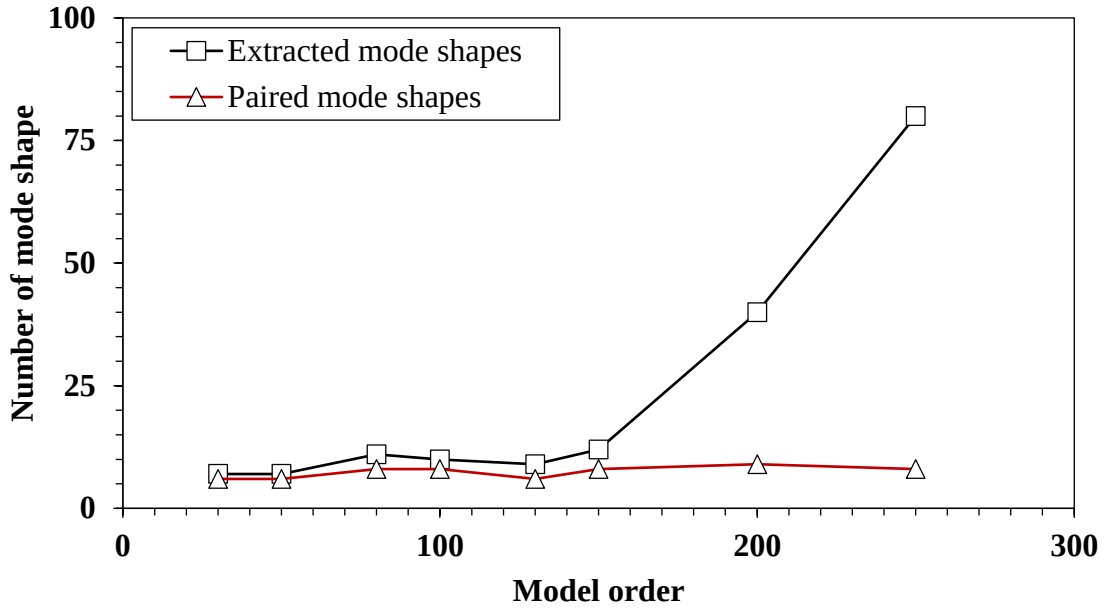


Figure 4.13: Parametric study of model order for test 5

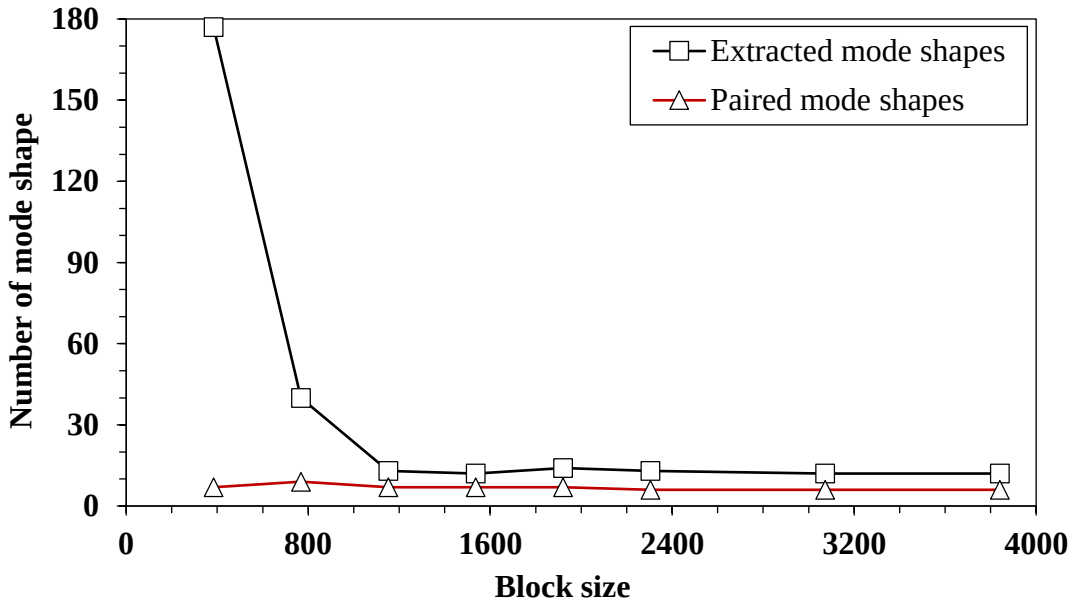
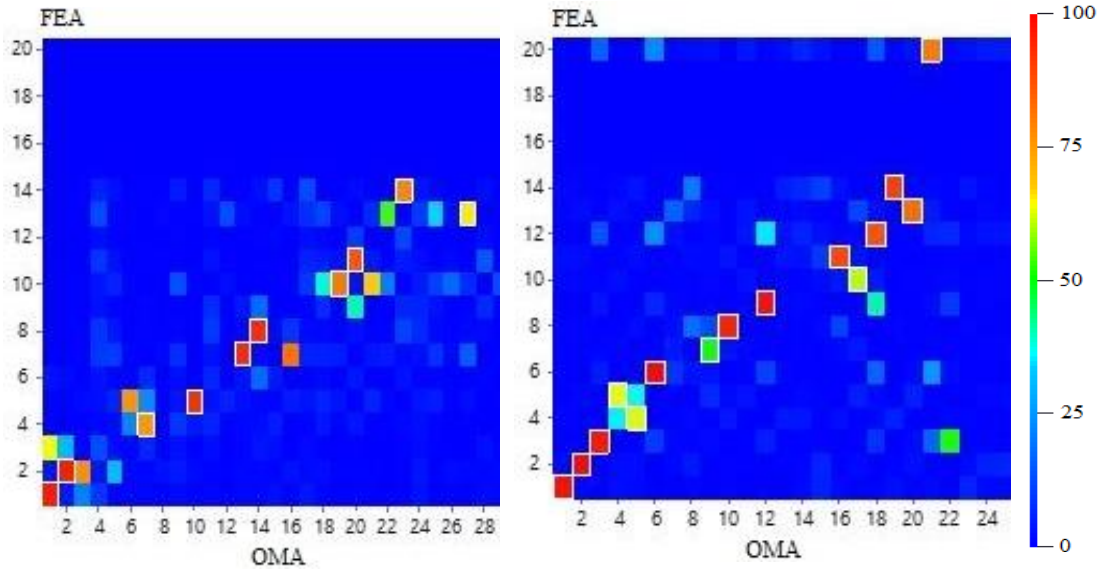


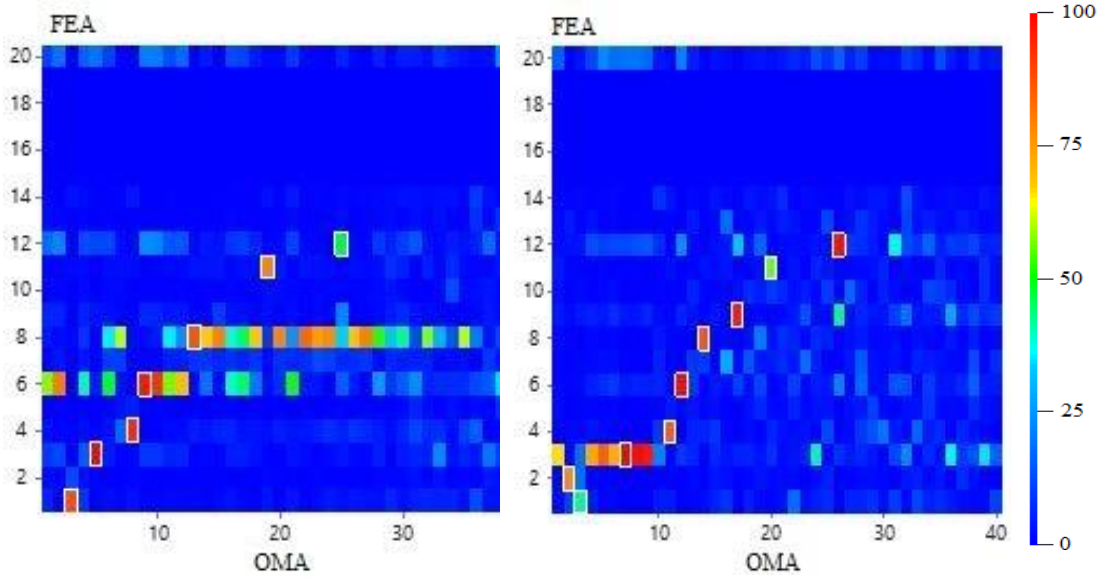
Figure 4.14: Parametric study of block size for test 5

OMA was then performed for all the vibration tests, using the selected OMA parameters. The MAC value matrix plots for each test are shown in Figure 4.15, the higher value of

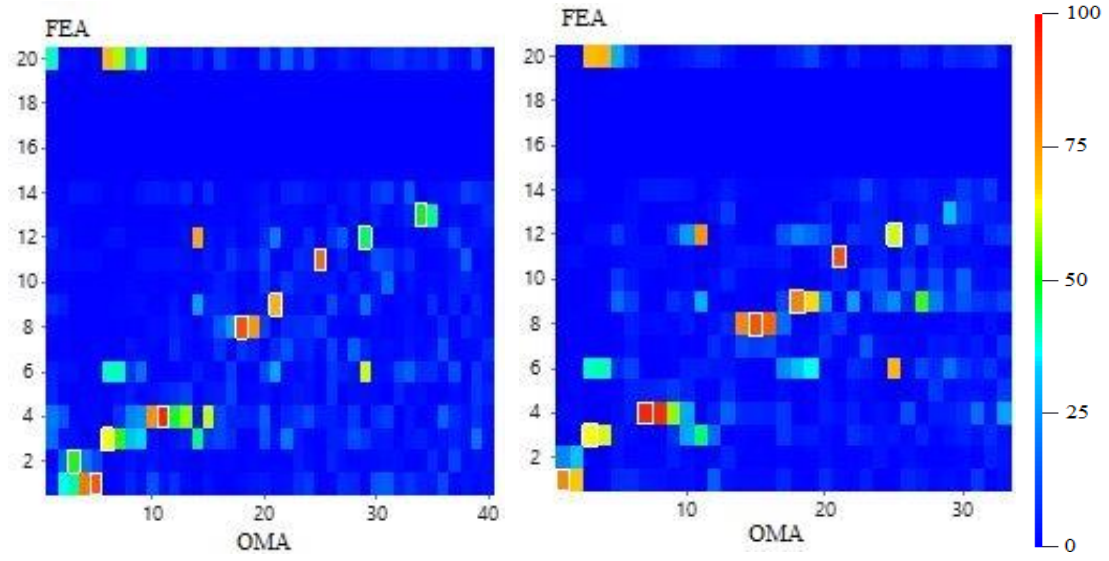
MAC means a better correlation between the numerical and experimental modes. As can be seen, test 3 to 6 extracted more modes since a higher model order was used. However, many of these modes are the noise modes with a low MAC value. Test 1 and 2 extracted fewer mode shapes with the majority of identified mode shapes being successfully paired with numerical modes.



a) b)



c) d)



e) f)

Figure 4.15: MAC matrix plots a) Test 1 b) Test 2 c) Test 3 d) Test 4 e) Test 5 f) Test 6

The best test setup that extracted the most number of paired modes with a higher MAC value is test 2, as shown in the following table.

Table 4.3: Extracted and paired modes from vibration tests

Test	1	2	3	4	5	6
Extracted modes	29	25	38	40	40	33
Paired modes	10	15	7	9	9	7

The test setup 2 was then used to conduct tests on the braced frame. The complete OMA results of the moment frame and the braced frame can be found in the following section.

4.5 Validation of FEMs and OMA Results

4.5.1 Validation of Finite Element Models

Several finite element models with different assumptions regarding the braces and member connections were developed in Chapter 3. The experimental results are used in

this section to validate the assumptions made in these models. The validation confirmed that the model without end-plates simulates the structural behaviour more realistically. The validation results of the first three modes are summarized in Table 4.4.

Table 4.4: Validation of the moment frame finite element model

Mode	ABAQUS without end-plates [Hz]	ABAQUS with end-plates [Hz]	OMA [Hz]
1	7.06	9.44	7.15
2	7.06	9.47	7.38
3	10.79	12.54	10.75

For the braced frame, it was found that the consideration of a reduced brace member stiffness is correct, as seen in Table 4.5. The ABAQUS model with a modified brace stiffness created a smaller discrepancy in natural frequencies than the original ABAQUS model.

Table 4.5: Validation of the braced frame finite element model

Mode	ABAQUS modified brace stiffness [Hz]	ABAQUS [Hz]	OMA [Hz]
1	7.01	7.01	7.15
2	12.42	21.13	11.70
3	14.82	30.91	14.37

Therefore, the ABAQUS model without end-plates is used for the moment frame studies. The ABAQUS model with a modified brace stiffness is used for the braced frame studies.

4.5.2 OMA Results of Moment and Braced Frame

The moment and braced frames modal parameters were successfully extracted with the first 9 mode shapes successfully paired. The MAC values are generally high for both braced and moment frame models, except for mode 7 of the moment frame. The natural frequencies are well correlated with minor differences. The results of the first 9 mode shapes for the moment and braced frames are summarized in Table 4.6.

Table 4.6: OMA results of moment frame

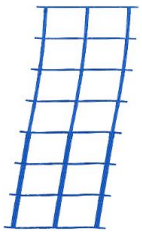
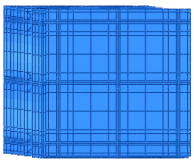
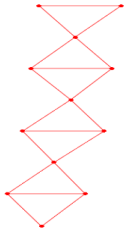
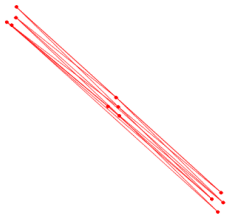
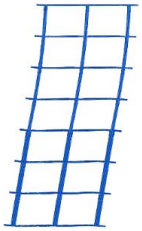
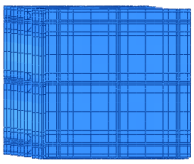
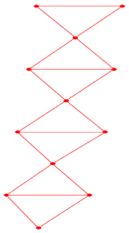
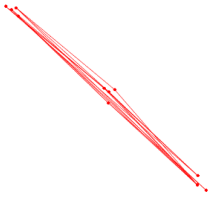
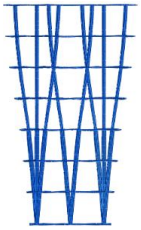
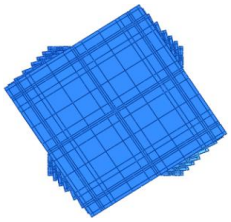
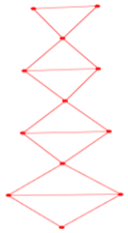
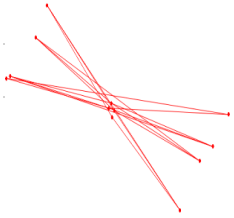
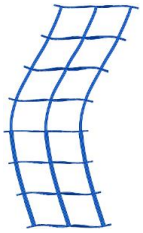
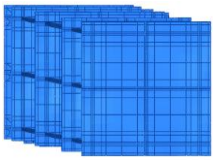
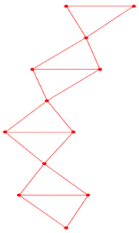
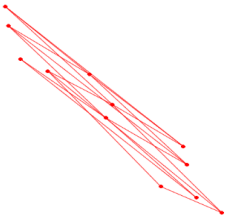
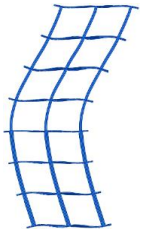
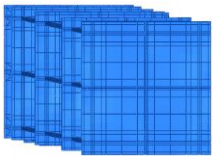
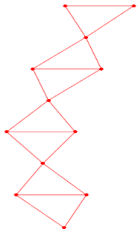
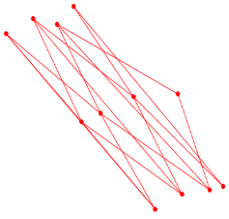
Pair	FEM		OMA		MAC
	Elevation view	Plan view	Elevation view	Plan view	
1 First Y direction	 7.06 Hz		 7.15 Hz, ζ= 0.56%		97.60%
2 First X direction	 7.06 Hz		 7.38 Hz, ζ= 0.71%		98.30%
3 First torsional	 10.8 Hz		 10.747 Hz, ζ= 0.23%		96.30%
4 Second Y direction	 21.28 Hz		 22.87 Hz, ζ= 0.26%		62.10%
5 Second X direction	 21.28 Hz		 22.453 Hz, ζ= 0.73%		62.70%

Table 4.6 Continue

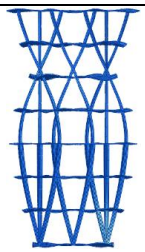
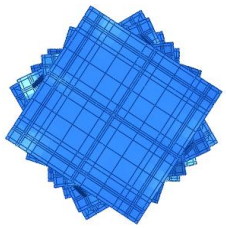
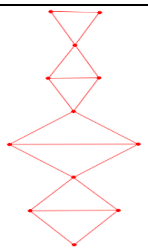
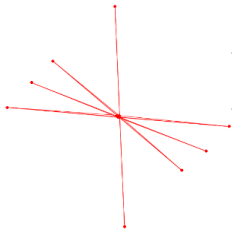
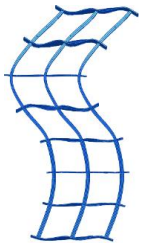
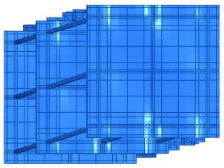
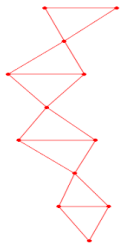
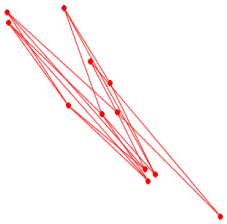
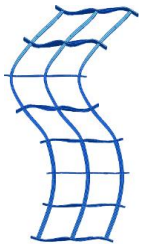
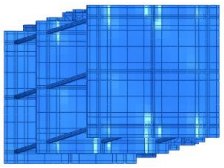
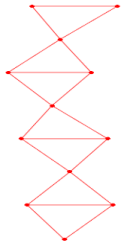
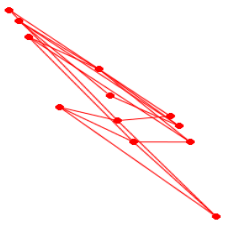
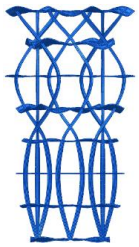
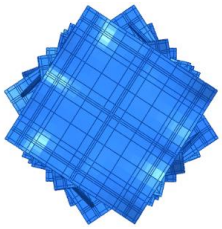
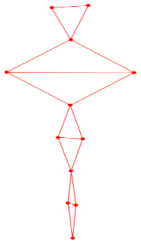
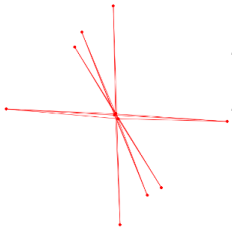
Pair	FEM		OMA		MAC
	Elevation view	Plan view	Elevation view	Plan view	
6 Second torsional					98.70%
	29.17 Hz		29.667 Hz, ζ= 0.2%		
7 Third Y direction					51.30%
	42.61 Hz		39.336 Hz, ζ= 1.8%		
8 Third X direction					94.40%
	42.61 Hz		42.618 Hz, ζ= 0.23%		
9 Third torsional					97.40%
	54.49 Hz		52.934 Hz, ζ= 0.16%		

Table 4.7: OMA results of brace frame

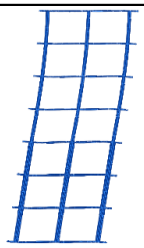
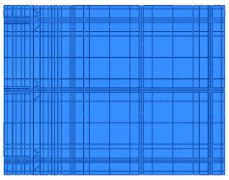
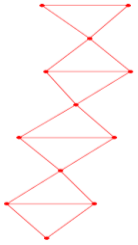
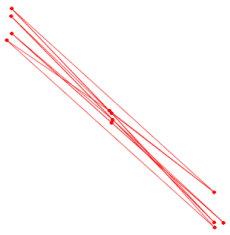
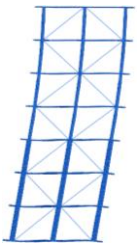
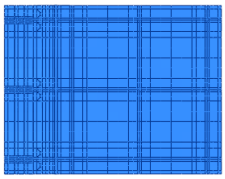
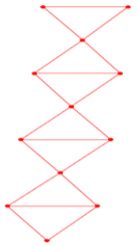
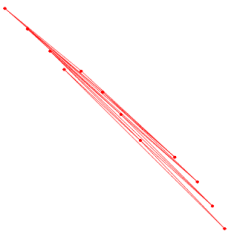
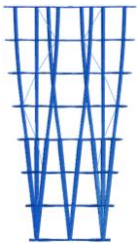
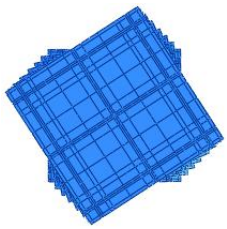
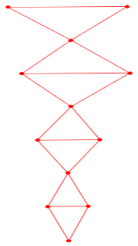
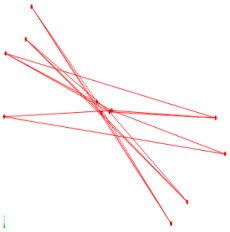
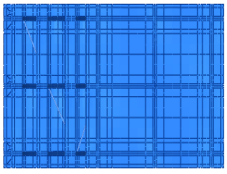
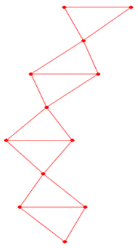
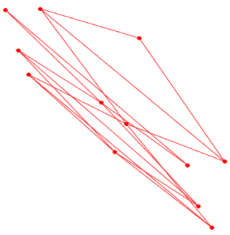
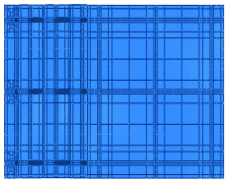
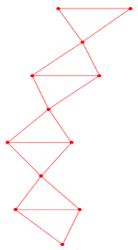
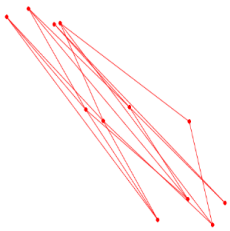
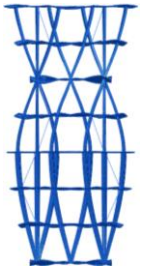
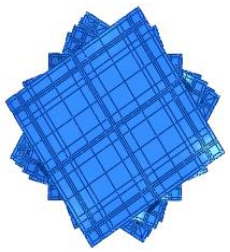
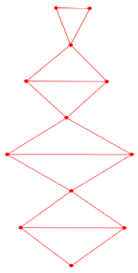
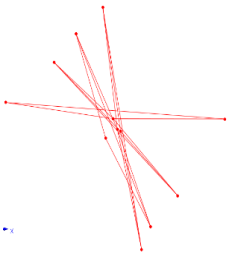
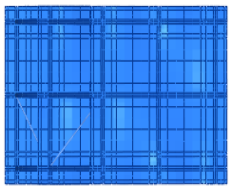
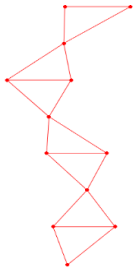
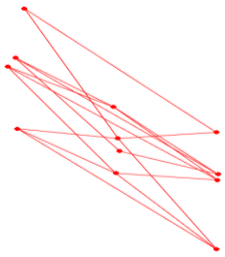
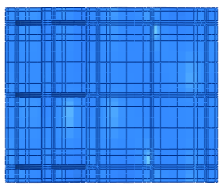
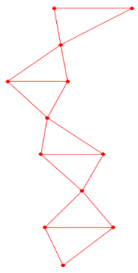
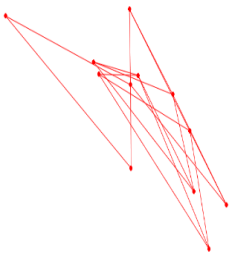
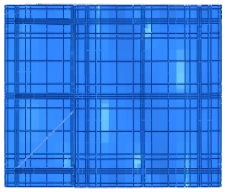
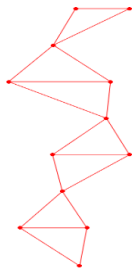
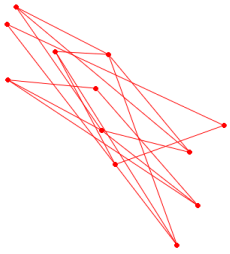
Pair	FEM		OMA		MAC
	Elevation view	Plan view	Elevation view	Plan view	
1 First Y direction	 7.01 Hz		 7.15 Hz, ζ= 0.6%		97.00%
2 First X direction	 12.4 Hz		 11.7 Hz, ζ= 0.58%		98.40%
3 First torsional	 14.8 Hz		 14.4 Hz, ζ= 0.25%		95.10%
4 Second Y direction	 21.1 Hz		 22.7 Hz, ζ= 0.23%		98.60%
5 Second X direction	 35.9 Hz		 35.9 Hz, ζ= 0.46%		95.70%

Table 4.7 Continue

Pair	FEM		OMA		MAC
	Elevation view	Plan view	Elevation view	Plan view	
6 Second torsional	 40.0Hz		 40.4 Hz, ζ= 0.17%		81.60%
7 Third Y direction	 42.3 Hz		 42.4, ζ= 0.29%		97.30%
8 Third X direction	 63.9 Hz		 60.5 Hz, ζ= 0.61%		72.10%
9 Fourth Y direction	 70.3 Hz		 66.6 Hz, ζ= 0.21%		71.60%

4.6 Discussion

The modal parameters were successfully extracted using the data obtained from the optimized test configurations. However, it was noted that the number of extracted and paired mode shapes were dependent on different test parameters, but the natural frequencies were successfully extracted from all the tests. The reason for this is because OMA is based on two assumptions. The first one is the input is assumed as a white noise which is a series of uncorrelated random variables. The second assumption is the uniform distribution of the force across the entire structure. The two assumptions were not fulfilled in this study which is the case in most practical applications. It can be concluded, when the two assumptions are not fulfilled, the extracted mode shapes are not completely reliable, and the results are affected by the test setup. However, these two assumptions did not affect the estimation of vibration frequencies. Also, because the scaled building is built out of aluminum, it is expected to have low damping ratios which was seen in the results.

The parametric study highlighted the importance of block size and model order, as the extracted and paired mode shapes are highly dependent on the two parameters. There is no unified estimation method to determine these parameters as it depends on the monitored system, signal length, and input excitation.

4.7 Conclusions

This Chapter focuses on performing operational modal analysis. Six different vibration tests were conducted on the scale building, and the best test setup which extracted the most paired mode shapes was determined. A procedure of finding the optimal parameters of block size and model order was developed. The modal parameters of the scale building (natural frequencies, mode shapes, damping ratio) were successfully extracted. Good correlation between the numerical results and OMA results was achieved. The results of this study will be used in the next chapter for calibrating the FE models.

5 Vibration-Based Damage Detection Using Model Updating

5.1 Introduction

Structural condition assessment is an important step in the maintenance and operation of civil infrastructure. Visual inspection is the most common method to assess structural damage caused by various sources such as ageing and material deterioration. However, with increasing the complexity of civil structures, visual inspection can be very expensive, time-consuming, and inadequate. For instance, if the structure experiences a natural disaster, often the damage appears in multiple structural members, and not all damage conditions are visible to human eyes. Thus visual inspection methods are often inadequate for detecting such damage.

In addition to visual inspection, non-destructive testing methods such as acoustic, ultrasonic, magnetic field, radiography and thermal field methods were developed in the late 1980s [1]. Successful application of these methods requires prior knowledge of the damage location, and in most cases the damage location needs to be accessible for inspection. The limitations of these traditional methods has led to the development of methods for detecting damage by examining the changes in the dynamic characteristics of the structure, which is known as vibration-based damage detection.

A change in structural parameters such as mass and stiffness can cause changes in the modal parameters of a structure. Thus, damage can be detected as the reduction of the structural stiffness. The common vibration-based damage identification methods detect damage by evaluating the change in modal frequencies and mode shapes of a structural system [53]. Cawley and Adams are the pioneer researchers for detecting damage by

evaluating the change in modal frequencies that is measured by placing sensors at specific points [54]. Salawu [55] in a state-of-the-art article reviews the methods that use changes in frequencies and conclude that they can be effective in the assessment of structural conditions.

The concept of detecting damage using the mode shape information was first presented by West [56]. The change in mode shapes is evaluated using the modal assurance criteria (MAC) to determine the correlation between the undamaged and damaged modes. Shortly after, Doebling [57] proposed that the damage can be effectively detected using the change in smoothness of mode shape curvature. In 2011, Fan and Qiao [58] in a comparative article reviewed the methods that use changes in mode shape and mode shape curvature. The article concludes that the damage can be roughly localized by assessing the mode shape change, and mode shape curvature-based method is effective in damage localization.

Doebling [59] summarized the applications of vibration-based damage detection that have been successfully applied on single structural members such as a beam, truss, plate, and shell and real structures such as bridges, offshore platforms, as well as the aerospace structures.

A case study of detecting damage by assessing the change in modal frequencies was conducted on a five-story shear building with a uniformly story height of 5 m [60]. Different damage scenarios with 20%, 30%, and 40% of stiffness loss were considered under two type of excitations, including single excitation at the top floor and full excitation. The damage was successfully detected for both tests. However, the results

indicated the full excitation test gives better results for damage identification. A prestressed concrete bridge in Zurich Switzerland was studied in [61]. Different damage scenarios including 20 mm, 40 mm, 80 mm, and 95 mm settlements of the pier were considered. The damage conditions were investigated by assessing the change in mode shape curvature. The measured mode shapes were smoothed prior to the damage detection process. Using the results of modes 1 and 3, the damage of 95 mm settlement was successfully identified.

Finite element model updating started to draw attention in civil engineering communities in the early 1990s. An overview of the major development of model updating in structural dynamics has been provided by Mottershead and Friswell [62], [63]. Assumptions that are used for developing the numerical model of an existing structure result in inaccuracies. The purpose of model updating techniques is to reduce the discrepancy and improve the correlation between the numerical model and the physical model. The objective of model updating is to create an updated model by modifying the system matrices (mass, stiffness, and damping) of the finite element (FE) model with respect to the experimental modal parameters (natural frequencies and mode shapes) through an iterative process.

Model updating has been successfully applied to a wide range of structures such as highway bridges [64], [65], high-rise buildings [66], cable-stayed bridges [67], and historical structures [68]. The mode updating technique was applied to a pontoon bridge with a floating span of 480 m that located in Norway [69]. The average natural frequency error was reduced and the MAC value was improved after 9 iterations of updating. However, in this study, it was found challenging for matching the FE model and identified result with closely spaced natural frequencies. To further reduce the errors, the reduction

of noise and refinement of updating parameters are required. In another study, model updating technique was applied on the Nanjing TV Tower, a high rise building with a height of 310 m located in Nanjing, China [70]. Good correlation of dynamic characteristics from the updated FE model and the experimental model were found. However, to maximize the accuracy of the updated FE model, it was found, it is important to select several groups of parameters and response and choose the one with the best result. Meanwhile, engineering judgement is an important part of this process.

Model updating uses the physical model properties to update the FE model. This means if the physical model is altered through experiencing damage, it would be detected in the updating process. Damage detection using model updating has became popular since the late 1990s. This technique was performed on a cracked beam in 1997 [71]; where it was found that a sensitivity-based approach of model updating is capable of localizing the damage. The successful localization of damage depends on the accuracy of the reference model. The same type of sensitivity based approach was applied to a bridge structure in 2001 [72]; the study reveals the limitation of the method is dependent on the accuracy of the reference FE model, and that engineering judgement is an important parameter when updating the FE model. It is evident that the result can be affected by the inaccuracy of the experimental data. In 2004, damage detection using model updating was applied to highway bridge Z24 in Switzerland [64]. The target responses were determined by assessing both the changes in natural frequencies and mode shape. The damage was successfully identified as a reduction in stiffness of the bridge girder.

In recent years, a similar method has been adopted for seismic damage detection [73]. An earthquake was simulated on a 7 storey reinforced concrete moment resistant frame that

was modelled in SAP2000, the structural damage caused by San Femando simulation was successfully identified by evaluating the change in mode shapes. However, in the Loma Prieta simulation, the damage was not successfully localized. Instead, it was identified in a floor next to the damaged floor.

In this chapter, first, a brief technical background of the sensitivity-based model updating method is presented. A damage detection method that uses model updating based on changes in natural frequencies is applied to both the moment resisting and braced frame models using different selection of responses. Lastly, the results of using the damage detection procedure for the experimental studies on the damaged moment and braced frame models are discussed.

5.2 Model updating

5.2.1 Technical background

In this research, FEMtools [22] was used to perform model updating. The software uses a sensitivity-based model updating method [74]. The method is based on the linearization of the relationship between the measured output which consists of the modal parameters such as natural frequency, mode shape, and the structural parameters that require correction. The functional relationship of measured output, and structural parameters can be expressed as:

$$\{\Delta R\} = [S]\{\Delta P\} \tag{5.1}$$

Where, ΔR is the response difference between the experimental data and analytical results, $[S]$ is the sensitivity matrix, ΔP is the difference between the updated parameter and the initial parameters. ΔR and ΔP can be written as:

$$\{\Delta R\} = \{R_e\} - \{R_a\} \tag{5.2}$$

$$\{\Delta P\} = \{P_u\} - \{P_0\} \tag{5.3}$$

Where, R_e is the vectors of experimental responses, R_a is the vector of numerical responses, P_u and P_0 are the vector of updated parameter and initial parameter, respectively. Thus, Equation (5.1) can also be expressed as:

$$\{R_e\} - \{R_a\} = [S](\{P_u\} - \{P_0\}) \tag{5.4}$$

Where, $[S]$ is the sensitivity matrix that can be obtained by computing the first derivative of selected responses (natural frequencies and mode shapes from the physical model) with respect to the selected parameters (member stiffness and geometry from the FE model):

$$[S] = \frac{\partial R_i}{\partial P_j} \tag{5.5}$$

Where, R is the response, P is the parameter, i and j are the index of response and parameters, respectively. The complete sensitivity matrix can be formed as:

$$[S] = \begin{bmatrix} \frac{\partial R_1}{\partial P_1} & \frac{\partial R_1}{\partial P_2} & \cdots & \frac{\partial R_1}{\partial P_j} \\ \frac{\partial R_2}{\partial P_1} & \frac{\partial R_2}{\partial P_2} & \cdots & \frac{\partial R_2}{\partial P_j} \\ \vdots & \vdots & \cdots & \vdots \\ \frac{\partial R_i}{\partial P_1} & \frac{\partial R_i}{\partial P_2} & \cdots & \frac{\partial R_i}{\partial P_j} \end{bmatrix} \tag{5.6}$$

The Bayesian parameter estimation method can be used to obtain the updated parameters in Equation (5.1). The Bayesian parameter estimation uses weighting coefficients on the parameters and responses; it reduces the discrepancy between the physical and FE model by minimizing the weighted error function E (Equation (5.7)). The error function E is calculated for every iteration until the convergence criterion (minimum E) is satisfied.

$$E = \{\Delta R\}^t [C_R]\{\Delta R\} + \{\Delta P\}^t [C_P]\{\Delta P\} \tag{5.7}$$

Where, ΔR is the response difference between the experimental data and analytical results, ΔP is the difference between the updated parameters and the initial parameters. C_R and C_P are the weighting coefficients of responses and parameters, respectively.

To minimize the error function, the updated parameters can be computed as:

$$\{P_U\} = \{P_0\} + [G]\{-\Delta R\} \tag{5.8}$$

Where, *[G]* is the gain matrix that can be computed from the sensitivity matrix and the weighting coefficients of responses and parameters. To obtain the updated parameter with minimum variance, the following equation for computing the gain matrix is developed by Collins [75]:

$$[G] = (\left[C_p\right] + [S]^t[C_R][S])^{-1}[S]^t[C_R] \quad (5.9)$$

Or

$$[G] = (\left[C_p\right])^{-1}[S]^t([C_R]^{-1} + [S](\left[C_p\right])^{-1}[S]^t)^{-1} \quad (5.10)$$

Equation (5.9) is used when the number of responses is more than the number of parameters. Otherwise Equation (5.10) should be used.

Once the updated parameter $\{P_U\}$ is calculated, the error function *E* (Equation (5.7)) can be computed for each iteration until the desired convergence is satisfied.

5.2.2 Damage Detection using Model Updating

Structural damage causes a reduction of stiffness in the FE model, which also affects the modal parameters. Model updating uses the structural responses in order to reduce the discrepancy between the FE and physical models. This means the FE model parameters can be updated with respect to the modal parameters that are extracted from the damage condition data. In this method, as long as the selected responses are sensitive to the damage, the damage can be identified. For this process, it is important to have an updated FE model that accurately simulate the sensitive modes. Such an FE model will be used as a baseline for detecting damages. A flowchart shown in Figure 5.1 was developed to show the method used for damage detection using model updating in this thesis.

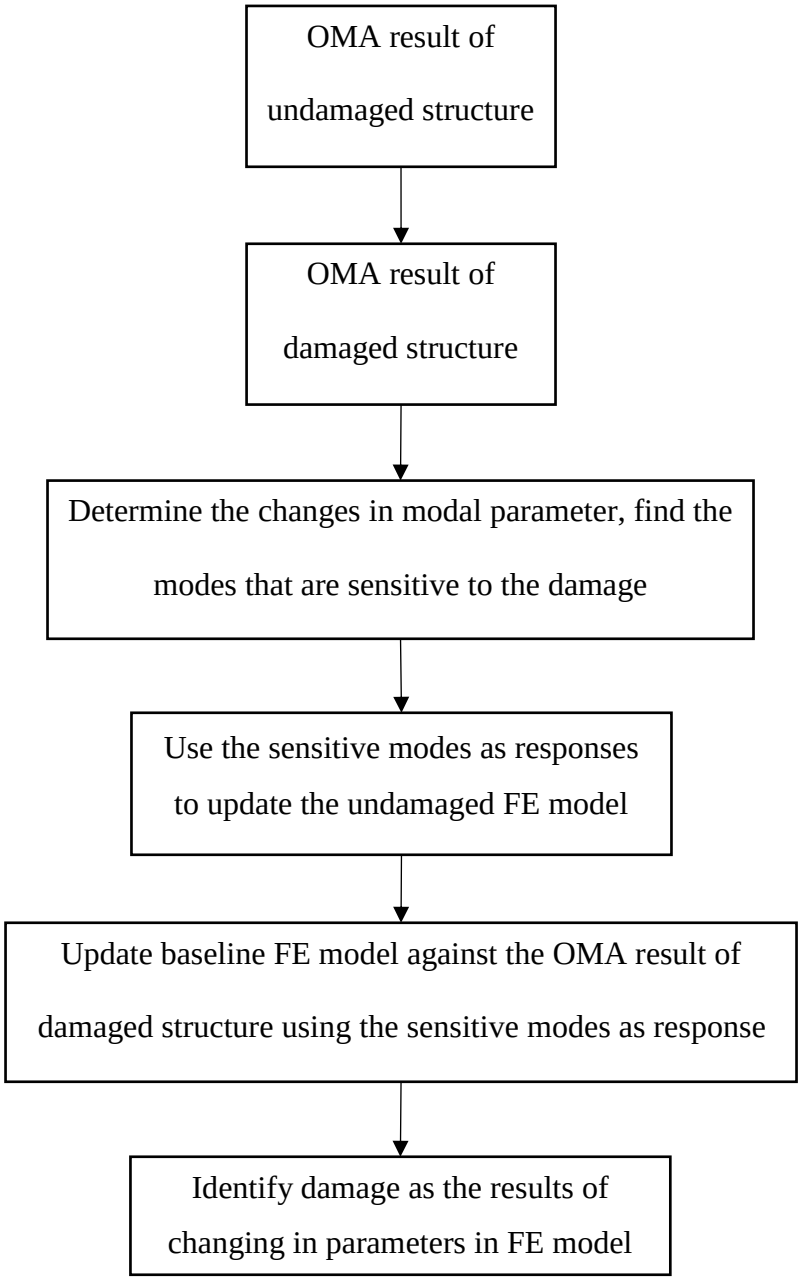


Figure 5.1: Procedure of damage detection using model updating

5.3 Experimental Studies on Undamaged Models

To investigate the effects that selected responses have on the updated results, different sets of responses were used to update the undamaged moment and braced frame FE models. Two correlation criteria were used to determine the convergence of the updated results. The first criterion is defined as the average of the absolute frequency difference between the OMA and FEA for the selected responses. This criterion was set to have a maximum of 1%. The second criterion is the improvement of the FE model between the two iterations and is adjusted to be smaller than 0.1%.

5.3.1 Moment Frame

The ABAQUS model without end-plates was used for moment frame study. The maximum allowable change of the structural parameters is shown in Table 5.1. Four different response combinations (Table 5.2) were used for updating the moment frame (MF) model. Table 5.3 summarizes the natural frequencies of the first 9 modes of OMA results and FEA results before model updating. The MAC values were calculated for indicating the correlation of the modes between the experimental and numerical results.

Table 5.1: Parameter limits of undamaged MF

Member	Parameter	Limits
Column	Young's modulus	±40%
Floor plates	Young's modulus	±40%

Table 5.2: Summary of Response Combination (RC) of undamaged MF

	RC1	RC2	RC3	RC4
Response combination	f1, f2, f3	f4, f5, f6	first 9 modes	Modes with MAC value smaller than 70

Table 5.3: Mode shape pairs of MF before updating

Mode pair	OMA [Hz]	FEA [Hz]	Δ frequency [%]	MAC [%]
1	7.15	7.06	-1.18	97.60
2	7.38	7.06	-4.30	98.30
3	10.75	10.80	0.49	96.30
4	22.87	21.28	-6.97	62.10
5	22.45	21.28	-5.25	62.70
6	29.67	29.17	-1.66	98.70
7	39.34	42.61	8.33	51.30
8	42.62	42.61	-0.01	94.40
9	52.93	54.49	2.94	97.40

Table 5.4 and Figures 5.2 to 5.5 summarize the updating results using different responses and the change in parameters. As can be seen, the updated results vary significantly depending on the selected response. The MAC values for mode 4 and 5 are improved in all cases, and the improvement of frequency agreement varies based on the selected responses. Overall, it was found to be difficult to have all the modes converge at the same time. Often the results diverge which means some modes are getting better while others may get worse during the updating procedure. This can be attributed to the complexity of the structural system. As shown in Figures 5.2 to 5.5, there were no changes in Young's modulus for the column members for all the cases, and the major adjustments were made

in floor plates. The changes in Young's modulus for the floor plates are ranged from -7.5% to 25%. It can be observed that the magnitude and location of the changes in floor plates highly depending on the selected response.

Table 5.4: Results of model updating of MF using different response combination

Mode pair	RC1		RC2		RC3		RC4	
	Δ frequency [%]	MAC [%]	Δ frequency [%]	MAC [%]	Δ frequency [%]	MAC [%]	Δ frequency [%]	MAC [%]
1	0.40	96.90	1.63	97.80	-0.69	97.00	1.79	97.90
2	-2.78	97.80	-1.58	98.40	-3.83	97.90	-1.43	98.50
3	1.39	96.30	2.60	96.30	0.68	96.30	2.46	96.30
4	-6.26	70.10	-1.75	82.60	-6.48	73.80	-2.26	82.30
5	-4.51	67.90	-3.54	96.40	-4.74	70.30	-4.04	95.60
6	-1.07	98.60	1.15	98.90	-1.28	98.70	0.79	98.70
7	8.74	49.40	10.47	51.80	7.78	46.60	8.92	57.00
8	0.37	94.30	1.97	94.50	-0.52	93.60	0.54	91.20
9	3.28	97.30	4.80	97.50	2.47	97.40	3.46	97.30

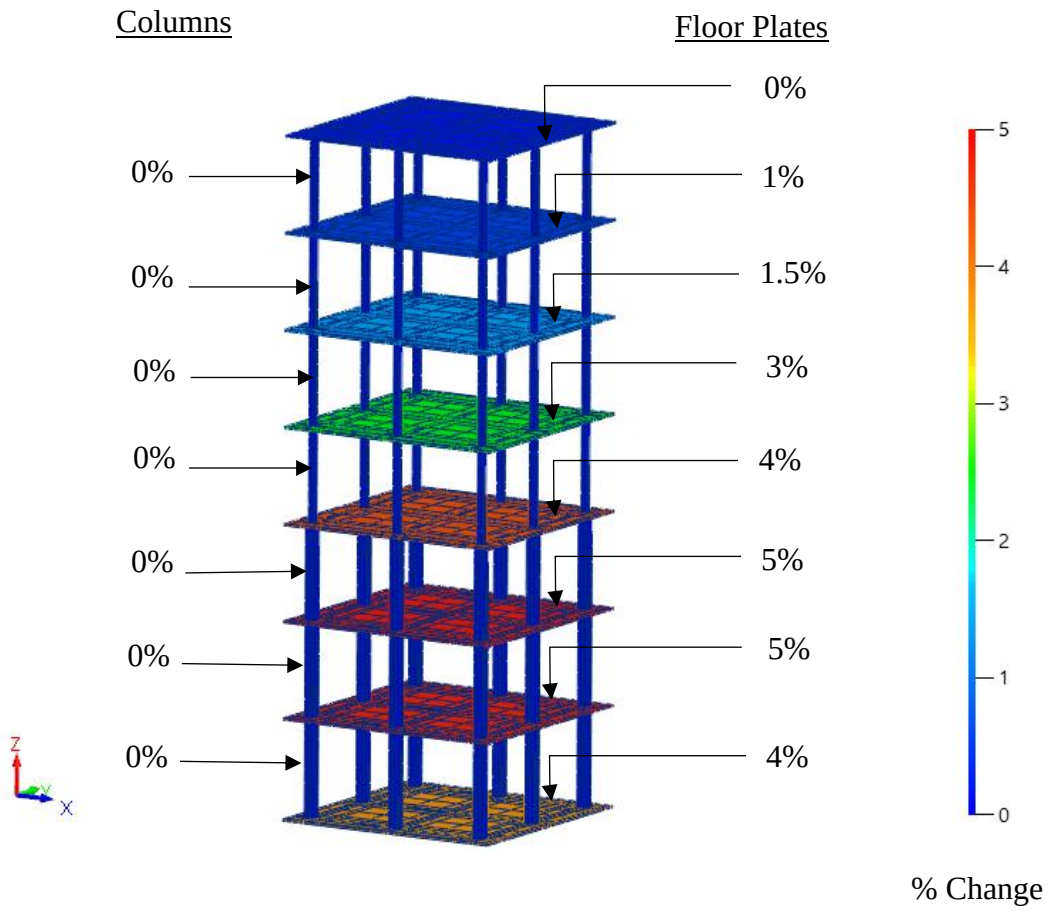


Figure 5.2: Changes in Young's modulus using 1st response combination [%]

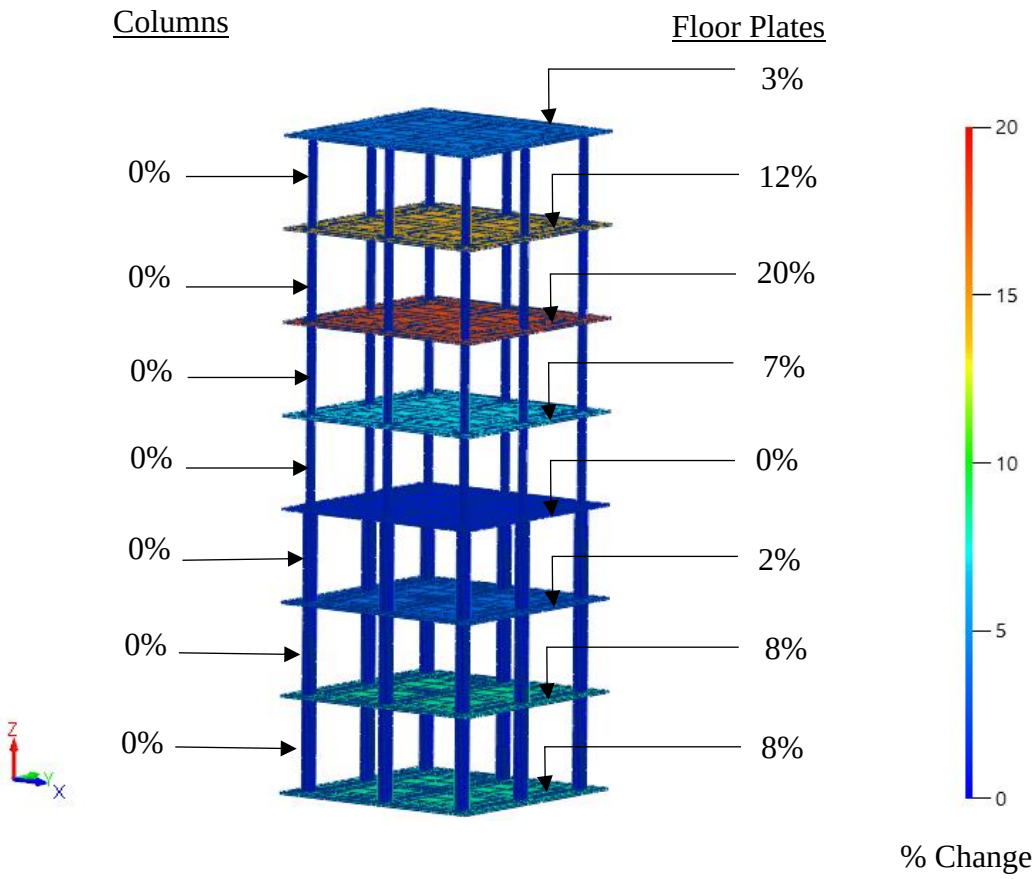


Figure 5.3: Changes in Young's modulus using 2nd response combination [%]

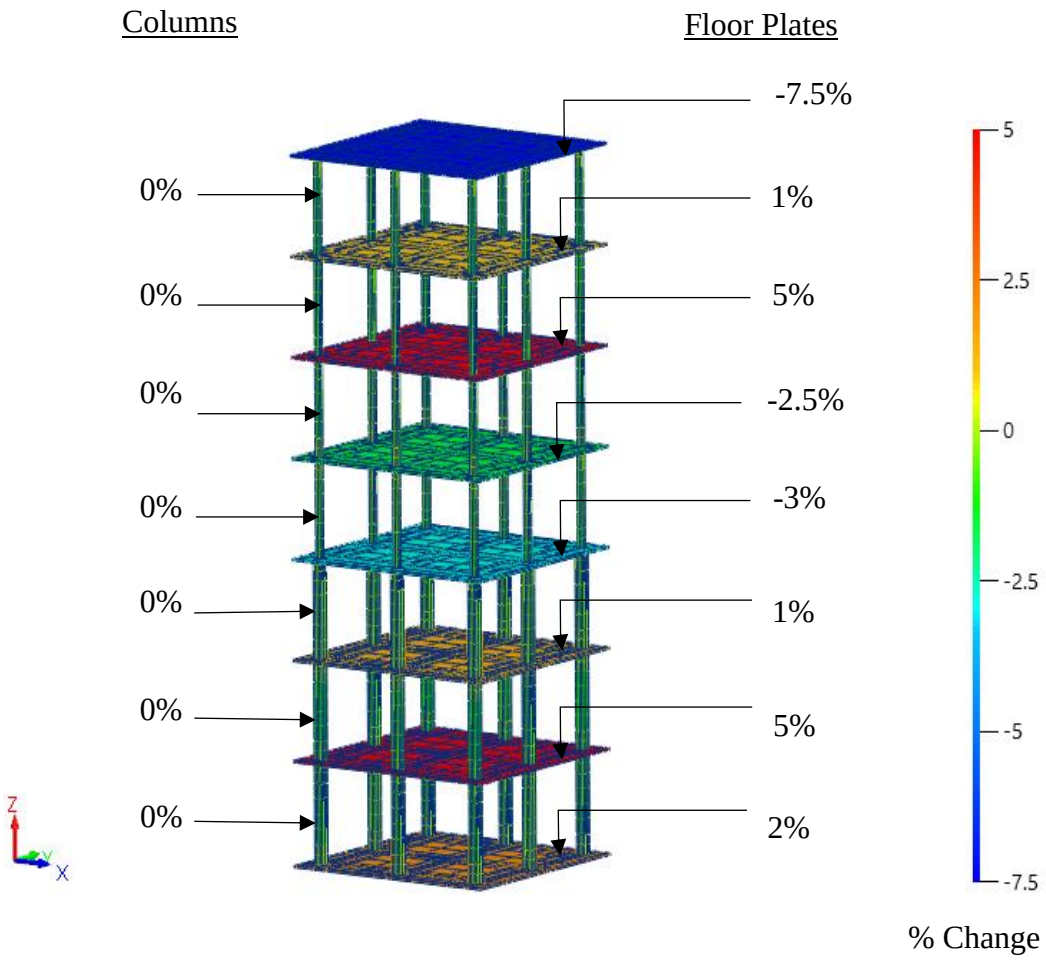


Figure 5.4: Changes in Young's modulus using 3rd response combination [%]

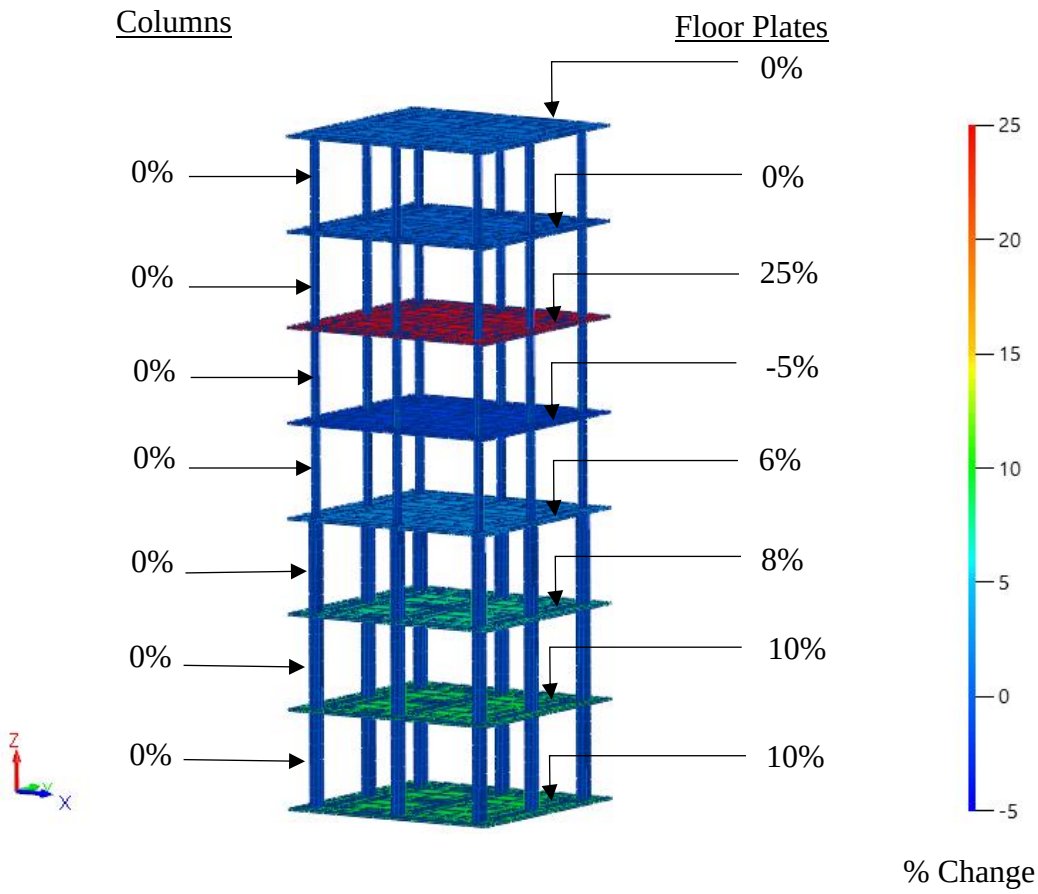


Figure 5.5: Changes in Young's modulus using 4th response combination [%]

5.3.2 Braced Frame

The ABAQUS model with modified brace stiffness was used for the braced frame study. Four different response combinations (Table 5.5) were used for updating the braced frame (BF) model. Combination 4 was selected as the modes that will be the most affected during damage condition as will be discussed in the next section. The summarized parameter limits and the results before updating are shown in Table 5.6 and 5.7.

Table 5.5: Summary of response combinations for the undamaged BF

	1	2	3	4
Response combination	f1, f2, f3	f4, f5, f6	First 9 modes	f2, f5, f8

Table 5.6: Parameter limits of undamaged BF

Member	Parameter	Limits
Column	Young's modulus	±40%
Floor plates	Young's modulus	±40%
Braces	Young's modulus	±40%

Table 5.7: Mode shape pairs of BF before updating

Mode pair	OMA [Hz]	FEA [Hz]	∆ frequency [%]	MAC [%]
1	7.15	7.01	-1.98	97.00
2	11.70	12.43	6.24	98.40
3	14.37	14.82	3.13	95.10
4	22.68	21.13	-6.81	98.60
5	35.87	35.86	-0.01	95.70
6	40.39	40.03	-0.90	81.60
7	42.38	42.31	-0.16	97.30
8	60.49	63.93	5.70	72.10
9	66.56	70.27	5.56	71.60

Table 5.8 and Figures 5.6 to 5.9 summarize the updating results using the different responses and the change in parameters. Similar to the MF results, the updated models significantly changed when using different responses. As shown in Table 5.8, using only the X direction modes (f2, f5, f8), not only improves the correlation and natural

frequencies of selected modes but also improved the torsional modes. The 8th and 9th mode had low MAC values, and using the RC4, the MAC value of mode 9 is improved from 71.6% to 76.4%. Moreover, it can be observed that the changes were mainly in the brace members. This is because the selected responses are X direction modes which are sensitive to the brace members. As shown in Figures 5.6 to 5.9, there were no changes in Young's modulus for the column members for all the cases, and the major adjustments were made in brace members and floor plates. The changes in Young's modulus for the floor plates are ranged from -25% to 25% depending on the selected responses. Young's modulus of the brace members was reduced for all the cases, amd the magnitudes are ranged from -2.5% to -25% depending on the selected responses.

Table 5.8: Results of model updating of BF using different response combination

	RC1		RC2		RC3		RC4	
Mode pair	∆ frequency [%]	MAC [%]	∆ frequency [%]	MAC [%]	∆ frequency [%]	MAC [%]	∆ frequency [%]	MAC [%]
1	-1.81	97.00	1.49	97.10	-2.16	97.00	-3.28	97.00
2	3.06	98.30	7.11	98.40	3.32	98.40	0.73	98.30
3	1.18	95.10	4.18	95.10	1.01	95.10	-0.52	95.10
4	-6.65	98.60	-2.45	98.70	-6.32	98.50	-7.52	98.60
5	-1.89	95.80	0.96	95.70	-2.53	95.60	-1.10	94.90
6	-2.21	81.60	0.50	81.60	-2.66	81.60	-3.20	81.60
7	-0.03	97.30	2.35	97.50	-1.48	97.00	-0.81	97.30
8	4.31	72.00	6.56	72.10	2.02	72.20	1.00	72.10
9	5.65	72.10	7.41	72.00	3.77	71.50	1.55	76.40

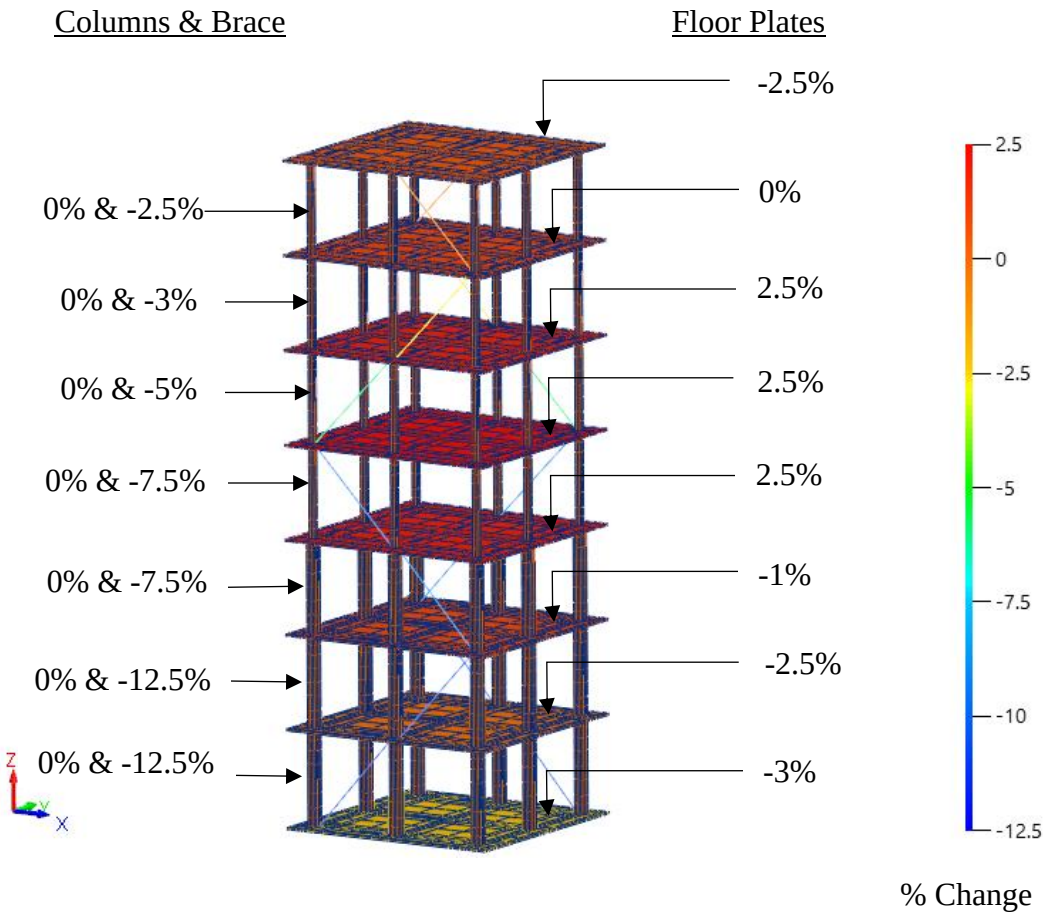


Figure 5.6: Changes in Young's modulus using 1st response combination [%]

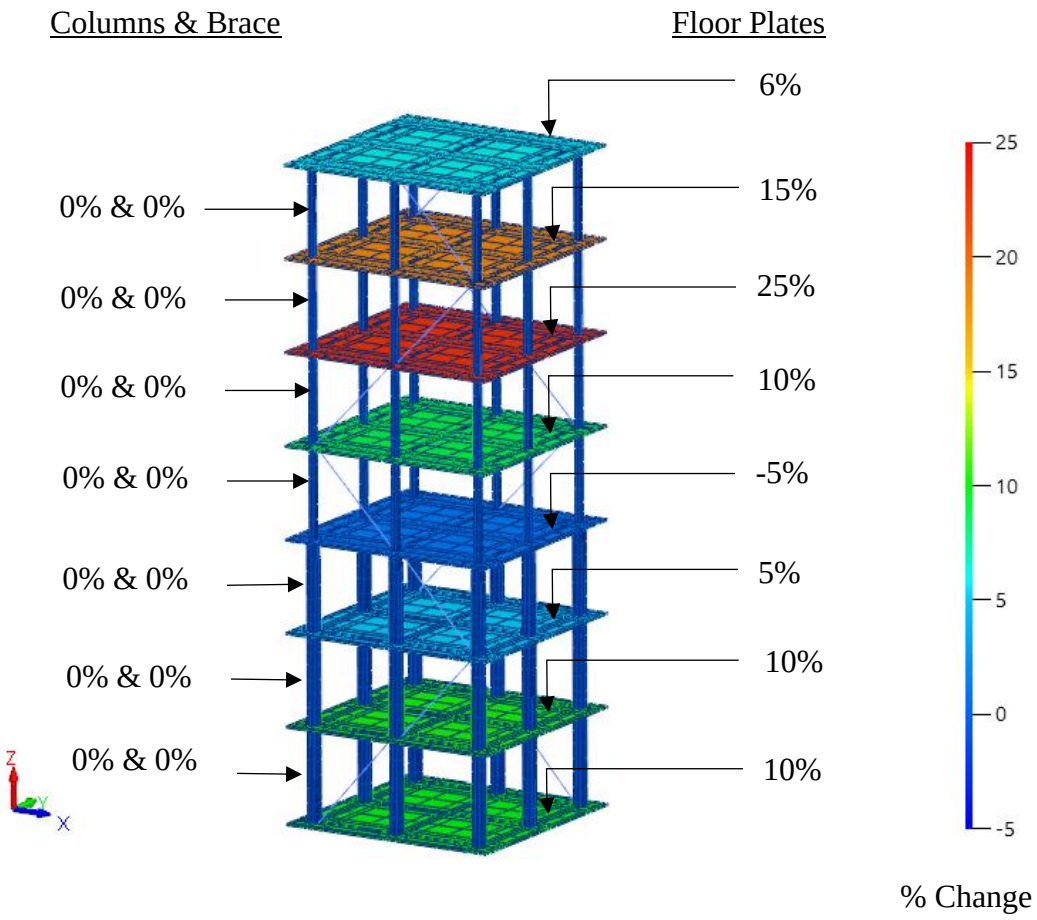


Figure 5.7: Changes in Young's modulus using 2nd response combination [%]

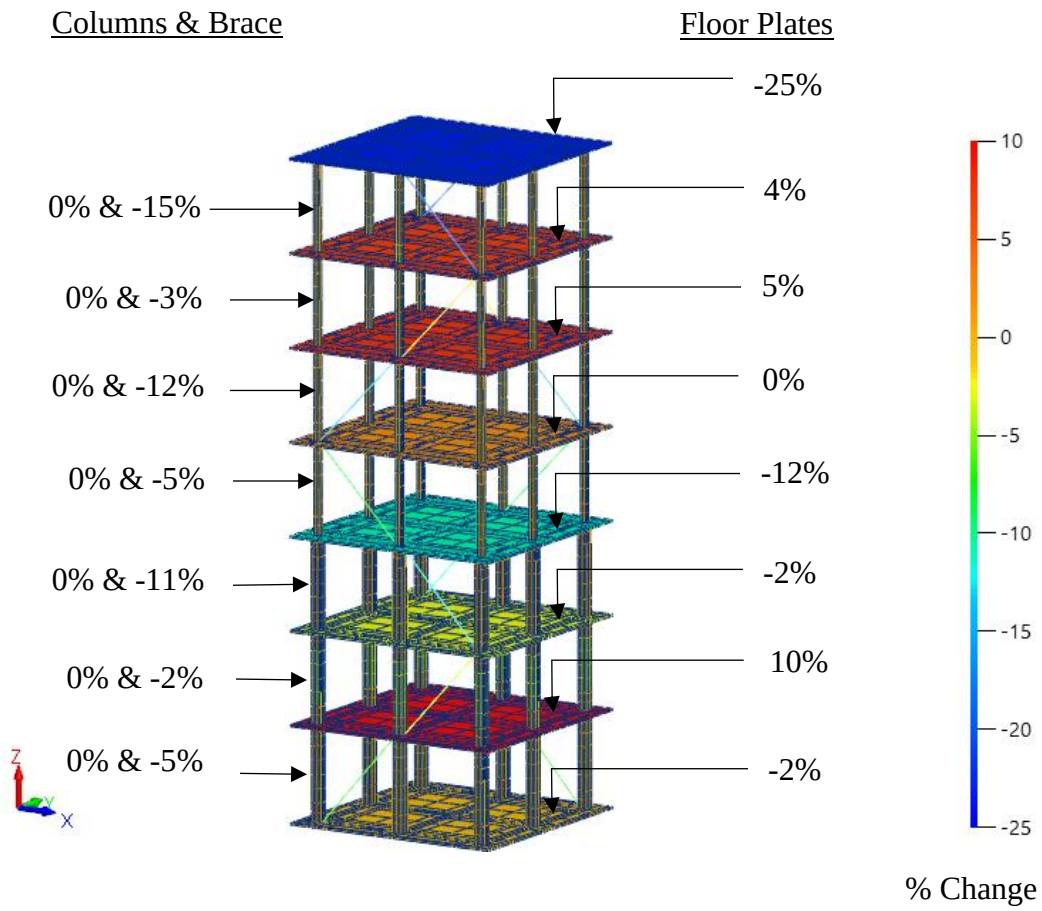


Figure 5.8: Changes in Young's modulus using 3rd response combination [%]

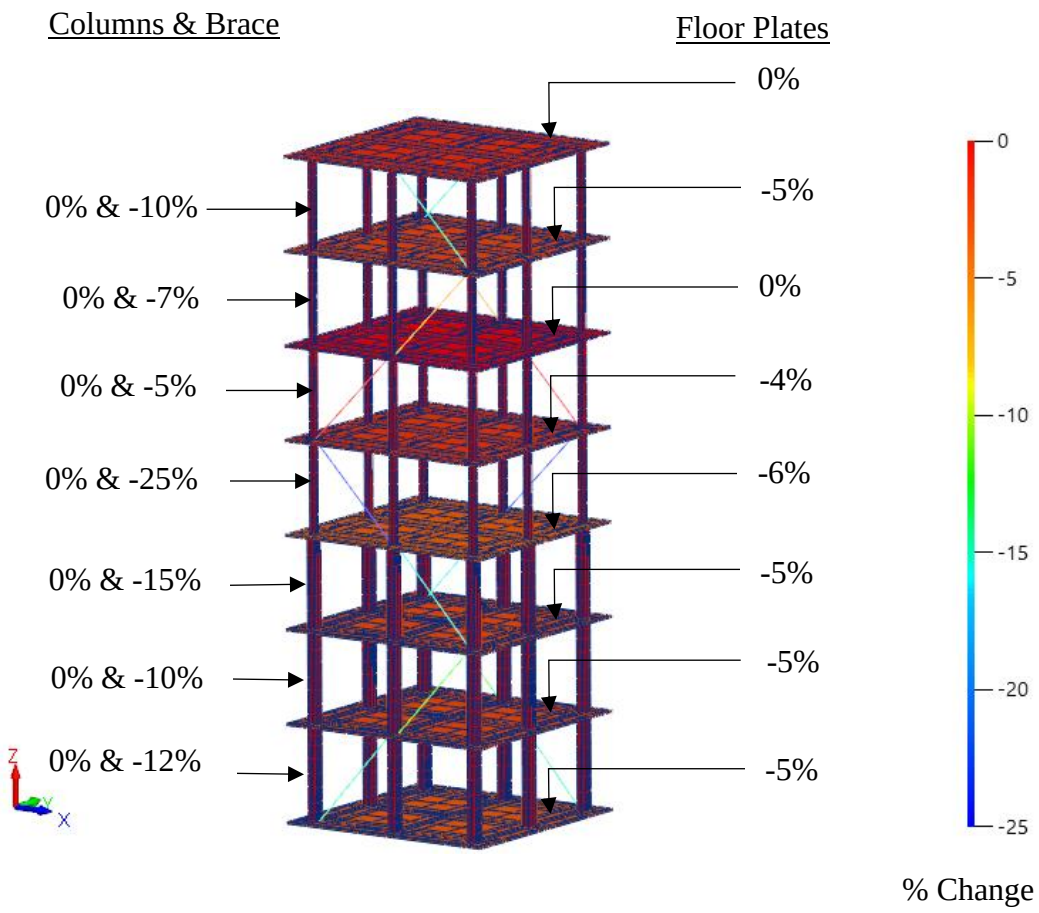
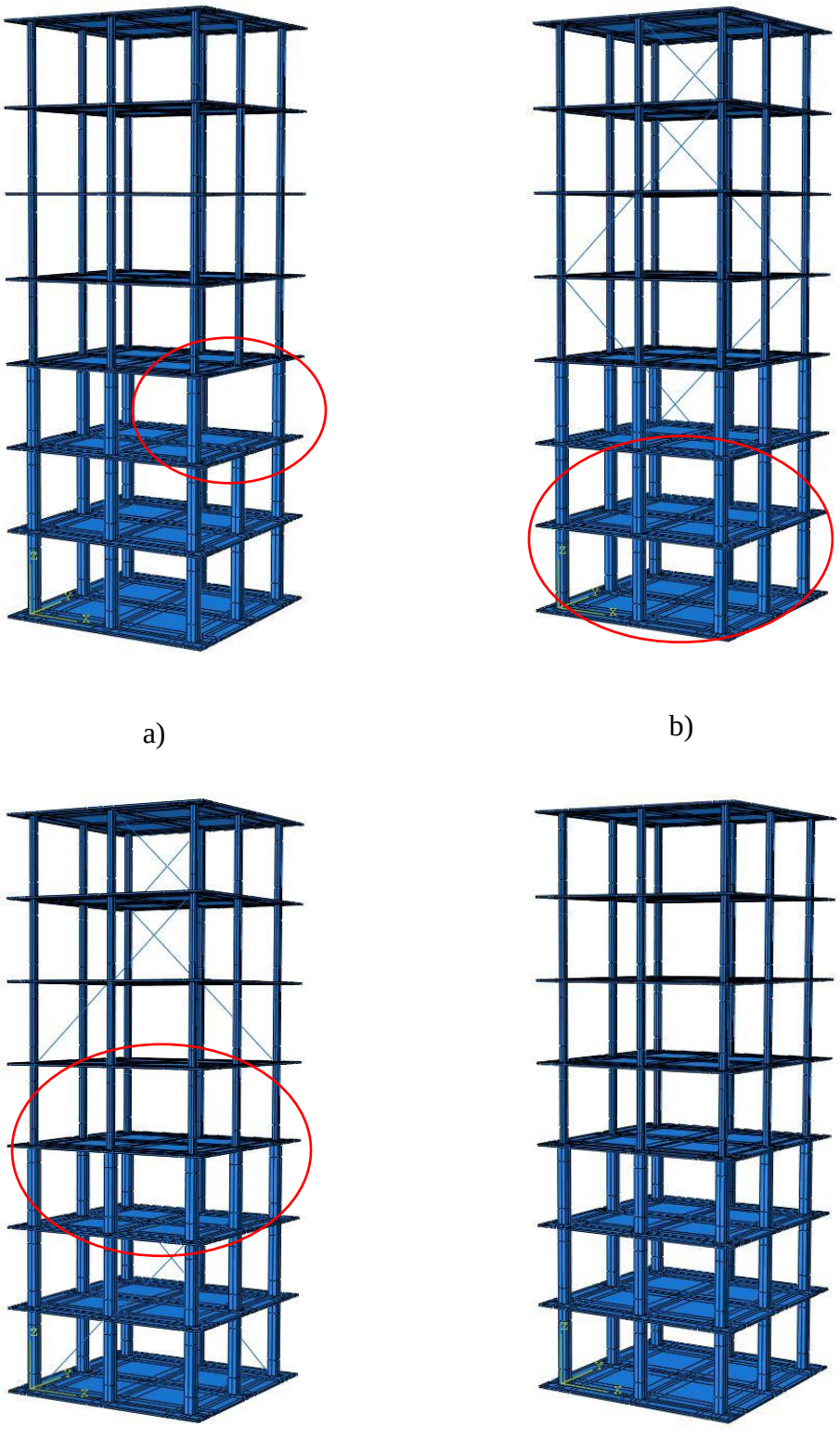


Figure 5.9: Changes in Young's modulus using 4th response combination [%]

5.4 Experimental Studies on Damaged Models

5.4.1 Damage Condition

Four different damage scenarios were created on the scale building. Vibration tests were then conducted on the damaged models in order to investigate the magnitude and location of damage. Minor damage was made to the moment frame model by taking out one of the third-floor columns. Three major damage conditions were made to the braced frame. The first damage condition was created by removing the first and second floors brace members. The second damage condition was created by removing the third and fourth-floor brace members. The third damage condition was created by removing all the brace members. Figure 5.10 illustrates the damage condition for each case.



a) b)

c) d)

Figure 5.10: Damage conditions a) MF b) BF case 1 c) BF case 2 d) BF case 3

5.4.2 Baseline FEM

As mentioned in the model updating study on the undamaged condition, it is difficult to update a finite element model to match all the modes of a physical model. However, compromise can be made to achieve good accuracy in partial modes depending on the considered problem. Therefore, the baseline FE model that is accurate in the modes that are sensitive to the damage can be developed. Vibration-based damage detection uses the change in dynamic characteristics to identify the damage. Therefore, it is important to develop an FE model that is as accurate as possible in the sensitive modes. The baseline FE model for the moment and braced frame will be discussed in Section 5.4.3 and 5.4.4.

5.4.3 Moment Frame

5.4.3.1 Selecting Parameters and Target Responses

In this research, changes in modal frequencies were used to find target modal responses that are sensitive to the damage. This was performed by comparing the OMA results of the undamaged and damaged models. As shown in Table 5.9, the frequencies of mode 5 and 7 of the damaged conditions are significantly higher than the undamaged condition; however, structural damage is expected to reduce the structural stiffness and decrease vibration frequencies. It can be concluded that an increase in the 5^{th} and 7^{th} mode vibration frequencies are introduced by the errors in OMA tests. Other than these two modes, the natural frequencies of MF model are not significantly affected by the damage; only minor changes are shown in some modes. Since none of the responses are significantly sensitive to the damage, the first x-direction and torsional modes (f1 and f3) are selected as the target response for performing damage detection. The maximum and minimum allowable change of the parameters are shown in Table 5.10.

Table 5.9: Comparison of OMA results of undamaged and damaged MF

Mode	Undamaged [Hz]	Damaged [Hz]	Δ frequency [%]
1	7.15	7.08	-1.01
2	7.38	7.43	0.72
3	10.75	10.66	-0.82
4	22.87	22.66	-0.95
5	22.45	22.99	2.33
6	29.67	29.77	0.36
7	39.34	42.01	6.37
8	42.62	42.68	0.14
9	52.93	52.80	-0.26

Table 5.10: Parameter limits for MF

Member	Parameter	Limits
Column	Young's modulus	±99%
Floor plates	Young's modulus	±40%

In this study, the updated FE model from Table 5.4 (RC1, used f1, f2, f3 as responses) has the best accuracy in the sensitive modes which are f1 and f3. Thus, this updated model is used as the baseline FE model to detect the damage for MF.

5.4.3.2 MF Damage Detection Results

As shown in Figure 5.11, damage in the MF model was not successfully localized. The main reason is that the damage condition of MF does not have enough effect on the natural frequencies, and none of the extracted mode shapes show high sensitivity to the damage.

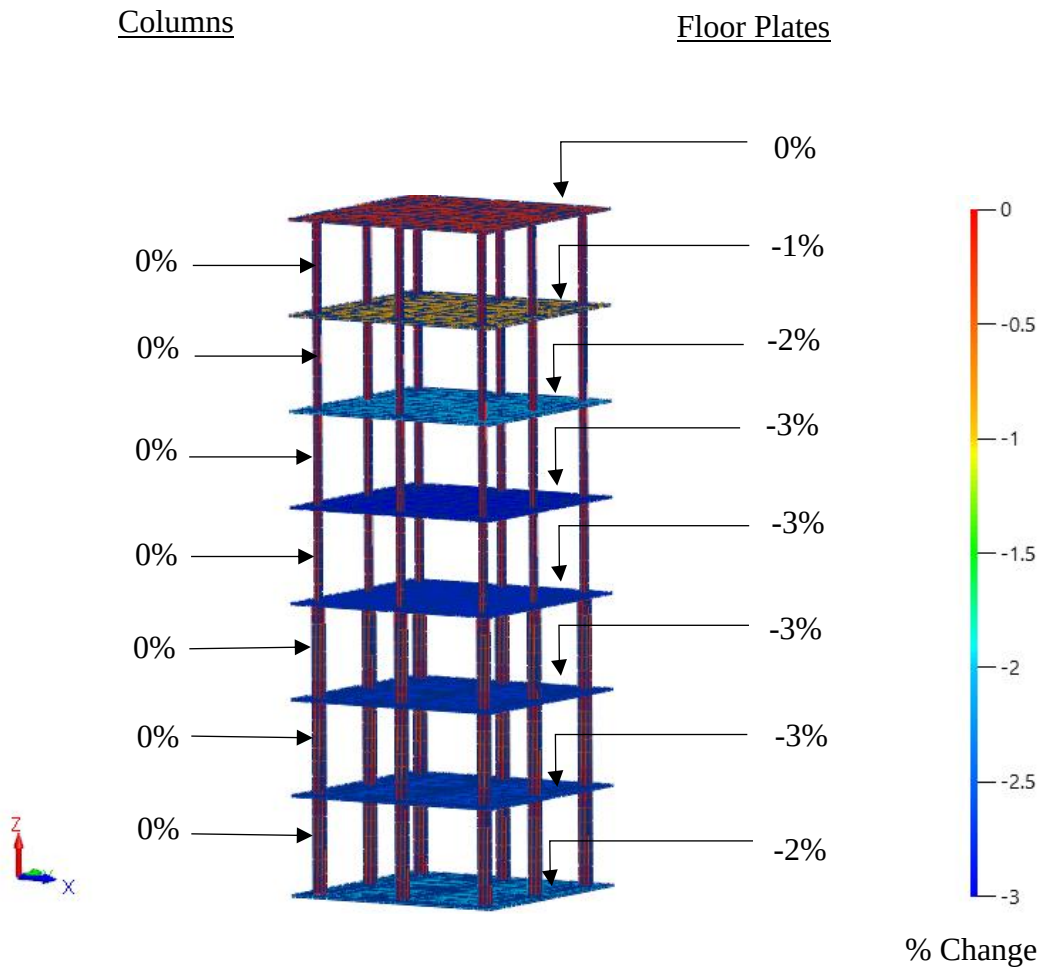


Figure 5.11: Parameter change in Young's modulus for damage detection of MF

5.4.4 Braced Frame

5.4.4.1 Selecting Parameters and Target Responses

The comparison of extracted natural frequencies from the undamaged and the damaged Braced Frames (BF) are summarized in Table 5.11. As can be seen, removing braces from different stories caused a significant level of reduction in natural frequencies, especially in the X direction modes (f2, f5, f8) and torsional modes (f3, f6, f9). Table 5.12 summarized the selected responses for the different cases of damage condition. Mode 2, 5 and 8 were selected as target responses for scenario 1 and 2 damage condition, since

these modes are all X direction modes which are the modes that are significantly affected by the damage. Torsional modes were not selected as responses for these two scenarios initially. This is because torsional modes consist of both X and Y direction vibration behaviour. However, for a larger damage condition such as scenario 3, it required more responses to add more constraints in order to successfully localize all damages. Thus, f3 and f9 torsional modes were added to the target response for scenario 3.

Table 5.11: Comparison of OMA results of undamaged and damaged BF

Mode		Case 1		Case 2		Case 3	
	Undamaged [Hz]	Damaged [Hz]	Δ frequency [%]	Damaged [Hz]	Δ frequency [%]	Damaged [Hz]	Δ frequency [%]
1	7.15	7.07	-1.13	7.23	1.08	7.15	-0.08
2	11.70	9.40	-24.37	10.21	-14.52	7.38	-58.48
3	14.37	12.68	-13.29	13.04	-10.17	10.75	-33.71
4	22.68	22.64	-0.14	22.75	0.34	22.87	0.85
5	35.87	31.24	-14.80	33.09	-8.40	22.45	-59.75
6	40.39	36.30	-11.26	39.76	-1.59	29.67	-36.14
7	42.38	42.38	0.00	42.30	-0.20	39.34	-7.74
8	60.49	59.02	-2.48	52.76	-14.64	42.62	-41.93
9	66.56	65.67	-1.35	62.76	-6.06	52.93	-25.75

Table 5.12: Selected response for model updating to detect the damage of the BF

	Case 1	Case 2	Case 3
Response combination	f2, f5, f8	f2, f5, f8	f2, f3, f5, f8, f9

Table 5.13: Parameter limits for BF damage detection

Member	Parameter	Limits
Columns	Young's modulus	±40%
Floor plates	Young's modulus	±40%
Braces	Young's modulus	±99%

The updated FE model from Table 5.8 (RC4, used f2, f5, f8 as responses) has good accuracy in the sensitive modes which are f2, f3, f5, f8 and f9. Thus it is used as baseline FE model to detect the damage for BF.

5.4.4.2 BF Damage Detection Results

Figures 5.12 to 5.14 show changes in the structural members' Young's modulus for the damaged BF models. Damage in the three cases was successfully identified and localized. For case 1, the largest parameter reduction of 60% was in the first and second-floor braces which matched the damage condition shown in Figure 5.10.b. The reductions of floor plates are in lower stories, and the changes are ranged from 25% to 5%. For case 2, the largest parameter reduction of 75% and 45% were in the third and fourth-floor braces which matched the damage condition shown in Figure 5.10.c. The reductions of floor plates are in all stories except 6^{th}-floor, the changes are ranged from 10% to 20%. For case 3, the largest reduction was the in the brace members which matched the damage condition shown in Figure5.10.d. The reductions of floor plates are in first to fifth-floor plates, the changes are ranged from 5% to 22%, and Young's modulus of 6^{th} and 7^{th}-floor plates increased 25% and 5% respectively. For all the cases, the column members are not sensitive to the selected responses.

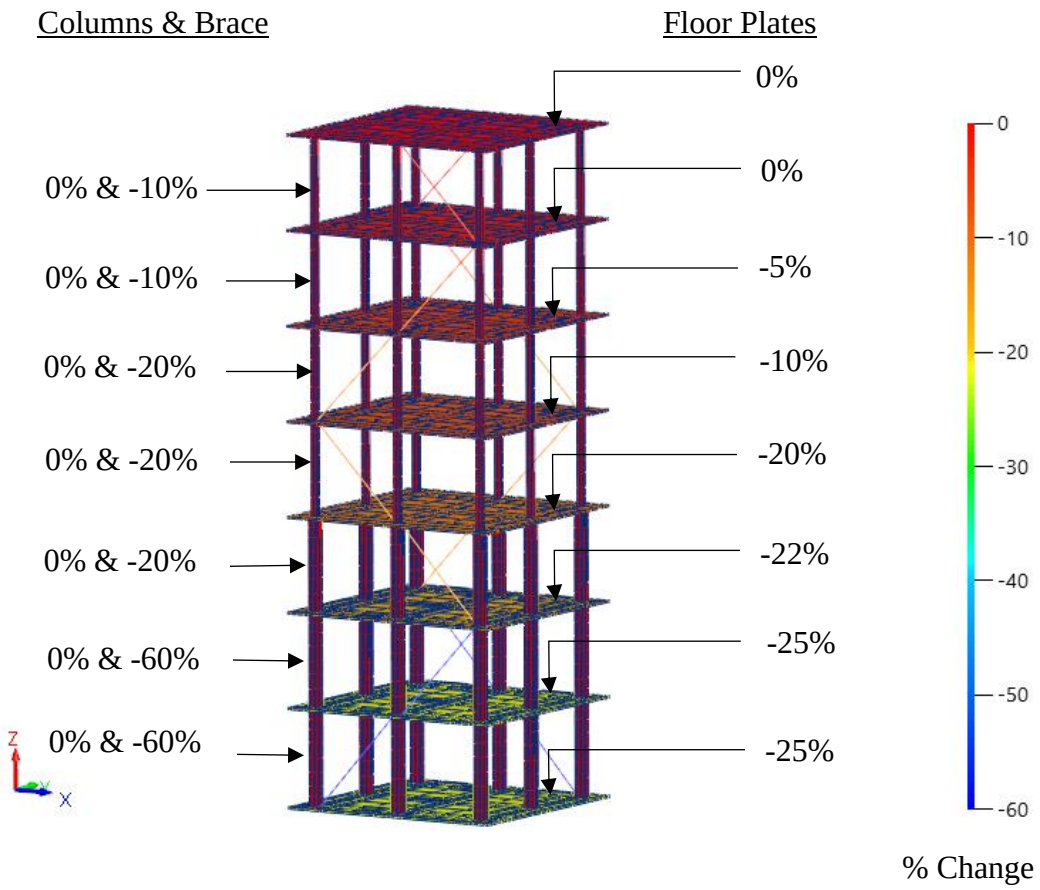


Figure 5.12: Parameter change in Young's modulus for damage detection of BF case 1

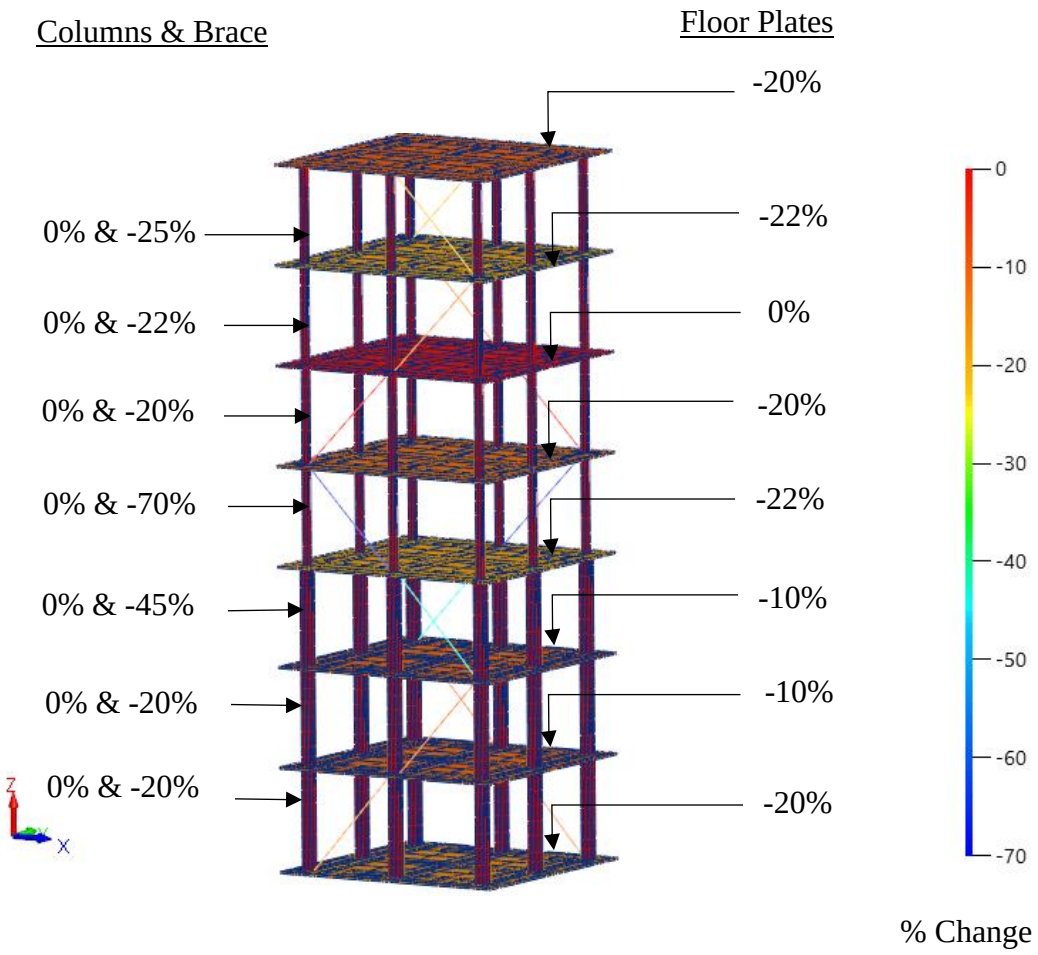


Figure 5.13: Parameter change in Young's modulus for damage detection of BF case 2

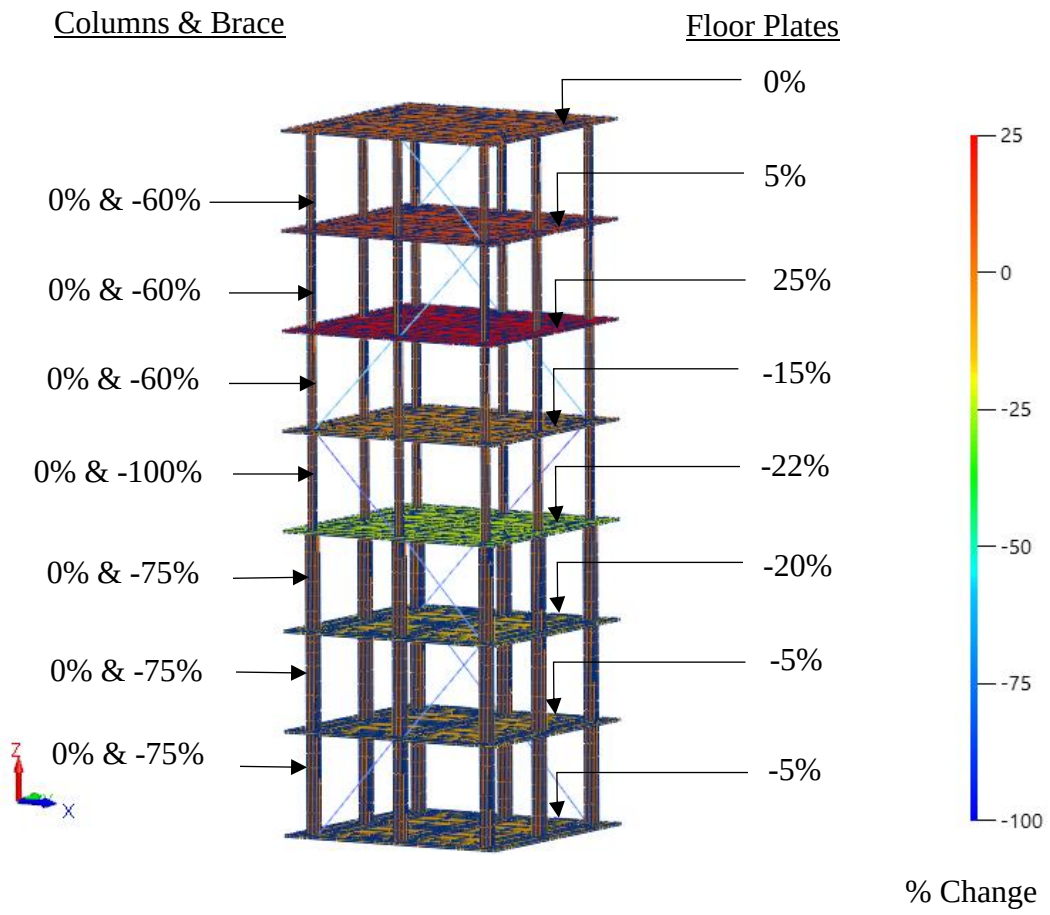


Figure 5.14: Parameter change in Young's modulus for damage detection of BF case 3

5.5 Conclusion

From this study, it can be observed that the model updating technique reduces the large discrepancy between numerical and physical models. However, creating an accurate FE model that has entirely the same modal parameters for a large number of mode shapes as the physical structure was found to be challenging. Instead, creating an accurate FE model with selected modes similar to the physical structure is achievable. Thus, compromise is required based on the considered problem when selecting the target responses for model updating.

Selecting the correct responses that are sensitive to the damage is crucial for damage detection using model updating. By assessing the change in natural frequencies, structural damage in the presence of major damage was successfully identified and localized. However, when minor damage is introduced which does not have a significant effect on the natural frequencies, the method cannot identify the damage. Promising results were achieved when structural damage caused significant change (in this case larger than 14%) in the modal frequencies.

This chapter investigated the effect of choosing different response on the results of model updating. Using the comparison between the undamaged and damaged condition OMA results, the target responses that are sensitive to the damage were successfully determined. The proposed procedure was successfully validated with three damaged brace frame models. The damage was successfully identified and localized as a reduction in Young's modulus of the structural members.

6 General Conclusions and Recommendations

6.1 General Conclusions

This thesis includes four topics pertaining to the study of structural damage detection using a vibration-based model updating method. The topics includes: (1) development of a physical model for a seven-story scale building, (2) development of a numerical model of the scale building, (3) operational modal analysis of the scale building, and (4) damage detection of different levels of damage using a vibration-based model updating method. The specific conclusions for each topic are given in Chapters 2 through 5, respectively, and have been summarized below:

1. A physical model of a seven-story scale building has been designed and constructed. It was found that similitude law is important for establishing the proper condition of similarity between prototype and scale model. However, when designing a scale model based on a prototype structure, necessary modifications are needed for the constructability, availability of material, as well as the considered problem.
2. Different FE models of the scale building have been developed using SAP2000 and ABAQUS. Mesh and element convergence studies provided the efficient mesh size and element type for accurate FE models. However, modelling assumptions such as the connection details and member stiffness that are used in the FE models resulted in tremendous differences between the idealized FE model and the as-built model. Therefore, to develop an accurate FE model, engineering judgment is required for making appropriate modelling assumptions.

3. Modal parameters of the scale building model including natural frequencies, mode shapes, and damping ratios have been successfully extracted using OMA. It was found that conducting multiple vibration tests using different types of excitation and sensor configurations is important, to find the best setup that can successfully extract the greatest number of modal parameters. The study also revealed that the results of OMA are highly dependent on block size and model order, highlighting the importance of conducting parametric studies to find the optimal parameter values.
4. Experimental studies of undamaged models were performed to investigate the effect of choosing different responses on the results of model updating. It was found that the model updating technique reduces large discrepancies between the numerical and physical models. However, it is challenging to create an accurate FE model that has entirely the same modal parameters as the physical structure. Thus, compromise is required based on the considered problem.

   Four different damage scenarios were investigated by assessing the change in natural frequencies using the model updating method. Three damage scenarios caused a significant change in modal frequencies and were successfully identified. One minor damage scenario was not successfully identified. It can be concluded that the following conditions are important to fulfill to successfully identify the damage:

   - The damage condition needs to be a major structural damage that has significant effect on the modal frequencies
   - Accurate results of extracted natural frequencies using OMA is required

- The modes that are sensitive to the damage need to be identified
- A FE model that accurately simulates the sensitive modes must be developed
- Only the sensitive modes should be used as the target response

6.2 Recommendations

The author wishes to make the following recommendations for future research:

- The extracted mode shape using OMA in Chapter 4 varied across different tests. This is because to conduct OMA it is necessary to assume the input is a Gaussian white noise which is uniformly distributed over the entire structure which is not true in practice. Thus, further study of extracting reliable mode shapes using OMA when these assumptions are not fulfilled is recommended.
- It is recommended to perform OMA on the experimental shake table test using the MTS system to simulate the actual earthquake. Then compare the extracted modal parameters with this research.
- It is recommended to apply damage detection using model updating to a full-scale civil structure.
- The damage detection method by assessing the change in natural frequency was able to detect the major structural damage. It is recommended that a damage identification method that is capable of detecting minor structural damages be developed by considering the change in mode shapes.

7 References

[1] J. E. Doherty, *Handbook on Experimental Mechanics*. Society for experimental mechanic, Inc., 1987.

[2] R. Brincker and C. Ventura, *Introduction to operation modal analysis*. John Wiley & Sons, Ltd, 2015.

[3] M. Friswell and J. E. Mottershead, *Finite element model updating in structural dynamics*, vol. 38. Springer Science & Business Media, 2013.

[4] H. Harry G and S. Gajanan M, "The theory of structural models," 1999.

[5] J. Li, J. Yan, T. Peng, and L. Han, "Shake table studies of seismic structural systems of a Taizhou Changjiang highway bridge model," *J. Bridg. Eng.*, vol. 20, no. 3, pp. 1–14, 2015.

[6] M. Garevski, V. Hristovski, K. Talaganov, and M. Stojmanovska, "Experimental investigations of 1 / 3 scale reinforced concrete frame With infill walls building structures," *13th World Conf. Earthq. Eng.*, 2004.

[7] M. Tomaževič and M. Gams, "Shaking table study and modelling of seismic behaviour of confined AAC masonry buildings," *Bull. Earthq. Eng.*, vol. 10, no. 3, pp. 863–893, 2012.

[8] E. Baglietto, M. Casirati, A. Castoldi, F. Demiranda, and R. Sammartino, "Mathematical and Structural Models of Zarate-Brazo Largo Bridges, Report No. 85," Bergamo, Italy, 1976.

[9] H. Harry G and S. Gajanan M, "Model applications and case studies," vol. 1, no. Phase I, 1999.

[10] R. W. Harris, H. G., Bertero, V. V., and Clough, "One-fifth scale model of a seven-story reinforced concrete frame-wall building under earthquake loading," *Proc. Jt. I. Struct. E./B.R.E. Int. Semin. Dyn. Model. Struct.*, 1981.

[11] W. Godden and D. Williams, “Seismic response of long curved bridge structures: Experimental model studies,” *Earthq. Eng. Struct. Dyn.*, vol. 7, no. 2, pp. 107–128, 1979.

[12] S. Stoyanoff, P. Irwin, J. Xie, M. Hunter, S. Stoyanoff, P. Irwin, and M. Hunter, “Wind Tunnel Testing of the Parallel Tacoma Bridges,” pp. 1–15, 2004.

[13] “Introduction to Physical Modeling in Structural Engineering,” 1999.

[14] Canadian Commission on Building and Fire Codes, *National Building Code of Canada 2010 (NBC)*, 2010th ed. NRC, 2010.

[15] “McMASTER-CARR supply company.” .

[16] K. J. Bathe, *Finite element procedures. Second edition*. 2006.

[17] Computers and Structures Inc., “CSI SAP2000 v.2015.” CSI, 2015.

[18] Computers & Structures Inc., “CSI ETABS v.2015.” CSI, 2016.

[19] “MIDAS.” MIDAS Information Technology Co., Ltd.

[20] “ANSYS.” ANSYS, Inc.

[21] M. Smith, “ABAQUS/Standard User’s Manual.” Simulia, 2009.

[22] Dynamic Design Solutions NV, “FEMtools.” DDS.

[23] M. T. Tucker, M. F. Horstemeyer, W. R. Whittington, and K. N. Solanki, “Structure / property relations of aluminum under varying rates and stress states,” no. January, 2010.

[24] D. D. Solutions, “FEMtools Model Updating User ’ s Guide,” *FEMtools user Guid.*, 2012.

[25] Y. Liu and G. Glass, “Effects of mesh density on finite element analysis,” no. May, 2013.

[26] C. E. Ventura, “Why output-only modal testing is a desirable tool for a wide range of practical applications,” 2003.

[27] S. Zivanovi, A. Pavic, and P. Reynolds, “Modal testing and FE model tuning of a lively footbridge structure,” vol. 28, pp. 857–868, 2006.

[28] W. Hu, C. Moutinho, E. Caetano, and F. Magalhaes, “Continuous dynamic monitoring of a lively footbridge for serviceability assessment and damage detection,” vol. 33, pp. 38–55, 2012.

[29] B. Peeters, H. Van Der Auweraer, F. Vanhollebeke, and P. Guillaume, “Operational modal analysis for estimating the dynamic properties of a stadium structure during a football game,” vol. 14, pp. 283–303, 2007.

[30] C. E. Ventura, J. F. Lord, and M. Turek, “FEM updating of tall buildings using ambient vibration data,” 2005.

[31] C. Ventura, “Dynamic analysis of a pedestrian walkway,” no. March 2015, 2002.

[32] M. Betti, L. Facchini, and S. Monchetti, “ScienceDirect Bayesian model updating of historic masonry towers through dynamic experimental data,” *Procedia Eng.*, vol. 199, pp. 1258–1263, 2017.

[33] C. Gentile and A. Saisi, “Operational modal testing of historic structures at different levels of excitation,” *Constr. Build. Mater.*, vol. 48, pp. 1273–1285, 2013.

[34] C. Gentile and A. Saisi, “Ambient vibration testing of historic masonry towers for structural identification and damage assessment,” vol. 21, pp. 1311–1321, 2007.

[35] E. Dascotte, “Vibration monitoring of the Hong Kong Stonecutters Bridge,” pp. 1–9, 2010.

[36] M. Turek, C. E. Ventura, and E. Dascotte, “Model updating of the Ironworkers Memorial Second Narrows Bridge,” 2009.

[37] A. Cunha, E. Caetano, and F. Magalhaes, “Vibration based structural health monitoring of an arch bridge : From automated OMA to damage detection,” vol. 28, pp. 212–228, 2012.

[38] L. F. Ramos, L. Marques, P. B. Lourenc, G. De Roeck, A. Campos-costa, and J. Roque, “Monitoring historical masonry structures with operational modal analysis : Two case studies,” vol. 24, pp. 1291–1305, 2010.

[39] S. R. Ibrahim and E. C. Mikulcik, “A method for the direct identification of vibration parameters from the free response,” *Shock Vib. Bull. 47*, 1977.

[40] H. Vold, J. KUNDRAT, G. ROCKLIN, and R. Russell, “A multi-input modal estimation algorithm for mini-computers,” *SAE*, 1982.

[41] P. Van Overschee and B. De Moor, “Subspace algorithms for the stochastic identi cation problem,” *Decis. Control. 1991., Proc. 30th IEEE Conf.*, pp. 1321–1326, 1993.

[42] C. Rainieri and G. Fabbrocino, *Operational modal analysis of civil engineering structures*. Springer Science & Business Media, 2014.

[43] L. Zhang, R. Brincker, and P. Andersen, “An Overview of Operational Modal Analysis : Major Development and Issues 1 . Major Developments of OMA,” no. 1, 2005.

[44] R. Brincker, P. Andersen, and L. Zhang, “Modal identification from ambient responses using frequency domain decomposition,” pp. 625–630, 2000.

[45] P. Guillaume, P. Verboven, and S. Vanlanduit, “Frequency-domain maximum likelihood identification of modal parameters with confidence intervals,” *Proc. Int. Semin. Modal Anal.*, vol. 1, no. JANUARY 1998, pp. 359–366, 1998.

[46] P. Guillaume, P. Verboven, and S. Vanlanduit, “A poly-reference impelementation of the least-squares complex frequency-domain estimator,” no. January, 2003.

[47] B. Peeters and H. Van Der Auweraer, “Polymax: a revolution in operational modal analysis,” *Proc. 1st Int. Oper. Modal Anal. Conf.*, no. January 2005, 2005.

[48] Structural Vibration Solutions A/S, “ARTeMIS Extractor.” .

[49] Dynamic Design Solutions NV, “Modal parameter extractor user ’ s guide,” 2017.

[50] M. H. Weik, “Nyquist theorem,” in *Computer Science and Communications Dictionary*, Boston, MA: Springer US, 2001.

[51] International Organization for Standardization, “Mechanical vibration and shock vibration of fixed structures- Guidelines for the measurements of vibrations and evaluation of their effects on structures,” no. ISO4866:2010.

[52] D. D. S. NV, “FEMtools framework user ’ s guide.”

[53] M. Y. He, J. W. Hutchinson, S. W. Doebling, C. R. Farrar, and M. B. Prime, “A summary review of vibration-based damage identification methods,” *J. Appl. Mech.*, vol. 111, no. 2, pp. 270–78, 1998.

[54] P. Cawley and R. D. Adams, “The location of defects in structures from measurements of natural frequencies,” *J. Strain Anal. Eng. Des.*, vol. 14, no. 2, pp. 49–57, 1979.

[55] O. S. Salawu, “Detection of structural damage through changes in frequency: A review,” *Eng. Struct.*, vol. 19, no. 9, pp. 718–723, 1997.

[56] W. M. West, “Illustration of the use of modal assurance criterion to detect structural changes in an Orbiter test specimen,” *Proc. Air Force Conf. Aircr. Struct. Integr.*, 1986.

[57] S. W. Doebling, C. R. Farrar, and M. B. Prime, “A summary review of vibration-based damage identification methods,” *Shock Vib. Dig.*, vol. 30, no. 2, pp. 91–105, 1998.

[58] W. Fan and P. Qiao, “Vibration-based damage identification methods: A review and comparative study,” *Struct. Heal. Monit.*, vol. 10, no. 1, pp. 83–111, 2011.

[59] S. W. Doebling, C. R. Farrar, M. B. Prime, and D. W. Shevitz, “Damage identification and health monitoring of structural and mechanical systems from changes in their vibration characteristics: A literature review,” 1996.

[60] B. Chen and Y. L. Xu, “Integrated vibration control and health monitoring of building structures using semi-active friction dampers: Part II - Numerical investigation,” *Eng. Struct.*, vol. 30, no. 3, pp. 573–587, 2008.

[61] M. M. Abdel Wahab and G. De Roeck, “Damage detection in bridges using modal curvatures: Application to a real damage scenario,” *J. Sound Vib.*, vol. 226, no. 2, pp. 217–235, 1999.

[62] J. E. Mottershead and M. I. Friswell, “Model Updating In Structural Dynamics: A Survey,” *Journal of Sound and Vibration*, vol. 167, no. 2. pp. 347–375, 1993.

[63] M. I. Friswell and J. E. Mottershead, *Finite element model updating in structural dynamics*. Dorcdrecht: Kluwer Academic Publishers, 1995.

[64] A. Teughels and G. De Roeck, “Structural damage identification of the highway bridge Z24 by FE model updating,” *J. Sound Vib.*, vol. 278, no. 3, pp. 589–610, 2004.

[65] J. M. W. Brownjohn, P. Moyo, P. Omenzetter, and Y. Lu, “Assessment of highway bridge upgrading by dynamic testing and finite-element model updating,” *J. Bridg. Eng.*, vol. 8, no. 3, pp. 162–172, 2003.

[66] J. R. Wu and Q. S. Li, “Finite element model updating for a high-rise structure based on ambient vibration measurements,” *Eng. Struct.*, vol. 26, no. 7, pp. 979–990, 2004.

[67] Y. Ding and A. Li, “FEM updating for the Runyang cable-stayed bridge tower using ambient vibration test results,” vol. 11, no. 3, pp. 323–335, 2008.

[68] W. Torres, J. L. Almazán, C. Sandoval, and R. Boroschek, “Operational modal analysis and FE model updating of the Metropolitan Cathedral of Santiago, Chile,” *Eng. Struct.*, vol. 143, pp. 169–188, 2017.

[69] Ø. W. Petersen and O. Øiseth, “Sensitivity-based finite element model updating of a pontoon bridge,” *Eng. Struct.*, vol. 150, pp. 573–584, 2017.

[70] J. R. Wu and Q. S. Ã. Li, “Finite element model updating for a high-rise structure based on ambient vibration measurements,” vol. 26, pp. 979–990, 2004.

[71] C. P. Fritzen, D. Jennewein, and T. Kiefer, “Damage detection based on model updating methods,” *Mech. Syst. Signal Process.*, vol. 12, no. 1, pp. 163–186, 1998.

[72] J. M. W. Brownjohn, P.-Q. Xia, H. Hao, and Y. Xia, “Civil structure condition assessment by FE model updating: methodology and case studies,” *Finite Elem. Anal. Des.*, vol. 37, no. 10, pp. 761–775, 2001.

[73] S. R. Shiradhonkar and M. Shrikhande, “Seismic damage detection in a building frame via finite element model updating,” *Comput. Struct.*, vol. 89, no. 23–24, pp. 2425–2438, 2011.

[74] FEMtools, “FEMtools: Model Updating Theoretical Manual,” 2014.

[75] C. J.D, Y. J, and K. L, “Methods and applications of system identification in shock and vibration,” *Syst. Identif. vibrating Struct.*, pp. 45–71, 1972.

Appendix A: FEMtools Command Script for OMA

```
# Define the points

define point 1 330.835 314.96 0

define point 2 86.675 551.62 327.75

define point 3 574.995 78.3 327.75

define point 4 330.835 314.96 642.8

define point 5 86.675 551.62 957.85

define point 6 574.995 78.3 957.85

define point 7 330.835 314.96 1272.9

define point 8 86.675 551.62 1587.95

define point 9 574.995 78.3 1587.95

define point 10 330.835 314.96 1903

define point 11 86.675 551.62 2218.05

define point 12 574.995 78.3 2218.05



# Define the trace lines

define connectivity 1 type line2 connect 1 2
```

define connectivity 2 type line2 connect 1 3

define connectivity 3 type line2 connect 2 4

define connectivity 4 type line2 connect 3 4

define connectivity 5 type line2 connect 4 5

define connectivity 6 type line2 connect 4 6

define connectivity 7 type line2 connect 5 7

define connectivity 8 type line2 connect 6 7

define connectivity 9 type line2 connect 7 8

define connectivity 10 type line2 connect 7 9

define connectivity 11 type line2 connect 8 10

define connectivity 12 type line2 connect 9 10

define connectivity 13 type line2 connect 10 11

define connectivity 14 type line2 connect 10 12

define connectivity 15 type line2 connect 11 12

define connectivity 16 type line2 connect 8 9

define connectivity 17 type line2 connect 5 6

define connectivity 18 type line2 connect 2 3

Define the channel

define channel 1 point 1 dof -ux type accelerationG

define channel 2 point 1 dof +uy type accelerationG

define channel 3 point 2 dof -ux type accelerationG

define channel 4 point 2 dof +uy type accelerationG

define channel 5 point 3 dof -ux type accelerationG

define channel 6 point 3 dof +uy type accelerationG

define channel 7 point 4 dof -ux type accelerationG

define channel 8 point 4 dof +uy type accelerationG

define channel 9 point 5 dof -ux type accelerationG

define channel 10 point 5 dof +uy type accelerationG

define channel 11 point 6 dof -ux type accelerationG

define channel 12 point 6 dof +uy type accelerationG

define channel 13 point 7 dof -ux type accelerationG

define channel 14 point 7 dof +uy type accelerationG

define channel 15 point 8 dof -ux type accelerationG

```
define channel 16 point 8 dof +uy type accelerationG

define channel 17 point 9 dof -ux type accelerationG

define channel 18 point 9 dof +uy type accelerationG

define channel 19 point 10 dof -ux type accelerationG

define channel 20 point 10 dof +uy type accelerationG

define channel 21 point 11 dof -ux type accelerationG

define channel 22 point 11 dof +uy type accelerationG

define channel 23 point 12 dof -ux type accelerationG

define channel 24 point 12 dof +uy type accelerationG



# Import test Data

load table timeseries file 'MeanSubedJune4MF600sec.txt' format ascii samplefreq 256



# Find the optimal references

dsp findreferences number 5



# Compute cross power spectra from the time histories
```

```
dsp xps blocksize 76800

set mpe maxorder 100

set mpe minfrequency 0

set mpe maxfrequency 130


mpe poles extract

mpe poles store

mpe modes extract


input fem format abaqus file 'NodeLimiteFreq.inp'

set solver abaqus.bas


compute stiffness mass

dynamic vector 20 fmin 1
```

Curriculum Vitae

Candidate's full name:

Shuxuan Li

Universities attended:

University of New Brunswick, B.Sc.E (Civil Engineering), 2016

Conference Presentations: None

Publications: None